Thermodynamic Simulation of HCCI Engine Systems

Olof Erlandsson

Doctoral thesis

Lund 2002

To my parents Sigurd and Maritha,
and my brother Henrik.

Department of Heat and Power Engineering
Lund Institute of Technology
P.O. Box 118
SE – 221 00 LUND
Sweden

ISBN 91-628-5427-5

ISSN 0282-1990
ISRN LUTMDN/TMHP--02/1007--SE

Printed in Sweden by Media-Tryck, Lund University
Lund 2002

Abstract

This thesis focuses on engine system simulation using thermodynamics and chemical kinetic models to investigate the performance and efficiency of Homogeneous Charge Compression Ignition (HCCI) engines for stationary applications.

It includes the development of software as well as models for engine, turbocharger, intercooler, inlet and exhaust manifolds, wastegate valve, inlet air humidifier, inlet air heater and more. The engine model can be classified as a one-zone, zero-dimensional and includes sub-models for in-cylinder heat transfer, exhaust port heat transfer, heat release and the valve flow process. The turbocharger model is developed in steps and is based on a polynomial fit to experimental compressor and turbine performance data. Inlet and exhaust manifolds are treated as well-mixed volumes. A simplified model for the humidifier is adopted in order to simulate a humid air motor (HAM) concept. The whole engine system is zero dimensional and the different system components are linked by means of mean values for mass flow, temperatures, pressures and gas composition. The NASA-polynomials are used for calculating thermal and transport properties. The extended Zeldovich mechanism is used as an indicator of significant NO formation. The models are validated through comparisons with experiments on mainly diesel and HCCI engines, both cycle and system results.

HCCI engine cycle simulations are made, showing the influence of various engine parameters e.g. compression ratio, engine speed, air-fuel ratio, exhaust gas recycling, inlet pressure and valve timing. Mainly natural gas and landfill gas are studied. The self-stabilizing feature of HCCI ignition timing is investigated using chemical kinetics. HCCI engine system simulations are made, both with (to find ignition timing) and without chemical kinetics, investigating turbocharging and the influence of turbine size. The HCCI - HAM concept is investigated and compared to simpler systems.

Preface

The mystery.

The Homogeneous Charge Compression Ignition (HCCI) engine is without a doubt a very thrilling concept because it uses a completely different form of ignition and combustion principle from the common engines. It does not use spark plug and propagating turbulent flame like the spark ignited engine, nor does it use high pressure fuel injection and luminous diffusion flame like the diesel engine. The combustion in a HCCI engine seems to have no single origin, it appear in many locations simultaneously with a light-blue fluorescence.

The usefulness.

The reason why HCCI is interesting is the never-ending search for power-sources with higher efficiency and lower emissions. HCCI engines use high compression ratio and lean homogeneous mixtures. This is also the key to high efficiency and low NOx emissions in internal combustion engines.

The invention.

There is very little new under the sun - that is in general very true. However, inventions and other artifacts can be before its time, and there exist several examples of that. When it comes to HCCI, the timing is perfect. Today we have all the basic electronics to monitor and control the HCCI engine, which is fundamental for performance, efficiency and emissions.

The challenge.

HCCI has drawbacks, and in this work, I have tried to tackle mainly one of them: the limited specific power output that follows from the lean mixtures. The goal is to achieve acceptable performance without loosing the benefits of HCCI.

The tool.

This thesis covers both use and development of engine system simulation software. The thesis is written with an increasing degree of simulation complexity, after a short introduction comes the theory behind the simulation software, then follows various validations, chemical kinetics, cycle simulations and finally the program is used to study HCCI engine systems.

Acknowledgements

First, and foremost, I would like to express my gratitude to Professor Bengt Johansson for allowing me to do this work, and then pushing me to finish it. He is a professor with many ideas and big demands and besides being a guru for me and other Ph. D. students at the division, he really put Lund on the map when it comes to HCCI engine research.

Another great professor is Gunnar Lundholm who really opened my eyes for internal combustion engines and allowed me to do my master thesis about variable compression ratio engines. Together with excellent lectures by Krister Olsson, I got the necessary basics to continue within this field.

I would also like to thank my colleagues at the division for all help. Either in the lab or in the office, they are always there for support. I would especially like to mention my office colleagues whom I had the pleasure of sharing office with these years: Magnus Christensen, Ola Stenlåås and Petter Strandh. Also thanks to Per Amnéus, a fellow from the Combustion Physics division, for giving excellent support with the chemical kinetics.

The financial support from the Swedish Energy Agency has been essential, so thanks to all Swedish taxpayers.

Olof Erlandsson

Lund, October 31, 2002

Previous publications by the author

This thesis is in a way a collection of material presented by the author in papers and other publications, although the material is updated and much more results are introduced. The idea is that the reader can read this thesis without having access to those papers. Below is a list of papers and publications the author somehow has been involved. Some of these, not all, are reviewed in this thesis.

- "Demonstrating the Performance and Emission Characteristics of a Variable Compression Ratio, Alvar-Cycle Engine", Olof Erlandsson, Gunnar Lundholm, Fredrik Söderberg, Bengt Johansson, Victor W. Wong, SAE 982682
- "Alvar Engine, An Engine with variable compression ratio, Experiments and tests", Olof Erlandsson, Master thesis, ISRN LUTMDN/TMVK-5304--SE
- "Hydrocarbon (HC) Reduction of Exhaust Gases from a Homogeneous Charge Compression Ignition (HCCI) Engine Using Different Catalytic Mesh Coatings", Olof Erlandsson, Bengt Johansson, Fredrik Silversand, SAE 2000-01-1847
- "Experiments and Simulation of a Six-Cylinder Homogeneous Charge Compression Ignition (HCCI) Engine", Jan-Ola Olsson, Olof Erlandsson, Bengt Johansson, SAE 2000-01-2867
- "Development of an Engine System Simulation Software Package – ESIM", Olof Erlandsson, Licentiate thesis, ISRN/LUTMDN/TMVK – 7043
- "Early Swedish Hot-Bulb Engines – Efficiency and Performance Compared to Contemporary Gasoline and Diesel Engines", Olof Erlandsson, SAE 2002-01-0115
- "Analysis of a 6 Cylinder Turbocharged HCCI Engine Using A Detailed Kinetic Mechanism", Guiseppe Cantore, Luca Montorsi, Fabian Mauss, Per Amnéus, Olof Erlandsson, Bengt Johansson, Thomas Morel, ASME Internal Combustion Engine Division, Spring Technical Conference, April 14 – 17, 2002 Rockford, Illinois
- "Simulation of HCCI - addressing compression ratio and turbo charging", Olof Erlandsson, Patrik Einewall, Bengt Johansson, Per Amneus, Fabian Mauss, SAE 2002-01-2862

Contents

1 Introduction

1.1 Internal Combustion Engines

The Internal Combustion (IC) Engine is perhaps the most wide-spread apparatus for transforming liquid and gaseous fuel to useful mechanical work. The reason why it's so well accepted can be explained by its overall appearance regarding properties like performance, economy, durability, controllability but also the lack of other competitive alternatives. However, the IC engine is certainly not the best apparatus in every aspect but seems to be a good compromise overall. It is possible to further develop the IC engine to be better in some property but this is usually at the "cost" of another. For example, it is not difficult to develop a highly powerful engine for racing, but at the same time keeping manufacturing cost and durability as for a regular car engine is quite difficult. It is also possible to develop a very cheep and lightweight engine for handheld equipment like chainsaws, but at the same time limit exhaust emissions becomes difficult. The delivered power per mass unit has to be high in order for the machine to be handheld, and the exhaust gases are expelled to the atmosphere, close to the human working area.

New engine applicable technology emerges continuously that, if or when economically sensible, can provide improvements in some or several aspects without cost in others. An example of this is the introduction of electronics in engine control that, combined with continuous development of engine design, has provided spark ignited engines with minimum emissions and with both higher power and efficiency. However, the demands are constantly increasing; less emissions, lower fuel consumption, more power and lower costs. A continuous development is always required.

1.1.1 The Diesel engine

The diesel engine has through its high compression ratio a very good thermal efficiency but due to the combustion principle (diffusion flame) it produces lots of nitrogen oxide (NOx) emissions. In addition, high peak pressures and soot formation limit the diesel engine load. The ignition principle is self-ignition and a high ignitability is wanted in order to get well-controlled combustion timing. The ignitability is measured by the cetane number (CN) of the fuel.

The high compression ratio causes high peak pressures that require a rigid engine design, which brings up the mass of the design. Nevertheless, this engine has found its major applications in especially trucks, trains and entrepreneur, agriculture and forestry machinery, mainly due to its combination of fuel economy, durability and the fact that engine mass plays a minor role in these applications. Turbo charging has opened a door for the diesel engine in the lighter car applications. The load control of the diesel engine is very simple, only the amount of injected fuel is controlled.

The major emissions of concern from the diesel engine are, besides CO_2, NOx and soot particulates. It is possible to use soot traps that collect a major part of the particulates but the traps have to be cleaned somehow. One way is to burn off the trapped particulates by temporarily increasing the temperature in the trap by using additional fuel injection during the

exhaust stroke or even upstream the trap. To better succeed with this catalytic materials can be used in the trap. It is more difficult with the NOx emissions because of the idea is to convert them into N_2. This is very difficult to do in diesel exhaust gases because the high amount of oxygen present. DeNOx catalysts exist but are in general very sensitive to sulfur, and most diesel engine fuels contain some amounts of sulfur. Technology that uses a reducing media, like urea or ammonia has also been tested but it then requires "refueling" in order to work properly.

1.1.2 The Spark Ignited (SI) engines

The SI engine uses a premix of fuel and air and it utilizes a spark plug (forced ignition) that sets of premixed turbulent flame combustion. This combustion principle makes it sensitive to self-ignition, "knocking", which can result in structural damage, mainly to the piston. This phenomenon limits the compression ratio of the SI engine, which in turn limits the thermal efficiency. The fuels for the SI engines have a certain degree of knocking resistance, measured by the octane number (ON) of the fuel.

The SI engine has through the lower compression ratio a possibility to use higher rpm's in order to get high specific power because the pressures are limited, thus a more lightweight design can be used that allows higher rpm's. Load control is achieved by throttling which means that the inlet pressure, and hence the air mass flow through the engine, is controlled by a restriction, usually a butterfly valve. This forces the engine to work like a compressor at part load, which also reduces efficiency. In car applications, the major operating point of the engine is low to medium load, which means that the overall efficiency becomes quite low. For the diesel engine, it is almost the opposite situation. This has contributed to an increase of the number of diesel-propelled cars.

The SI engine uses (in general) stoichiometric mixtures, which opens a door to exhaust gas after treatment using a 3-way catalyst. This means that carbon monoxide, CO, and unburned hydrocarbons, HC, can be oxidized, and nitrogen oxides, NOx, can be reduced, simultaneously. The spark-ignited engine with 3-way catalyst is therefore the environmentally friendly alternative. It becomes even better if bio-fuels are used, which do not contribute to a net CO_2 increase in the atmosphere in the long perspective, like petroleum products do.

1.1.3 Modern and novel engine technology

The dream of every engine designer is to find a combination of the diesel engine and the spark ignited engine that only inherit the good properties of the diesel and SI engine i.e. efficiency like a diesel engine and exhaust emissions that are as clean as from the SI engine, or at least possible to after-treat to the same level. This is quite difficult and there have been very few attempts that have reached any commercial success. There are two such concepts that are worth to be mentioned: lean burn SI engines with either homogeneous mixtures or stratified charge.

Lean burn SI engines simply uses a mixture with less fuel per mass air, and hence burns with lower temperature. By lowering the combustion temperature, NOx formation (heavily temperature dependant) is limited, but unfortunately this limits the power output of the engine, so this technology is often used as a part load operation mode of a, in other aspects, conventional SI engine. One difficulty with lean mixtures are the ignition process itself, it requires improved ignition technology to get as good early flame propagation with lean mixtures as with stoichiometric ones. Turbo charging together with lean mixtures becomes difficult due to lower exhaust gas energy levels, however in large stationary engines with

quite low heat transfer losses, this is a successful technology. The problem to be solved is the ignition process. Wärtsilä NSD uses a prechamber were a stoichiometric mixture is ignited by a spark plug, the burning gas then flows out of the prechamber, into the main combustion chamber through several nozzles, resulting in a very good and secure ignition process of an overall diluted mixture. However, the compression ratio is still limited by knocking combustion.

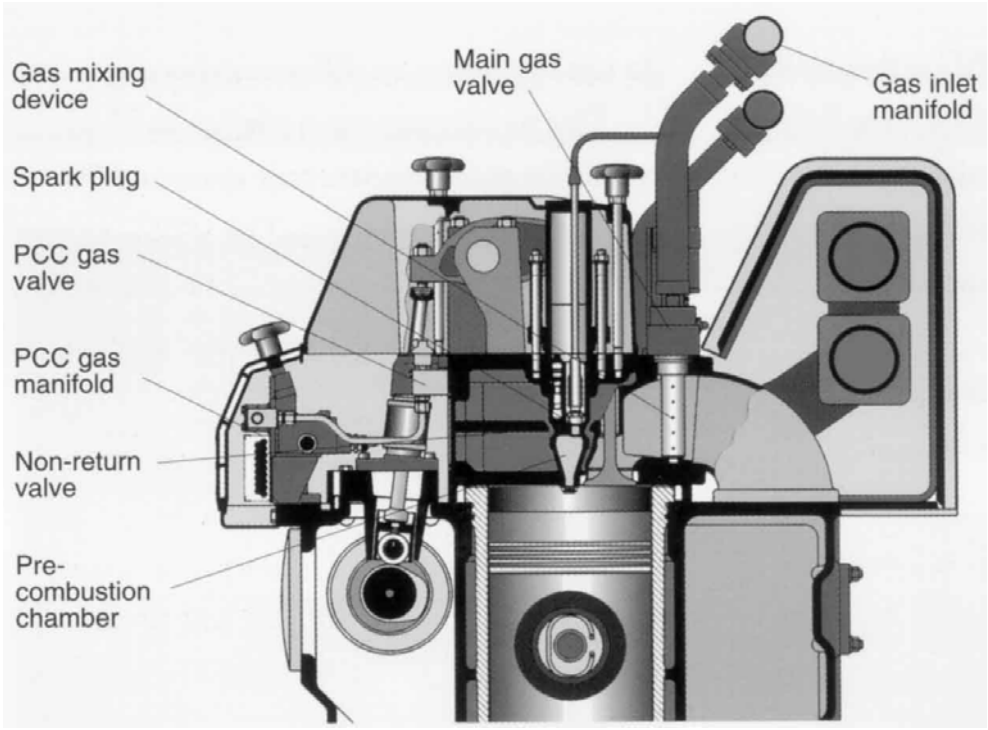

Figure 1 Wärtsilä pre combustion chamber (PCC) spark ignited natural gas engine [1].

Stratified charge SI engines uses direct injection of the fuel towards the spark plug and by using the proper injection timing and duration it is possible (but certainly not trivial) to get a fairly stoichiometric mixture around the spark plug surrounded by pure air. The idea is that load control is achieved by varying the amount of air-fuel mixture around the spark plug, instead of control the total amount of mass inside the cylinder, and this limits the throttle losses. At maximum load, the engine works more or less like a normal SI engine. Unfortunately, it becomes difficult to achieve a perfect homogeneous mixture and the emissions, especially particulates, increase with this technology.

It is the compression ratio of the diesel engine that are the main design factor that give the diesel engine its high efficiency, and it is the diluted homogenous mixtures that give low NOx emissions form the lean burn SI engine. The compression ratio of the latter cannot be increased due to knocking phenomena that destroy the engine. Instead of looking at knocking as a negative phenomenon, it is actually possible to use it as an ignition process and this is the basic idea of Homogeneous Charge Compression Ignition - HCCI. This means an engine without spark plug or direct injection of the fuel, i.e. in its basic configuration, a very simple design. Unfortunately, the ignition process becomes uncontrolled, or to be more specific; there is no parameter that directly controls ignition timing like a spark plug or the injection timing in the diesel engine. Everything is determined when the intake valve closes: Will the temperature and pressure become high enough in order to get auto-ignition and combustion? Will ignition occur at a desired crank angle degree? The advantage is that we will get high efficiency, ultra low NOx emissions and no particulates, because it uses high compression ratios and well-diluted mixtures (leaner mixtures than used in lean burn SI engines).

1.1.4 Fuels for IC engines

The IC engine transforms chemically bonded energy of a combustible fuel into useful mechanical work. As long as the fuel is relatively safe, efficient and convenient to handle, transport and store, the IC engine an excellent choice for automotive applications. Since the IC engine is a compromise between properties the whole engine development becomes very sensitive to fuel accessibility and technology. This has allowed two major IC engine types to evolve: the diesel engines and the gasoline engines. If all combustion engines are considered, the third engine type is the gas turbines; these will not be discussed any further in this thesis but has its most common application in aircrafts due to its superior power density ratio (power-to-weight). Oil drilling, cracking and distilling gives a spectrum of different petroleum products with different combustion characteristics. This fuel refining is obviously adapted to the major markets, the automotive and aeronautical applications, so proper blends of distilled products become suitable for a specific application e.g. gasoline for SI engines. Natural gas is the most economical alternative for stationary applications as long as the access is sufficient and as long as it can be transported in pipelines.

Fuels that are “renewable” start to appear on the market today, which means fuels that do not contribute to a net increase of CO_2 in the atmosphere, unlike coal and oil products (fossil fuels). During rationing in wartimes these were quite widely used, a typical example was gasifiers (gas generators) mounted on European vehicles, during the 2’nd world war, in order to run the cars on wood-chips. Today it is perhaps ethanol mixed into the gasoline that is the most frequent example. Other examples are landfill gas or similar biogases.

1.2 Homogeneous Charge Compression Ignition (HCCI)

1.2.1 The basic principle of the HCCI engine

Homogeneous charge compression ignition (HCCI) uses a lean premixed air-fuel mixture that is compressed with a high compression ratio. During the end of the compression stroke, ignition occurs through self-ignition in the whole combustion chamber at once.

Since the mixture is lean, the maximum temperature, both locally and overall, becomes low compared to other engines, which effectively reduces NO_x formation. However, at richer mixtures the combustion becomes too fast and knocking, or ringing, occurs. Therefore, if a higher load is desired, supercharging, or turbocharging is necessary. The load limit (without supercharging) is said to be either the engine structure capabilities (knocking limit) or NO_x emissions.

The emissions from the HCCI engine are mainly hydrocarbons (HC) caused by incomplete combustion and quenching due to wall effects. HC emissions are in general considered more treatable than NOx emissions. The problem with the HCCI engines is related to the lean mixtures, the fast combustion, and the high compression ratio (high engine efficiency) that causes the exhaust temperature to become quite low. This can make it difficult to get both turbocharging and oxidizing catalysts to work.

1.2.2 HCCI combustion characteristics

The HCCI engine relies on self-ignition of the fuel-air mixture. This means that there is no mechanical or electrical device controlling the exact time of ignition. The condition for ignition to take place is determined the moment the intake valve closes and compression starts. The only factor that could affect the ignition timing somewhat at this point is if the

engine speed would be changing tremendously. In this way the volume – time curve, and hence pressure and temperature trace, prior combustion would be changing and allow shorter/longer time for the chemistry resulting in earlier or later ignition timing.

As mentioned earlier, the HCCI engine uses a high compression ratio; this is generally true but depends on the fuel that we would like to run the engine on. A fuel that easily ignites, like a modern diesel fuel, requires low compression ratio in order to get ignition close to TDC. I fact diesel is a quite poor fuel to run the HCCI engine on because the required compression ratio becomes as low as 7:1. This would mean that we actually would get lower efficiency than in a spark-ignited engine and that is certainly not our goal. The selected fuel should give us an optimum compression ratio of about 15:1 – 17:1, this is a good compromise, if we use higher compression ratio, not only do we increase the mechanical load on the engine, we also increase the area-to-volume ratio and the heat transfer, crevice and blow by losses become more significant. With this high compression ratio and lean mixtures, high octane number fuels like natural gas and gasoline are more adequate. Anyway, some sort of parameter for combustion timing control is required in order to optimize both efficiency and emissions.

The combustion duration at high load operation has shown to be extremely short and it is easy to get knocking combustion, i.e. the combustion produces an oscillating pressure trace after the main combustion, and in general a “pinging” noise outside the engine. This phenomenon is the same as found in spark-ignited engines. The question is what degree of knocking is acceptable from an engine durability point of view. In general, the combustion duration depend on several parameters like fuel, air-fuel ratio, burned gas fraction (EGR), engine speed, compression ratio and several other parameters, but also the degree of homogeneity in terms of e.g. fuel and thermal distribution. Turbulence smoothes out most of these distributions (and it is perhaps in this way turbulence plays its most important role). The turbulence itself is distributed over the combustion chamber.

However, there are better methods to control combustion. It can be done by varying the compression ratio or by using blends of two or several different fuels or additives that affects the ignition timing and combustion duration. A variable compression ratio also makes it possible to run the HCCI-engine on practically any fuel with an acceptable ignition temperature of the air-fuel mixture. CFR-, Atkinson -, Alvar-cycle [2, 3] and variable valve timing is examples of engines and methods used to achieve a variable compression ratio in an engine.

1.2.3 HCCI background – 2 stroke engines

The first published results of using compression ignition of a homogeneous mixture was made by Onishi et. al. [4] at Nippon Clean Engine Research Institute Co. with the Active Thermo Atmosphere Combustion, ATAC concept. The basic idea was to run a 2-stroke engine with lean mixtures during part load operation. At throttled operation, lots of burned gas was trapped inside the cylinder during the scavenging phase. This increased the mean charge temperature to a degree where auto ignition (self ignition) occurred. Since lean mixtures were used, it was possible to use an oxidizing catalyst and hence achieve clean exhaust emissions.

Onishi also provided an ideal model (Figure 2) of the ATAC principle, which became very famous and discussed in many later HCCI and ATAC papers. It explains in a simple way the basic difference between an ATAC and a spark-ignited engine. In a spark-ignited engine, the fuel is burnt in a reaction zone – the flame front, which propagates across the combustion chamber and hence consumes the fuel. This means that there is a clear separation between a burned and an un-burned zone. In the ATAC case all the fuel is consumed simultaneously, but at a lower rate. The fuel is split up into intermediate species during the oxidation process,

which terminates when there is no combustible species left. Onishi also showed that the cycle-to-cycle variations became very small compared to normal spark ignition operation, which improved the overall efficiency of the engine. Detailed studies of the ATAC combustion followed shortly after Onishi's first publications [5-16].

The ATAC technology was adopted in commercial products, first small generators ("NiCE", electrical power of 1 kW) but later Honda Motorcycle Company introduced a similar concept where they adjusted the burned gas fraction with an exhaust port valve. They implemented the technology in small motorcycles and they gave the concept the name Active Radical Combustion [9, 16]. A brief but comprehensive summary of ATAC and HCCI publications is made by A. Hultqvist [17].

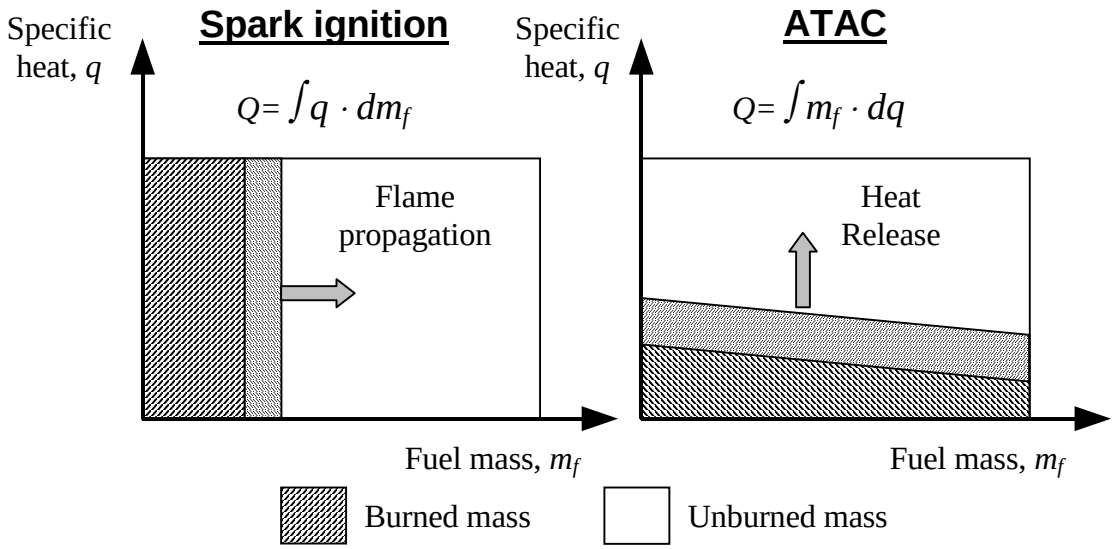

Figure 2 Onischi´s ideal model of spark ignition and ATAC. The area inside the rectangle symbols total amount of heat released, Q.

Another, commercial 2-stroke product, although in every aspect much smaller scale, are engines for model airplanes, often denoted as "diesel" engines by model plane enthusiasts. The more common engine type in these lightweight applications is the glow-plug engine. The major difference between these two engines is that the "diesel" model engine has an adjustable compression ratio, which is set for best performance, and does not have an ignition improvement part i.e. a glow plug or spark plug. These facts imply that these "diesel" engines are some kind of ATAC engines. This type of engine is reported to be more powerful and less noisy compared to the glow plug engine. The fuel blend used for these engines is a mixture of 15% castor oil, 50% paraffin, 33% ether and 2% isopropyl nitrate. The fuel blend varies with model and degree of run-in. Compared to the ATAC 2-stroke engines mentioned earlier these engines probably run with much richer air-fuel mixtures (λ well below 1). Heavy heat transfer and lots of residual gas in these small engines probably gives an acceptable heat release rate and knocking is not a problem. One interesting feature is that it can be cold-started without any preheating of inlet air, fuel or cylinder head.

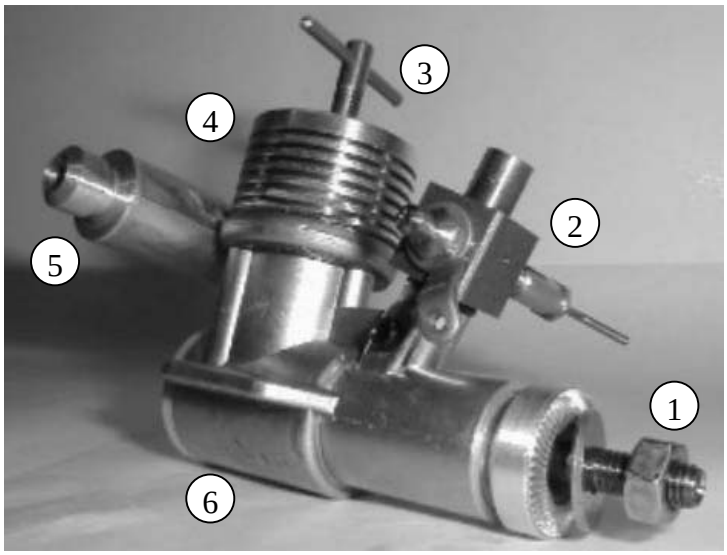

Figure 3 The PAW 09 TBR – R/C engine. Weight: 140g Power: 0.24hp at 19500rpm. 1 – propeller shaft, 2 – carburetor, 3 – compression ratio adjusting screw, 4 – Cylinder, 5 – exhaust pipe, 6 – crankcase [18].

1.2.4 HCCI background – 4 stroke engines

There have been numerous experiments with port injected four-stroke HCCI engines where either diesel engines or so-called CFR engines are rebuilt to work with HCCI combustion [19-93]. Diesel engines are often very robust and they work more or less with the same overall air-fuel mixtures as the HCCI engines do. The fuel injector can also be removed and an ordinary port injector from a SI-engine can be placed in the inlet port. In order to obtain auto ignition temperature and be able to adjust the point of ignition, an inlet air heater is often used. If the inlet air is heated the temperature over the whole engine cycle is elevated. This means that auto ignition temperature is reached earlier in the cycle and thereby combustion is phased earlier. The HCCI engine has proved to have very small cycle-to-cycle variations, although if the combustion is phased very late, unstable or modal behavior may occur. The perhaps most comprehensive HCCI experimental work is made by M. Christensen who has, on one and the same engine, performed a massive parametric study regarding e.g. load, compression ratio, fuel and inlet conditions [94].

Besides a few of the 2-stroke concepts described earlier, the most successful commercial concept is made by Nissan Motor Co. who, through their Modulated Kinetics (MK) system [37, 49], has created something that is quite close to HCCI and with the same advantages. Basically, it's a 4 stroke direct injected diesel engine with quite high compression ratio. The injection timing is retarded and by using EGR, the ignition delay becomes longer. This means that there is longer time for vaporization and mixing. In combination with high swirl gas motion, the premixed part of the combustion increases. EGR and late ignition timing reduces the NOx formation and soot is suppressed by the high fraction of premixed combustion.

1.2.5 Emissions and exhaust gas after treatment

As stated earlier, the NOx emissions are extremely low due to the very lean and homogeneous mixture. The major emissions are unburned hydrocarbons from the fuel and lubricating oil (from cylinder walls and piston ring crevices). The ignition process is temperature sensitive and thus cold spots near the combustion chamber walls can escape combustion, especially at

very low load (high λ-values). In addition, fuel can be trapped in top land crevices[1], and evaporate late in the expansion-, or even during the exhaust stroke. The temperature is then too low for this mixture to ignite or burn completely, which results in UHC emissions. Some CO emissions are also produced from partial burn in regions where combustion rate is reduced due to the expansion.

To completely get rid of the UHC and CO emissions some sort of oxidizing catalyst is required. The temperatures in the exhaust manifold from the HCCI engine is quite low due to several factors:

- High compression ratio – high efficiency
- Fast combustion
- Lean mixtures

This may require more expensive catalyst technology e.g. coatings that have a low activation temperature, or complex regenerative catalyst designs. Very few solutions have been presented to this problem.

1.3 "ATAC in Systems" - project description

1.3.1 The challenge

There are two major problematic concerns to overcome before the HCCI engine is a viable alternative: engine control and specific power. HC emissions are seen upon as a smaller problem because the HCCI engine is constantly running on lean mixtures and that there is oxidizing catalysts that should work if properly sized. Several experimental studies have proved that NOx emissions are ultra-low, if the air-fuel mixture is lean enough.

Engine control is much more than controlling power output on a HCCI engine. The problem is to find a control system for the ignition and combustion itself. This system or method has to be fast in order to cope with transients if the engine is to be used in a vehicle.

Regarding specific power, the traditional way has been supercharging or turbocharging i.e. increasing the inlet air pressure (or density) of the engine and thereby increasing the mass flow through the engine. Since the HCCI-engine has quite high efficiency, the energy left in the exhaust gas is limited and thus it becomes difficult to achieve turbo-charging. However, one can argue that since the HCCI engine has about the same compression ratio and operates with lean mixtures like the diesel engine, it should be possible to successfully turbocharge the HCCI engine as well. The difference is that it is possible to temporarily use richer mixtures in the diesel engine, before there is any boost pressure, resulting in higher exhaust temperature and hence, higher boost pressure. This will not work in a HCCI engine due to too fast combustion resulting in knocking phenomena. In addition, fore some fuels the inlet air temperature has to be slightly higher in the HCCI engine in order to ensure auto ignition, which reduces the mass flow through the engine. Therefore, the turbine will probably have to be smaller on the HCCI engine. Furthermore, the exhaust temperature of the diesel engine becomes higher at higher loads, not only because of the higher amount of fuel injected, but also due to the slower combustion that is limited by the mixing between the fuel-spray and air. At higher loads, the injection duration becomes longer which also delays the combustion,

[1] Crevices formed by the small volume between piston crown and cylinder wall, above the top piston ring.

causing a lower efficiency and a higher exhaust temperature. From a turbocharging point of view, the higher exhaust temperature provided, the more energy is available to be transformed in the turbine, which then gives a higher boost pressure. Supercharging by using a crank driven compressor is not an option if a high efficiency system is wanted. One exception may be as a temporary action in automotive applications, when performance is more important than fuel economy.

The project that includes this study has the goal to find working HCCI engine system solutions and this study provides a tool, or workbench, for that purpose. The primary task for the project is to find a HCCI engine solution to stationary engine applications such as small combined heat and power plants. The purpose of choosing stationary applications as a first step is that the control problems are believed to be smaller since the control system does not have to cope with heavy transients, as is the case in a mobile application.

1.3.2 Goals, limits tools and material

The more descriptive name of this project is: "Homogeneous Charge Compression Ignition of Natural Gas and Biofuel for High Efficiency and Ultralow NOx". The project is funded by the Swedish Energy Agency (former Swedish National Energy Administration, former NUTEK, project number P10025). The goal of this work is to find a cogeneration power plant that utilizes the HCCI principle in order to limit NOx emissions and increasing the efficiency. The first stage in the project started November 1997 with a quite wide goal formulation; the goal was to study:

- Turbocharging/Supercharging
- The influence of pressure gradients on the engine structure
- Exhaust gas composition – FTIR measurements
- Experiments with low expansion, catalyst and turbocharger
- Exhaust gas after treatment (low temperature HC oxidation in catalysts)

Most work was put into the first one, it was decided that the major tool should be simulation and that in-house software should be produced in order to gain knowledge and competence. This decision obviously caused long periods of modeling and programming but allowed a lot of freedom since all the code was accessible. The second goal would probably have required complex FEM methods that can handle not only load, but also vibration and thermal loads. There is no effort made in this field in this project, and to the author's knowledge, very little is made elsewhere. No structural damage is reported in experimental HCCI engines (often rebuilt diesel engines) that can be explained by normal HCCI combustion itself. One or two engines with optical access have experienced cracked or even exploding quartz rings, but this is quite common in optical engines. One engine was exposed to too high peak pressures through stoichiometric mixtures, causing a slight compression of the connecting rods. Other than the connecting rods, there was no structural damage (mechanical adaptive conrod's!).

A small experiment with FTIR was made in order to evaluate the method, it was concluded that the major exhaust HC emission was the fuel itself (in this case isooctane). There were also a wide range other species but it was difficult to get a good quantitative figure if more species (spectra) with individually low concentrations were added to the analysis, the method was abandoned but could perhaps be more suitable if simpler fuels like hydrogen, methane, methanol, or carbon monoxide were studied.

Some experimental efforts were made with several catalysts. Mesh-type catalysts were developed in Lund by Catator AB (former Katator AB) and could be doped with various precious metals. The results were documented in a paper [95] and showed that carbon monoxide was quite simple to handle regardless of coating; however higher amount of platinum nitrate ($PtNO_3$) gave much higher oxidation. It was a little bit more difficult with HC emissions (Figure 4). By adding some ceria or stannic oxide (CeO_2 or SnO_2) some gain could be seen, although there were some variations between the different experiments, e.g. the amount of HC emissions upstream catalyst; the conclusions were not that precise. Anyway, it seemed like if the catalyst were properly sized it would be possible to reduce the CO and HC emissions to acceptable levels.

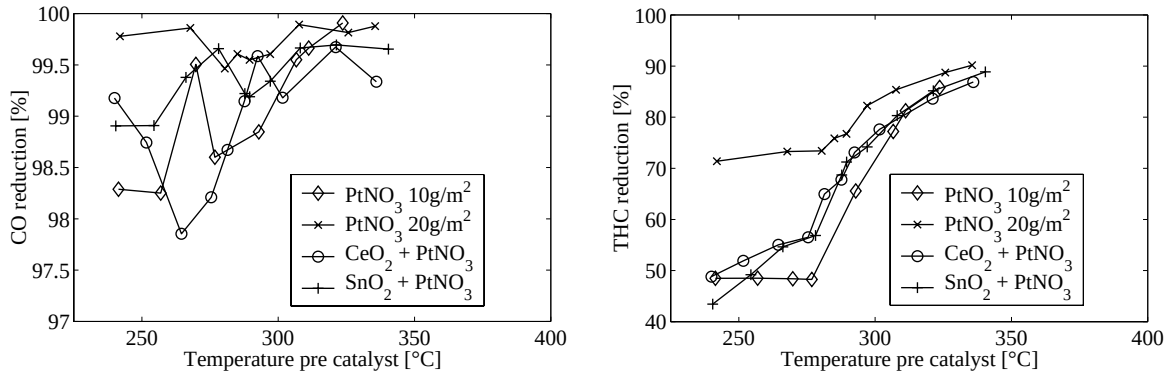

Figure 4 Reduction in CO (left) and THC (right) emissions for various catalyst coatings

The second stage in the project started April 1999 and this time the goal was more explicit into three part goals: 1 – further develop the simulation software, 2 – show a full scale HCCI engine system and 3 – make new experiments with catalysts. The funding was however quite limited which limited all experimental efforts within the project alone. A new project started with separate funding and with a new Ph. D. student. A 6-cylinder diesel engine was converted to HCCI by adding a dual-fuel port injection system. Varying the fuel mixture of n-heptane and isooctane i.e. the RON number of the fuel controlled the ignition timing. Cooperation resulted in a joint paper [68] and this fulfilled the second part goal. There were however very little boost pressure and thus the engine load was quite small. In addition, valuable validation was made of the software. The engine was fitted with its diesel size turbocharger. Later, smaller turbines were tested with promising results. The results with the catalysts described above were also published during this stage. Discussions were made with catalyst developers about a regenerative catalyst design but it felt like it was a little bit too early to start the development of full-scale catalysts at this time.

During the third stage, which started November 2000 the simulation software was fitted with a chemical kinetics part that provided a prediction of the ignition timing. This is quite demanding calculations that were not that suitable to use in direct combination with full system simulations. Instead, cycle simulations were used to find proper control strategies (fuel composition, inlet temperature or compression ratio) depending on engine speed, inlet and exhaust conditions and air-fuel ratio. Then system simulation was then performed with a fixed heat release function and the previously determined control model. Another part goal was still to do experiments with catalysts but this felt again too early i.e. there were no bright ideas on how to overcome the problem more than making a sufficiently large catalyst. The funds were also quite limited and therefore catalysts experiments were considered a less prioritized area at that time. Other part goals were simulations with exhaust gas recirculation (EGR) and variable compression ratio (VCR). EGR has an effect of dilution and can be used to decrease the air-fuel ratio for the same amount of fuel (heat) input. This reduces the heat release rate

during the combustion and hence suppresses knocking combustion. However, the ignition temperature increases with EGR and higher inlet temperature reduce the mass flow through the engine. In spark ignition and diesel engines EGR usually decreases the NOx formation. In the HCCI engine the required higher inlet temperature balances this effect, however the NOx levels are overall ultra low in comparison with SI and diesel engines.

1.4 Engine related definitions

In order to make discoveries and results understandable for others it is important to use the same language and terminology, especially in the field of combustion engine that is very broad. In order to reduce the risk of being misinterpreted, some important properties and relations are shown. A Sankey diagram illustrating the definitions and the energy flow of an arbitrary engine is seen in Figure 5.

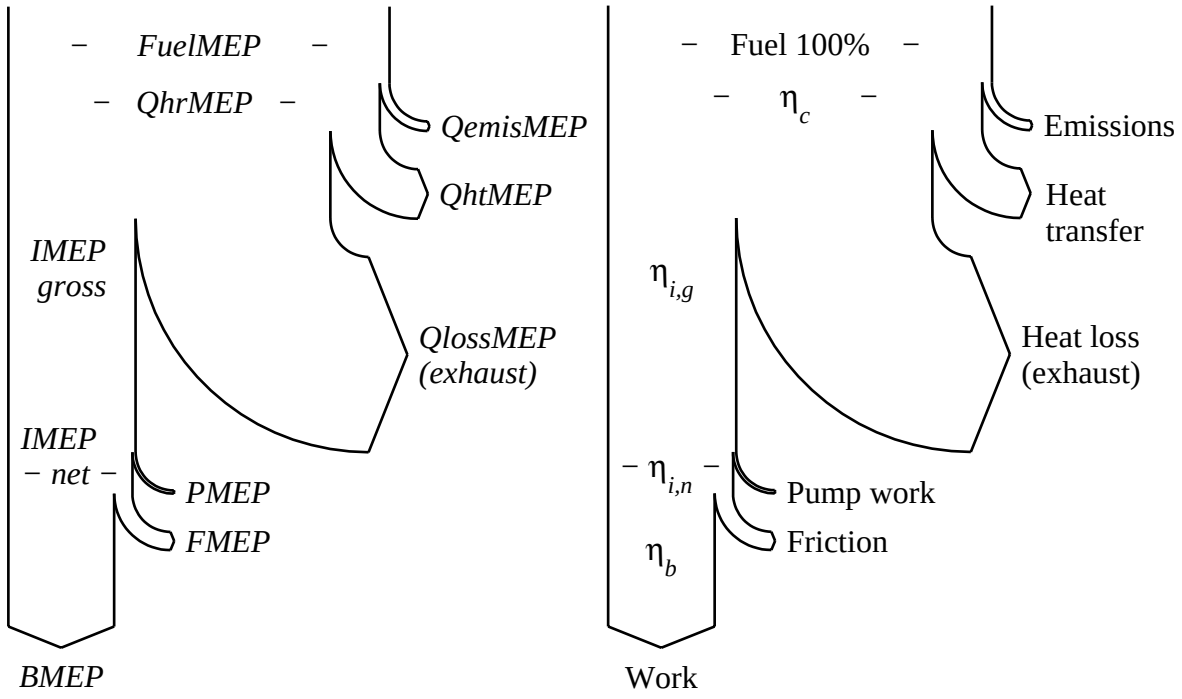

Figure 5 Sankey graph illustrating the energy flow of an engine, in this case a naturally aspirated, spark ignited, car-size engine running at 3500 rpm at WOT conditions, selected to give significant pumping and friction. Mean effective pressure representation to the left and efficiency representation to the right.

1.4.1 Performance

Starting at the end, the performance of an engine is in general described by the maximum brake[2] output power of an engine. This power, P_b [W] is the product of speed, n [rpm] and torque, T_b [Nm] on the outgoing shaft and can be expressed as:

$$P_b = \frac{2\pi \cdot n}{60} \cdot T_b \qquad \text{Eq.1}$$

[2] The word "brake" refers to the usual way to determine the performance of an engine; connect it to a dynamometer and brake the engine to a desired torque (load) and speed.

In general, it is sometimes necessary to compare, or to normalize, with the respect to the size of the engine in order to make relevant comparisons between different engines and this is usually done by looking at what *Brake Mean Effective Pressure*, *BMEP* [Pa], is delivered by the engine. This is a ratio between the delivered torque and the displaced volume, V_d [m^3] of the engine. In addition, the number of revolutions per power strokes is considered in order to make it possible to compare 2-stroke (n_R = {revolutions per cycle} = 1) and 4-stroke engines (n_R = 2). Another way to look at it is that it is the delivered work per cycle and displaced volume [96].

$$BMEP = \frac{2\pi \cdot n_R \cdot T_b}{V_d} = \frac{60 \cdot n_R \cdot P_b}{n \cdot V_d} \qquad \text{Eq.2}$$

The engine is an apparatus that transforms energy and the transformation can be separated into different steps, each represented by a mean effective pressure. The difference between the steps of this transformation may often be considered as losses (or gains) and can be expressed as differences in mean effective pressures. Into the engine flows the energy carrier – the fuel. The fuel flow rate introduces a certain amount of fuel per cycle, m_f [kg]. Fuel corresponds to a certain amount of energy through the heating value of the fuel, Q_{LHV} [J/kg]. This means that we can express this fuel flow as a delivered energy per cycle, *Fuel Mean Effective Pressure*, *FuelMEP* defined as:

$$FuelMEP = \frac{m_f \cdot Q_{LHV}}{V_d} \qquad \text{Eq.3}$$

Note that the lower heating value (LHV) of the fuel is used, normally any condensation of the water content is difficult to implement in combustion engines. The lower heating value corresponds to the maximum possible heat released per mass fuel during combustion if combustion is allowed to go to completion. The energy carried by fuel is released through combustion inside the cylinder, at least some of it, depending on how effective the combustion process is. This means that the amount of energy that is released, Q_{hr}, may not be as much as the amount that was carried by the fuel. The amount of energy released may be expressed as a *Heat Release (Qhr) Mean Effective Pressure*, *QhrMEP* defined as:

$$QhrMEP = \frac{Q_{hr}}{V_d} = \frac{\oint_{cycle} dQ_{hr}}{V_d} \qquad \text{Eq.4}$$

The difference between *FuelMEP* and *QhrMEP* corresponds to energy that is chemically bonded to unburned components like hydrocarbons and carbon monoxide or any other species (e.g. NO, NO_2, H_2, H_2O_2, ...) that is an undesired product of combustion and that "steals" energy by escaping out of the engine with the exhaust gases or into the crank case. We can interpret this as an *Emission (Qemis) Mean Effective Pressure*, *QemisMEP*:

$$QemisMEP = FuelMEP - QhrMEP \qquad \text{Eq.5}$$

The released energy, or heat, then increases the temperature and pressure during combustion and, thanks to the cyclic operating principle of the engine, mechanical work can be extracted by the moving piston. The energy that is transformed into work per cycle is called indicated work, W_c , and an *Indicated Mean Effective Pressure*, *IMEP*, can be calculated. In 4-stroke engines, it is sometimes convenient to separate this work into $IMEP_{net}$ and $IMEP_{gross}$ depending on the gas exchange, is considered or not.

The definitions are:

$$IMEP_{net} = \frac{W_c}{V_d} = \frac{\oint_{cycle} p \cdot dV}{V_d}$$

$$IMEP_{gross} = \frac{\int_{V(180°)}^{V(540°)} p \cdot dV}{V_d} \qquad \text{Eq.6}$$

360° ⇔ TDC combustion

The released energy that that is not transformed into work, is partly transferred to the cylinder walls by the temperature difference between the gas and the walls and some escape with the exhaust gas; exhaust temperatures are significantly higher than the intake temperatures of the engine. *Heat Transfer-*, *QhtMEP*, and the *Heat Loss Mean Effective Pressures*, *QlossMEP*, can be calculated as:

$$QhtMEP = \frac{Q_{ht}}{V_d} = \frac{\oint_{cycle} dQ_{ht}}{V_d} \qquad \text{Eq.7}$$

$$QlossMEP = QhrMEP - IMEP_{gross} - QhtMEP$$

An internal combustion engine is partly an open system, it breathes fuel, air and burned exhaust gases. The breathing part of the process is difficult to do totally without work input since the valves and other inlet and exhaust devices are restrictions in some sense. To force a mass flow through these devices requires pumping work. In engines, this pumping work, *Pump Mean Effective Pressure*, *PMEP*, is defined as the difference between the gross and net indicated mean effective pressure:

$$PMEP = IMEP_{gross} - IMEP_{net} \qquad \text{Eq.8}$$

The internal combustion engine consists of several moving parts. They are very well lubricated but not totally frictionless, so some mechanical work has to be used to keep them moving. This work can be expressed as a *Friction Mean Effective Pressure*, *FMEP*, and is defined as the difference between indicated and brake mean effective pressures:

$$FMEP = IMEP_{net} - BMEP \qquad \text{Eq.9}$$

With this final definition, the whole chain from fuel input to shaft output is covered and the engine can be thermodynamically analyzed by looking at these factors.

1.4.2 Efficiency

Using the previously defined mean effective pressures it is possible to normalize one more step by using the *FuelMEP* as reference, and by doing so, several efficiencies are easily defined. To start with, the combustion efficiency, η_c , that simply state how much of the energy in the fuel is converted into heat during the combustion:

$$\eta_c = \frac{QhrMEP}{FuelMEP} = \frac{\oint_{cycle} dQ_{hr}}{V_d} \cdot \frac{V_d}{m_f \cdot Q_{LHV}} = \frac{\oint_{cycle} dQ_{hr}}{m_f \cdot Q_{LHV}} \qquad \text{Eq.10}$$

Two different indicated efficiencies could be defined based on $IMEP_{net}$ and $IMEP_{gross}$ respectively. The next step is incorporates the basic cycle and in the same way as there are two different IMEP, two indicated efficiencies, net – whole cycle, and gross – compression and expansion, are defined as:

$$\eta_{i,n} = \frac{IMEP_{net}}{FuelMEP} = \frac{\oint_{cycle} p \cdot dV}{m_f \cdot Q_{LHV}}$$

$$\eta_{i,g} = \frac{IMEP_{gross}}{FuelMEP} = \frac{\int_{V(180°)}^{V(540°)} p \cdot dV}{m_f \cdot Q_{LHV}} \qquad \text{Eq.11}$$

And the more interesting brake efficiency that includes the frictional loss is simply calculated through either the mean effective pressures, or in the more common way from experimental data; from power output and fuel flow:

$$\eta_b = \frac{BMEP}{FuelMEP} = \frac{2\pi \cdot n_R \cdot T_b}{m_f \cdot Q_{LHV}} = \frac{60 \cdot n_R \cdot P_b}{n \cdot m_f \cdot Q_{LHV}} = \frac{P_b}{\dot{m}_f \cdot Q_{LHV}} \qquad \text{Eq.12}$$

Sometimes it is interesting to only look at the thermal process and not include combustion. Then the reference is changed from being the heat equivalent of the fuel to the actual released heat instead, and thermal conversion efficiency can be calculated as:

$$\eta_{Th.} = \frac{IMEP_{Gross}}{QhrMEP} = \frac{\int_{V(180°)}^{V(540°)} p \cdot dV}{\oint_{cycle} dQ_{hr}} = \frac{\eta_{i,g}}{\eta_c} \qquad \text{Eq.13}$$

The gas exchange process also has some degree of efficiency, the gas exchange efficiency, and it is simply the ratio between the indicated net and gross mean effective pressures, or indicated efficiencies:

$$\eta_{G.e.} = \frac{IMEP_{net}}{IMEP_{gross}} = 1 - \frac{PMEP}{IMEP_{gross}} = \frac{\eta_{i,n}}{\eta_{i,g}} \qquad \text{Eq.14}$$

The mechanics of transforming the piston motion to shaft rotation has mechanical efficiency, which is the ratio of work leaving the engine shaft and work delivered to the pistons:

$$\eta_{M.e.} = \frac{BMEP}{IMEP_{net}} = 1 - \frac{FMEP}{IMEP_{net}} = \frac{\eta_b}{\eta_{i,n}} \qquad \text{Eq.15}$$

The brake efficiency can now also be calculated as a product of several part efficiencies, each representing the efficiency of an essential step of energy transformation in the IC engine:

$$\eta_b = \eta_c \cdot \eta_{Th.} \cdot \eta_{G.e.} \cdot \eta_{M.e.} \qquad \text{Eq.16}$$

2 The tool - ESIM

2.1 Engine simulations

Engine calculations along with experimental activities have been performed ever since the beginning of the internal combustion engine era. The first man to actually use a thermodynamic approach to study heat engines was Rudolf Diesel [97]. There are often several reasons behind a theoretical approach and some of them can be connected to terms like dimensioning of engine mechanics, system behavior, performance studies or understanding of in-cylinder processes.

There exist several different levels of simulation, some includes both turbulence and chemistry calculations of the in-cylinder gas, whereas others only treat the engine as a black box with some inputs and outputs.

The program package that is developed here is primarily for thermodynamical system analyses and performance studies. “System” refers to the engine and surrounding components like manifolds, turbocharger, intercooler etc.

2.2 The ESIM package

2.2.1 Description

The Engine SIMulation (ESIM) software package is written in MATLAB© and consists of several functions that correspond to a certain engine system components. These different components are linked together by state, mass and energy conservation equations. The engine part is a zero-dimensional, one-zone model that considers heat transfer and mass-flow calculations over the valves. This section focuses on describing the different models and how to connect them, building an entire engine system, e.g. a turbocharged HCCI engine.

2.2.2 Limitations

The engine part handle only thermodynamics, i.e. there are no mechanical calculations regarding e.g. friction losses. That means that result as mean effective pressure and efficiency is shown as *indicated*, i.e. based on the in-cylinder gas calculations only. Various friction models often use the indicated mean effective pressure, *IMEP* and engine speed to determine friction mean effective pressure, *FMEP*. Then a simulated brake mean effective pressure, $BMEP_{sim}$ can be calculated and hence brake power, $P_{b,\,sim}$.

The program is not fully dynamical i.e. it cannot fully handle transients. However, it can cope with changes in the operating situation if these are not to swift. The potential and kinetic part of the total energy is somewhat neglected yet commented on in this report when necessary.

At first the combustion is treated empirically through a simple model i.e. there are no calculations of the chemical reactions. The heat release is described by a shape function; the level is determined by the amount of fuel present and a combustion efficiency factor. As an

alternative, an external chemical kinetic program can be linked to the engine module that provides an estimation of ignition timing.

When linking the different system components, mean values are used i.e. mass flow into and out of the engine is averaged when linked to the manifolds. The process itself, flow over intake or exhaust valves, works with a varying in-cylinder pressure and a constant manifold pressure. Flow is allowed ”backwards” over the valves and regarding the inlet valve this process is assumed to work as a plug flow process i.e. mixing does not occur between the back-flowing gas and the inlet manifold gas.

2.3 General assumptions

In order to limit some calculations and computational time there has to be some simplifications. Therefore it is important as user to know what the limitations are and when they have to be compensated for.

2.3.1 Ideal-gas equation of state

All gases are assumed to be ideal i.e. the *ideal-gas law,* or the ideal-gas *equation of state,* are assumed to be valid:

$$p \cdot V = n \cdot R \cdot T \qquad \text{Eq.17}$$

The universal gas constant is set to 8.3145 J/(mol·K) [98]. For a gas mixture the law becomes:

$$p \cdot V = \sum_{i=1}^{N} (n_i) \cdot R \cdot T \qquad \text{Eq.18}$$

This means that there are no mixing effects accounted for.

In order to show the validity of this law for engine applications the following simple analysis is done. Among different gases there are some that does not behave as an ideal gas. The usual way to describe this is to modify the right hand side of the ideal gas law, Eq.17 by multiply with a *compressibility factor*, *Z* that depends on both pressure and temperature.

$$p \cdot V = Z(p,T) \cdot n \cdot R \cdot T \qquad \text{Eq.19}$$

However, it is shown that the Z factor is approximately same at the same reduced temperature and pressure, defined by Eq.20, for different pure species.

$$p_r = \frac{p}{p_{cr}} \qquad T_r = \frac{T}{T_{cr}} \qquad \text{Eq.20}$$

p_{cr} and T_{cr} is the critical pressure and temperature, specific for different substances. The relation between reduced states and Z is e.g. given in the Nelson-Obert generalized compressibility charts [reviewed in 99] and some examples are shown in Table 1. It has been shown that very low pressure ($p_r << 1$, regardless of temperature) and at high temperature ($T_r > 2$) the gases can be treated as ideal gases with good accuracy. The error becomes larger close to the critical point. Gas mixtures of real gases are a little more complicated due to the influence of dissimilar molecules. In combustion engines the state are usually close to normal atmosphere in the inlet manifold and during the compression stroke both pressure and temperature increases. Higher pressure results in an increasing compressibility factor but this is balanced to some extent by the increasing temperature. During combustion, expansion and exhaust stroke, the temperature is high and the gas can be treated as ideal. Liquid fuel, or fuel

that undergoes vaporization is definitely not an ideal gas and situations were vapor is present, e.g. fuel or water injection must be treated a little bit careful. So the conclusion is that in an engine the gas can be treated as ideal without any larger error. In addition, most of the working gas is nitrogen, which is a gas that is very close to ideal gas in all states, this also give a high accuracy. In this study all gases are treated as ideal gases and equation Eq.17 and Eq.18 are assumed valid. However, this assumption requires that the mixture be well known which maybe difficult in some cases. At high temperatures, species can dissociate, affecting number of moles and mixture composition, a phenomena that is not treated here unless chemical kinetics is involved.

Table 1 Examples of compressibility factors, Z for some gases at engine related pressures and temperatures. The table is based on generalized compressibility chart readouts.

Gas	T[K]	p[bar]	T[K]	p[bar]	T[K]	p[bar]	T[K]	p[bar]
	300	1	700	50	1000	100	2500	250
	Z		Z		Z		Z	
N2	1,00		1,02		1,04		1,02	
O2	1,00		1,01		1,02		1,01	
Ar	1,00		1,02		1,03		1,02	
CO2	1,00		0,99		1,01		1,01	
H2O	n.a.		0,93		0,97		1,01	
CH4	1,00		1,02		1,03		1,02	
C2H6	1,00		1,00		1,03		1,02	
C3H8	0,99		0,95		1,01		1,04	

2.3.2 Thermal and physical gas properties

Thermal and physical properties for pure substances have been taken from the NASA-polynomials [98][3]. It provides a compact way to calculate gas properties for different species at different states. The data are a large set of polynomial coefficients. For some compounds of substance such as ”gasoline” or ”diesel", there exist no polynomials. In those cases it is easiest to either assume that they have the same properties as similar pure substance, or set up a polynomial set that are equal to a constant specific heat i.e. enthalpy becomes a straight line. The errors will probably be small in engine calculations since the fuel fraction of most fuel-air mixtures is quite small.

The species that are treated in this study is Nitrogen (N2), Oxygen (O2), Argon (Ar), Carbon dioxide (CO2), Water vapor (H2O) and Fuel. Fuel is treated here as single specie regardless of what it is. For example, gasoline is treated as a ”synthetic” fuel $C_{7.76}H_{13.1}$, diesel as $C_{10.8}H_{18.7}$ and natural gas is set up depending on its individual mole fractions, of typically methane, ethane, propane and so on. Thermal properties for fuels like gasoline and diesel is taken from data reviewed by Heywood [96], although converted to NASA-polynomials. Thermo physical properties for gasoline and diesel vapor is missing completely but since viscosity and conductivity is only needed in the exhaust gas, were fuel is only present as a very small unburned fraction, viscosity and conductivity properties for butane was used instead.

[3] Another very useful source for this type of data (and more) is the NIST Chemistry WebBook, http://webbook.nist.gov/chemistry/.

The easiest way to display how this data is stored and handled is by an example. For nitrogen (N2) the coefficients for thermal properties are shown in Figure 6.

```
N2                J 3/77N   20   00   00   0G   300.000  5000.000              1
 0.28532899E+01 0.16022128E-02-0.62936893E-06 0.11441022E-09-0.78057465E-14    2
-0.89008093E+03 0.63964897E+01 0.37044177E+01-0.14218753E-02 0.28670392E-05    3
-0.12028885E-08-0.13954677E-13-0.10640795E+04 0.22336285E+01                   4
```

Figure 6 Example of a set of polynomial coefficients for calculating thermodynamic properties, in this case for nitrogen, N2.

The first line contains various information e.g. name, reference and valid temperatures (between 300 and 5000K). Then there are 14 coefficients, first 7 high- (>1000K) and then 7 low temperature coefficients. Seven coefficients c_1–c_7, either the high temperature or the low temperature set, is then used to calculate heat capacity (*Cp*), enthalpy (h^0) and entropy (s^0) [4]:

$$\begin{aligned} C_p(T) &= R\cdot\left(c_1 + c_2T + c_3T^2 + c_4T^3 + c_5T^4\right) && \left[\mathrm{J/(mol\cdot K)}\right] \\ h^0(T) &= R\cdot\left(c_1T + c_2\frac{T^2}{2} + c_3\frac{T^3}{3} + c_4\frac{T^4}{4} + c_5\frac{T^5}{5} + c_6\right) && \left[\mathrm{J/mol}\right] \\ s^0(T) &= R\cdot\left(c_1\cdot\ln(T) + c_2T + c_3\frac{T^2}{2} + c_4\frac{T^3}{3} + c_5\frac{T^4}{4} + c_7\right) && \left[\mathrm{J/(mol\cdot K)}\right] \end{aligned} \qquad \text{Eq.21}$$

Now it is very important to point out that enthalpy calculated from the expression above is calculated at a reference state at 298.15 K and includes enthalpy of formation, for liquids the vaporization heat is also included. This means that enthalpy above is written as:

$$h^0_{f,298}(T) = \left(\bar{h}^0(T) - \bar{h}^0_{298}\right) + \Delta\bar{h}^0_{f,298} + \Delta\bar{h}^0_{vap,298} \qquad \left[\mathrm{J/mol}\right] \qquad \text{Eq.22}$$

When calculating chemical reactions it is very convenient to have the formation enthalpy included because heat from combustion will be added directly following the specie concentration. However, if there are species present like gasoline or diesel, where polynomials like those above is missing but the heating value is known, then it is easier to ignore the formation enthalpy, as shown in equation Eq.23, and instead add energy as heat during combustion. This approach is used mostly in this study.

$$h^0_{298}(T) = h^0_{f,298}(T) - h^0_{f,298}(298) = \left(\bar{h}^0(T) - \bar{h}^0_{298}\right) \quad \left[\mathrm{J/mol}\right] \qquad \text{Eq.23}$$

The reverse calculation, from enthalpy to temperature becomes also important. Several numerical methods are possible but here is the well-known Newton-Rhapson method chosen manly because in this case it becomes simple since the needed derivative of enthalpy, is the same as specific heat and the enthalpy - temperature relation is monotonically increasing for most species. The iterative process of the Newton-Rhapson can thereby be written as:

$$T_{k+1} = T_k - \frac{h^0_{298}(T_k) - h^0_{298}}{C_p(T_k)} \qquad [\mathrm{K}] \qquad \text{Eq.24}$$

[4] Note: Notation of the coefficients and the polynomials is different here than in the original reference, hopefully this notation is a little bit simpler to grasp.

The reference state for entropy is at 0K and 1bar in order to only having to ”table” a function of temperature only. Entropy change for an arbitrary process is then calculated as:

$$\Delta s = \left(s_2 - s_1\right) = \left(s_2^0 - s_1^0\right) - R \cdot \ln\left(\frac{p_2}{p_1}\right) \qquad \left[\mathrm{J}/\left(\mathrm{mol}\cdot\mathrm{K}\right)\right] \qquad \text{Eq.25}$$

In analogy with the ideal gas law, it is assumed that there are no mixing effects and specific heat, enthalpy and entropy for the mixture is calculated with respect of the property of each individual species and their mole fractions e.g. enthalpy for a mixture is calculated as:

$$\begin{aligned} h_{mix}\left(T\right) &= \sum_{i=1}^{N} h_i\left(T\right)\cdot y_i \qquad [J/mol] \quad \text{or} \\ H_{mix}\left(T\right) &= \sum_{i=1}^{N} h_i\left(T\right)\cdot n_i \qquad [J] \end{aligned} \qquad \text{Eq.26}$$

Mole fraction, y_i is calculated as:

$$y_i = \frac{n_i}{\sum_{k=1}^{N} n_k} \qquad \text{Eq.27}$$

Viscosity and thermal conductivity for pure substances are taken from the same source as the thermodynamical data [98]. An example is shown Figure 7.

```
N2                                V2C2  GORDON; NASA TM86885, OCT 1984
 V  300.000 1000.000 0.60443938E 00-0.43632704E 02-0.88441949E 03 0.18972150E 01
 V 1000.000 5000.000 0.65060585E 00 0.28517449E 02-0.16690236E 05 0.15223271E 01
 C  300.000 1000.000 0.94306384E 00 0.12279898E 03-0.11839435E 05-0.10668773E 00
 C 1000.000 5000.000 0.65147781E 00-0.15059801E 03-0.13746760E 05 0.21801632E 01
```

Figure 7 Thermophysical coefficients for nitrogen, N2.

The first line contains the substance name, phase and some reference data. Then there are four lines that start with a ”V”, for viscosity, or a ”C”, for conductivity. The two first values in each of these rows are the temperature boundary, which the coefficients are valid. The following four values are the coefficients, A–D for the specific property and temperature interval. Viscosity and conductivity is then calculated as:

$$\begin{aligned} &\text{Viscosity:} \quad \eta\left(T\right) = \exp\left(A_V \cdot \ln\left(T\right) + \frac{B_V}{T} + \frac{C_V}{T^2} + D_V\right) \quad [\mu\mathrm{P}] \\ &\text{Conductivity:} \quad \lambda\left(T\right) = \exp\left(A_C \cdot \ln\left(T\right) + \frac{B_C}{T} + \frac{C_C}{T^2} + D_C\right) \quad [\mu\mathrm{W}/\mathrm{cm}\cdot\mathrm{K}] \end{aligned} \qquad \text{Eq.28}$$

Note that viscosity given by Eq.28 is the so-called *dynamical viscosity*[5], which is temperature dependent only. *Kinematical viscosity* is calculated as:

$$\upsilon\left(T,p\right) = \frac{\eta\left(T\right)}{\rho\left(T,p\right)} \qquad \text{Eq.29}$$

[5] Note: In some literature, μ is used as symbol for dynamical viscosity, instead of η.

Now, viscosity and conductivity calculated from Eq.28 gives properties for pure substances. When mixing substances it is not as simple as with thermodynamical properties. Several approximate methods exist for mixture calculations and the one is chosen for this work is derived from Brokaw (1961), as reviewed by Ferguson [101]. This method is briefly reviewed here.

Thermal conductivity in pure species is split into a translational- and internal transport of energy:

$$\lambda_i = \lambda_i' + \lambda'' \qquad \text{Eq.30}$$

The internal contribution, λ'' is approximately given by:

$$\lambda_i'' \approx 0.88\left(\frac{2}{5}\frac{C_{p,i}}{R} - 1\right)\lambda_i' \qquad \text{Eq.31}$$

Equation Eq.30 and Eq.31 gives:

$$\begin{cases} \lambda_i' \approx \lambda_i \Big/ \left(1 + 0.88\left(\frac{2}{5}\frac{C_{p,i}}{R} - 1\right)\right) \\ \lambda_i'' \approx \lambda_i - \lambda_i' \end{cases} \qquad \text{Eq.32}$$

Now, the two parts is calculated for the mixture:

$$\begin{cases} \lambda_{mix}{}' \approx \sum_{i=1}^{N} \dfrac{\lambda_i'}{1 + \sum\limits_{\substack{j=1 \\ j\neq i}}^{N} \Psi_{i,j} \dfrac{y_j}{y_i}} \\ \lambda_{mix}{}'' \approx \sum_{i=1}^{N} \dfrac{\lambda_i''}{1 + \sum\limits_{\substack{j=1 \\ j\neq i}}^{N} \Phi_{i,j} \dfrac{y_j}{y_i}} \end{cases} \qquad \text{Eq.33}$$

where *y* denotes mole fraction and:

$$\begin{cases} \Phi_{i,j} = \dfrac{\left[1 + \left(\dfrac{\eta_i}{\eta_j}\right)^{1/2}\left(\dfrac{M_j}{M_i}\right)^{1/4}\right]}{2\sqrt{2}\left(1 + \dfrac{M_i}{M_j}\right)^{1/2}} \\ \Psi_{i,j} = \Phi_{i,j}\left[1 + 2.41\dfrac{\left(M_i - M_j\right)\left(M_i - 0.142M_j\right)}{\left(M_i + M_j\right)^2}\right] \end{cases} \qquad \text{Eq.34}$$

The conductivity for the mixture is then calculated as:

$$\begin{aligned} \lambda_{mix} &= \lambda_{mix}' + \lambda_{mix}'' && \text{Non reacting media} \\ \lambda_{mix} &= \left(\lambda_{mix}' + \lambda_{mix}''\right)\frac{C_p}{C_{p,\,frozen}} && \text{Reacting media} \end{aligned} \qquad \text{Eq.35}$$

In this study, all calculus that needs conductivity is using the first expression in Eq.35 e.g., heat transfer calculations in exhaust port and manifold are assumed to be under non-reacting conditions. Viscosity for mixtures is calculated trough:

$$\eta_{mix} \approx \sum_{i=1}^{N} \frac{\eta_i}{1 + \sum_{\substack{j=1 \\ j \neq i}}^{N} \Phi_{i,j} \frac{y_j}{y_i}} \qquad \text{Eq.36}$$

with $\Phi_{i,j}$ given by Eq.34.

2.3.3 Energy relations

One fundamental relation in this study is the *first law of thermodynamics* for an open system (Eq.37), which is based on the *conservation of energy* principle of a control volume, as illustrated in Figure 8.

$$Q - W + \sum E_{IN} + \sum E_{OUT} = E_2 - E_1 = \Delta E_{CV} \qquad \text{Eq.37}$$

Q is heat transferred to the system (or control volume, CV), W is work done by the system, E_{IN} and E_{OUT} is energy related to mass flowing into and out of the system respectively, *E2 - E1* is the change of energy in the control volume.

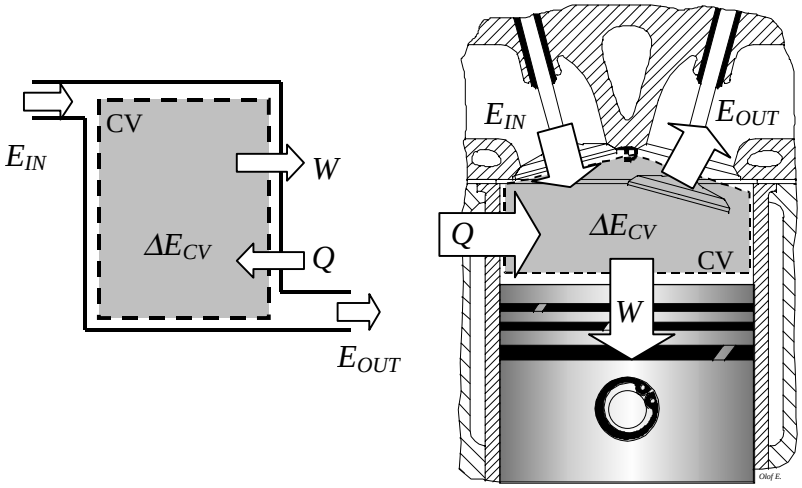

Figure 8 Left: Energy flow in and out of a system. Right: Engine interpretation.

The total energy, E in the system can be written as a sum of internal, potential and kinetic energy:

$$E = U + PE + KE \qquad \text{Eq.38}$$

Assuming potential and kinetic energy very small and insignificant (gas has usually a quite low density), the total energy difference in the control volume will essentially be the same as difference in internal energy. Consider small changes and assume that the flow can be described uniform. Now, this assumption may be a limitation but normally, when solving the following equations, these are usually made over small time-steps over which the properties of the fluids may me treated uniform, or averaged, without any large errors. For a short time-step and with the assumptions mentioned above, we get:

$$\partial Q - \partial W + \sum \partial n_{IN} \cdot e_{IN} + \sum \partial n_{OUT} \cdot e_{OUT} = U_2 - U_1 \qquad \text{Eq.39}$$

For a flowing fluid, the *flow work* has to be considered (which can be seen upon as a part of potential energy) when the flowing media is passing the control volume boundaries:

$$E = U + p \cdot V \quad (+KE + PE) \quad \text{or}$$
$$e = u + p \cdot v \quad \text{on mass-unit basis} \qquad \text{Eq.40}$$

It is very convenient to introduce enthalpy into the calculations for three reasons: Enthalpy depends on temperature only (see section), gas properties are given in enthalpy and the definition includes the $p \cdot v$ term:

$$H = U + p \cdot V \quad \text{or}$$
$$h = u + p \cdot v \qquad \text{Eq.41}$$

The change in heat is governed by heat transfer models e.g. heat transfer between in-cylinder gas and inner cylinder surface, the combustion is also seen upon as heat transferred to the system as mentioned earlier. The definition is set so that positive ∂Q means heat transferred to the control volume. Work is boundary work, and positive values on ∂W means work is done by the media in the control volume. In addition, mass transfer, e.g. valve flow, is governed by models also which also depends on various state variables.

$$\partial Q = \partial Q(T, p, \ldots)$$
$$\partial W = p \cdot \partial V \qquad \text{Eq.42}$$

Inserted in Eq.39 we get:

$$\partial Q(T, p, \ldots) - p\partial V + \sum \partial n_{IN} \cdot h_{IN} + \sum \partial n_{OUT} \cdot h_{OUT} =$$
$$\left(H(T_2) - p_2 V_2\right) - \left(H(T_1) - p_1 V_1\right) \qquad \text{Eq.43}$$

This is an ordinary differential equation and it is, like most other large, differential equations, quite often impossible to solve analytically, numerical solutions seem more appropriate.

2.3.4 Numerical solutions

There exist many different methods for solving ordinary differential equations. Although it would be appropriate, there has not been any room in this study to test and select an optimum method. Instead, one has been selected that works and is quite simple to handle and understand. It is called *trapezoid method* and can simply be described as an integrating method where states are represented by their mean values over a time-step.

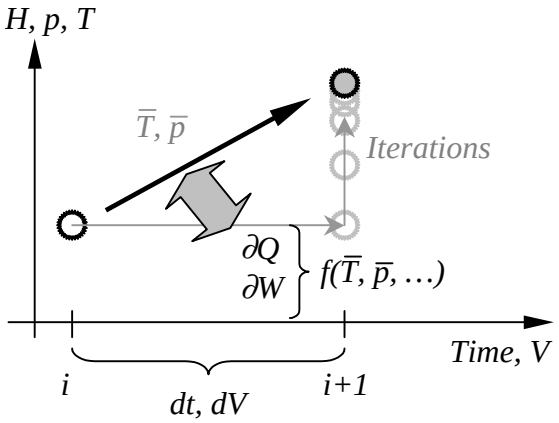

Figure 9 Principle of trapezoid method

Schematically this can be described as shown in Figure 9. From one step to another, work, heat and mass transfer are calculated as functions of the mean value representation of temperature and pressure between the two steps. The state in the one point (*i*) is used as start values for the next point (*i+1*). Trough iterative calculations, pressure and temperature are calculated in the next point. This means that Eq.43 is written as:

$$\partial Q\left(\overline{T},\overline{p},...\right)-\overline{p}\partial V+\sum\partial n_{IN}\cdot\overline{h}_{IN}+\sum\partial n_{OUT}\cdot\overline{h}_{OUT}\approx$$
$$\left(H\left(T_{i+1}\right)-p_{i+1}V_{i+1}\right)-\left(H\left(T_i\right)-p_iV_i\right)$$

with: Eq.44

$$\overline{T}=\frac{T_i+T_{i+1}}{2}\qquad\overline{p}=\frac{p_i+p_{i+1}}{2}$$

Note that the left-hand terms in expression Eq.44 are functions of the mean state variables and these causes a change in state between two points, which is described on the right-hand side. The ideal gas law Eq.18 then connects the state variables in the next point (*i+1*):

$$p_{i+1}\cdot V_{i+1}=n_{i+1}\cdot R\cdot T_{i+1}$$ Eq.45

The relation between enthalpy and temperature is then given by Eq.23 and Eq.24. It is thus possible to set up an iterative calculation scheme (simplified):

1. Given: T_i, p_i, V_i, n_i (including mole fractions) and V_{i+1}.
2. As start values for the next point, set $T_{i+1}=T_i$, $p_{i+1}=p_i$ and $n_{i+1}=n_i$ (or a better guess).
3. Calculate mean values $\overline{T},\overline{p}$
4. Use models to calculate heat and mass transfer, functions of $\left(\overline{T},\overline{p},...\right)$
5. Calculate mole fractions in the next point, n_{i+1} , which changes due to combustion and mass transfer.
6. Use Eq.44 to calculate enthalpy in the next point, $H(T_{i+1})$
7. Use Eq.24 to calculate temperature, T_{i+1} from enthalpy and Eq.45 to calculate pressure, p_{i+1}
8. Iterate 3 to 7, until stable pressure and temperature in the next point.

The description above is somewhat influenced by in-cylinder calculations i.e. to calculate in-cylinder temperature and pressure trace. The time step used is set to be equal to the time corresponding to 1 crank angle degree (CAD) at the specific engine speed. Test were made were the step was set to 0.2 CAD with almost the same results (about 1% difference in resulting variables). At 10 CAD per step the still generate acceptable results as shown in Figure 10, indicating that the numerical method is very robust.

The expressions and method is very similar when calculating the whole engine system. In some cases there has to be some numerical ”dampers” in order to achieve convergence due to e.g. singularities in mass transfer functions. These dampers are inside the iteration loop above and do not affect the results; they ensure convergence but cost calculation time.

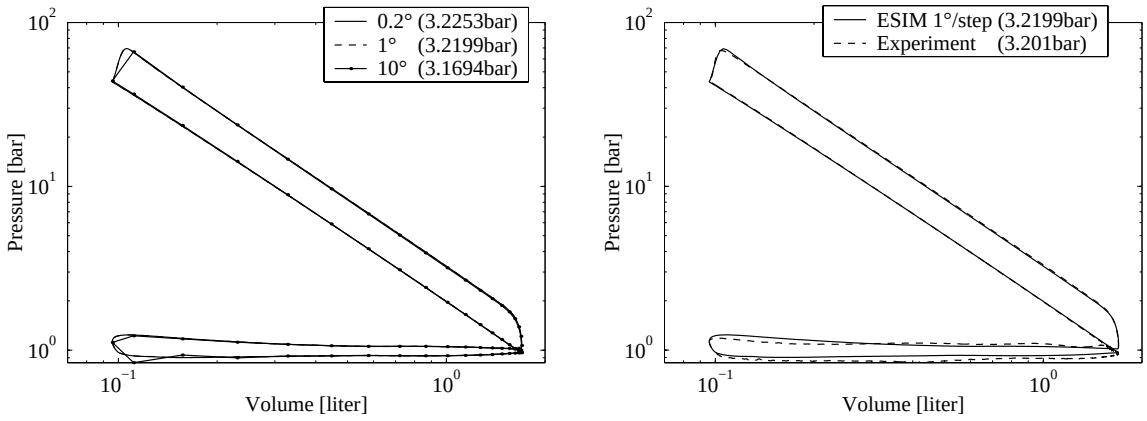

Figure 10 Comparison between different calculation resolution of 0.2, 1, and 10 CAD (left) and a comparison with experiment (right). $IMEP_{net}$ is shown in brackets. Volvo TD100 engine running with HCCI combustion at $\lambda = 3$, isooctane.

2.4 System buildup

In this section, the different models of engine system components are described in more detail. The idea is also to point out what effects are considered and which are not.

The different components are in the software represented by different functions and it becomes the user role to give the necessary inputs and to connect the different components together.

When linking these functions together, with respect of pressure, temperatures, mixtures and mass flows, an engine system can be simulated. The engine cycle calculation can be treated a little bit different from the other components. By leaving the engine calculations out when calculating the surrounding components, computational time can be saved without any larger errors in the calculations. The error that this causes is taken out over time, i.e. if the flow into the engine is under-predicted then the next cycle will experience a higher inlet pressure that increases the flow. In a way, this procedure is an assumption that the dynamic changes is small, and that the engine cycles have a damping effect in the system. An example of a system is schematically described in Figure 11.

If better accuracy of dynamic, multi-cylinder engine simulations is needed, then the cylinders should be calculated separately, but overlapped in time, and together with the rest of the system i.e. inside the iteration loop shown in Figure 11, resulting in a tremendous increase in computational time.

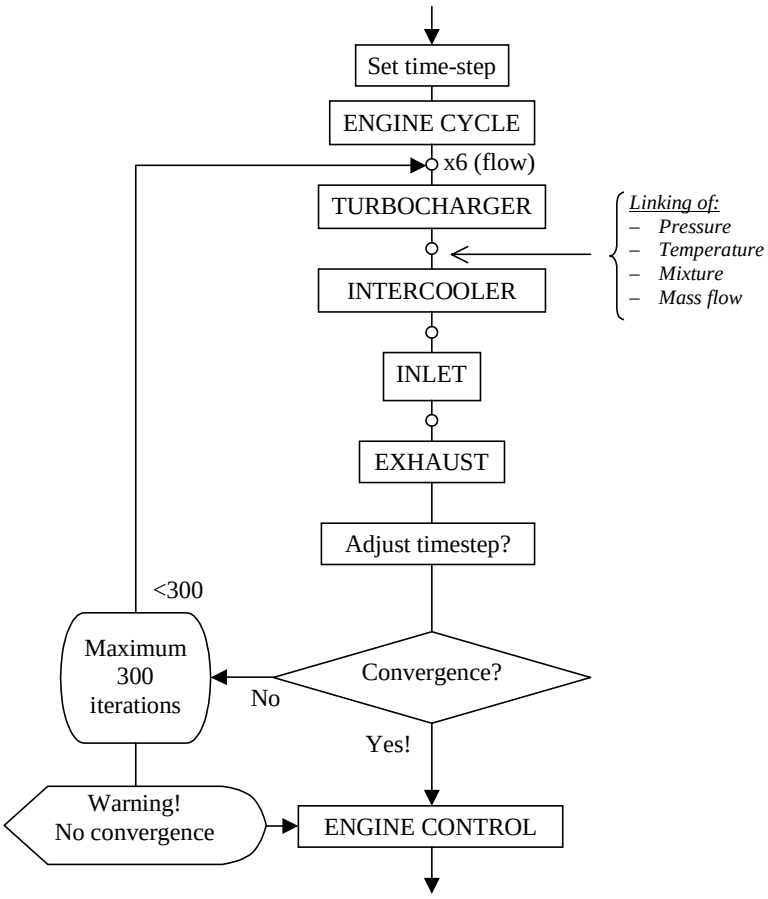

Figure 11 Schematical illustration of the system calculation, in this case a 6 cylinder engine.

2.5 Engine model

The engine calculation includes geometry-, heat transfer-, heat release- and valve-flow calculations. There also exist two different layouts depending on the engine type, port injected or direct injected engine. The engine is here seen upon as a component with a varying volume, exposed to heat transfer (including heat release) and connected to two ports with variable restrictions.

First, before doing any thermodynamic calculations or simulations, some constant data can be set up representing the geometry of a specific engine. These are typically volume, combustion chamber area and effective valve flow area. An expression for the piston movement is set up, which includes an offset in crankshaft-cylinder centerline. TDC is set to be when the piston reaches its uppermost position, see Figure 12. The following expression for the piston position can be set up:

$$x(\theta) = (r+l)\cdot\cos(\varsigma) - \left[r\cdot\cos(\theta+\varsigma) + \sqrt{l^2 - \left(r\cdot\sin(\theta+\varsigma) - \delta\right)^2} \right]$$

where: Eq.46

$$\varsigma = \arcsin\left(\frac{\delta}{r+l}\right)$$

This position is then used to calculate in-cylinder volume and combustion chamber area trough:

$$V(0...720°) = \frac{\pi D^2}{4} \cdot x(0...720°) + V_c$$

$$A(0...720°) = A_{cylinder}(0...720°) + A_{piston} + A_{cylinderhead} = \quad \text{Eq.47}$$

$$\pi D \cdot \left(x(0...720°) + x_0 \right) + A_{piston} + A_{cylinderhead}$$

V_c is the minimum compressed volume and should include crevice volumes. Area should also include piston topland area, valve slot area and cylinder head gasket area.

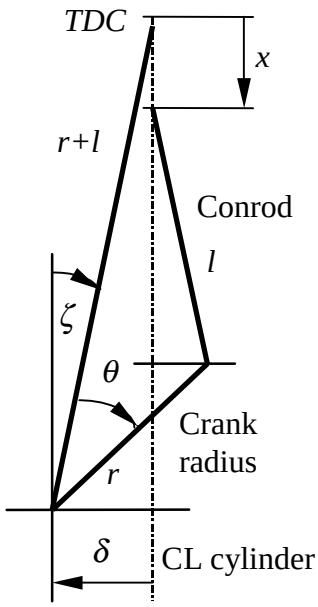

TDC	=	*Top dead center, the piston is in the upper position*
x	=	*Piston position, x = 0 ⇔ TDC*
ς	=	*Angle between the connecting rod (conrod) and the cylinder when x = 0*
l	=	*Conrod length*
r	=	*Crank arm length ⇔ Crank radius*
δ	=	*Offset, i.e. shortest distance between the crankshaft and the cylinder centerlines*
θ	=	*Crank angle, θ = 0 ⇔ TDC*

Figure 12 Geometry for piston movement

Valve lift is calculated trough the cam profile determined by mechanical analysis (Bensinger, 1968, reviewed by Söderberg [102]). For a given desired maximum valve lift and duration a cam profile is calculated. This is then used to calculate the lift curve. Further description will not be made here more than it can be mentioned that the lift curve is determined with e.g. respect of maximum acceptable valve acceleration and deceleration. One alternative is to use measured valve lift. This data can be stored in a suitable format and read by the program during initialization.

The valve lift is used to calculate the minimum geometrical flow area (A_{min}) but for the valve flow calculation, an effective valve flow area (A_E) is used. There are some flow effects that depend on valve and port geometry and friction against port and seat surfaces. The ratio between effective flow area and minimum flow area is usually called “discharge coefficient” (C_D) and can be seen upon as port and valve geometry efficiency (Eq.48). An alternative is the A_E/A_C ratio, which is the effective valve flow area divided by the valve curtain area (A_C). The valve curtain area is simply the cylindrical area defined by lift and valve diameter. The minimum flow area depends on the geometrical layout of the valve and the port and is calculated through Eq.49, the geometrical parameters given in Figure 13. An example of calculated lift and flow areas is seen in Figure 14.

$$C_D = \frac{A_E}{A_{\min}} \qquad \left[A_E / A_C \qquad A_C = \pi \cdot D_v \cdot L_v \right] \quad \text{Eq.48}$$

$$\begin{cases} A_{\min} = \pi \cdot L_v \cdot \cos(\beta) \cdot \left(D_v - 2w + {L_v}/{2 \cdot \sin(2\beta)} \right) & \text{when } 0 < L_v \le L_{v1} \\ A_{\min} = \pi \cdot (D_v - w) \cdot \sqrt{\left(L_v - w \cdot \tan(\beta)\right)^2 + w^2} & \text{when } L_{v1} < L_v \le L_{v2} \\ A_{\min} = \dfrac{\pi}{4} \cdot \left(D_p^2 - D_s^2\right) & \text{when } L_{v2} < L_v \end{cases}$$

where valve lifts L_{v1} and L_{v2} is calculated through: Eq.49

$$\begin{cases} L_{v1} = {w}/{\left(\sin(\beta) \cdot \cos(\beta)\right)} \\ L_{v2} = \sqrt{\left(\dfrac{D_p^2 - D_s^2}{4 \cdot (D_v - w)} \right)^2 - w^2} + w \cdot \tan(\beta) \end{cases}$$

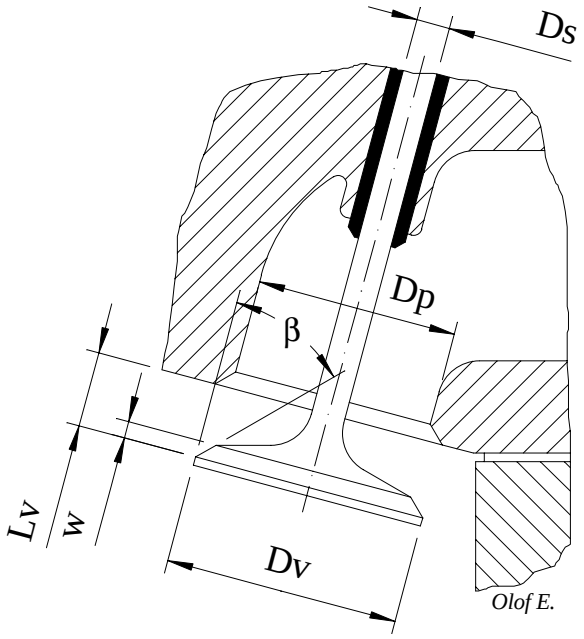

Figure 13. Valve geometry

Initially models for the discharge coefficients were adopted, based on measurements reviewed in Heywood [96]. Although based on rather limited amount of data, it provided at least an estimate of the effective flow area. The discharge coefficient was dependent on relative valve lift (lift divided by valve diameter). However, some limitations were found with this approach. According to the reviewed results the C_D factor tended to go down at high lifts but the review did not say if A_{min} was constant or not at high lifts. If constant it would mean that the effective flow area would go down at high lifts and this seems quite unrealistic since it would also mean that the pressure drop given a certain mass flow then would be higher. If the effective flow area is determine by the A_E/A_C ratio it is possible that the effective flow area becomes higher than the A_{min}, which also seems quite unrealistic. Therefore, in the absence of measured data on effective flow area, a constant discharge coefficient, C_D of 0.7 is adopted, regardless of flow direction. If there is some knowledge about the flow process of the real engine, it is quite simple to add this information into the calculations.

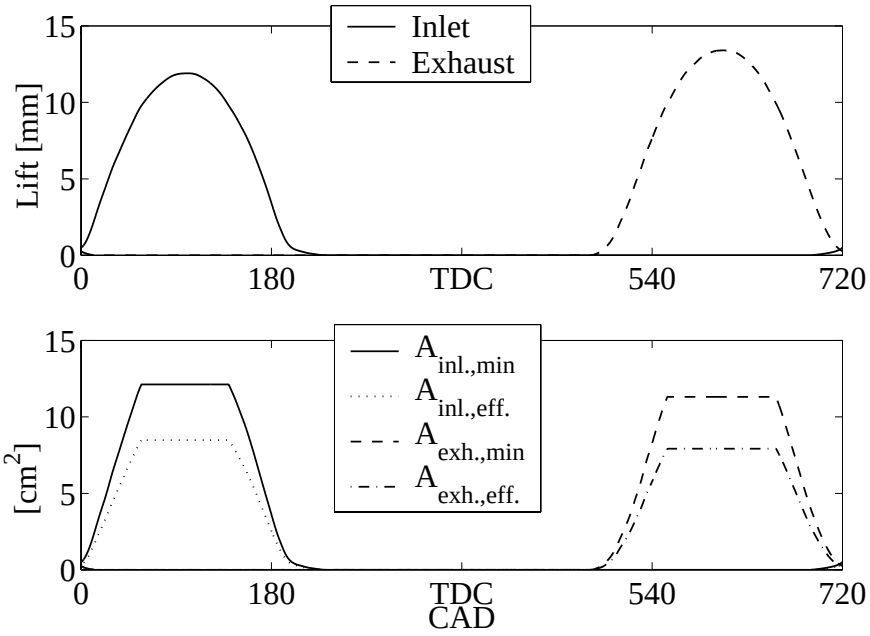

Figure 14 Example of calculated valve lift (top), minimum and effective flow area (bottom). Note that the C_D factor is set constant.

The effective valve flow area and the pressures in the inlet port and in the cylinder are then used to calculate mass-flow over the valves. The expression below is derived with an ideal, steady flow and isentropic assumption [96], resulting in:

$$\begin{cases} \dot{m} = \dfrac{1000 \cdot A_E \cdot p_{up}}{\sqrt{1000 \cdot T_{up} \cdot R/M}} \left(\dfrac{p_{down}}{p_{up}} \right)^{1/\gamma} \sqrt{\dfrac{2\gamma}{\gamma - 1} \left(1 - \left(\dfrac{p_{down}}{p_{up}} \right)^{(\gamma-1)/\gamma} \right)} \quad [g/s] \\ \dot{m}_{choked} = \dfrac{1000 \cdot A_E \cdot p_{up}}{\sqrt{1000 \cdot T_{up} \cdot R/M}} \sqrt{\gamma} \left(\dfrac{2}{\gamma + 1} \right)^{(\gamma+1)/2(\gamma-1)} \quad [g/s] \end{cases} \qquad \text{Eq.50}$$

Choked flow occur when: $\dfrac{p_{down}}{p_{up}} \leq \left(\dfrac{2}{\gamma + 1} \right)^{\gamma/(\gamma-1)}$

Note that the expressions are written as function of γ, up to now this has been avoided since gas properties are given by enthalpy. However, in this case it is simpler due to the non-choked/choked check has to be done, which is easiest described as a function of γ, calculated through:

$$\gamma(T) = \frac{C_p(T)}{C_p(T) - R} \qquad \text{Eq.51}$$

Note that specific heat also depends on what mixture flows trough the valves. The mixture is set to be a mixture of air-fuel-EGR when flowing over the inlet valves, except when backflow occurs and when this flow is pulled back into the cylinder again. In this case the mixture is assumed to be the same as inside the cylinder. This is also is assumed to be the case regarding the exhaust valve flow. The cylinder is assumed to be a well-mixed volume. In order to fit into the energy conservation equation, the flow is represented as:

$$\partial n \cdot \bar{h} = \partial t \cdot \dot{m}/M \cdot h(\bar{T}) \quad [J] \qquad \text{Eq.52}$$

2.5.1 Simple heat release model

Since this model does not have any built-in chemical kinetic calculations or an empirical model of the heat release during combustion, a simple shape function is used for the heat release. The amount of heat released is determined of the amount of fuel (and oxygen) that is trapped inside the cylinder at IVC. This amount of fuel, its lower heating value and an assumed combustion efficiency is then used to calculate the heat released. Together with the shape-function the heat release for each CAD can be calculated and inserted in the left-hand side of Eq.44. Several different shape functions have been tested and a function first described by Wiebe, as reviewed by Heywood [96] (see also Vibe [103]) was found appropriate. In a slightly modified form it can be described as:

$$x_b = 1 - \exp\left(a'\left(\theta - \theta_0\right)^{m'}\right) \qquad \text{Eq.53}$$

where x_b is the percentage heat released, or combustion progress. The parameters θ_0, a' and m' is often hard to give values with direct physical meaning, it is easier to think in terms of *A0*, *A10* and *A90*, which represent the crank angle of 0,10 and 90%, of total heat release. It is possible for a set of *A0*, *A10* and *A90*, find a θ_0, a' and m':

$$\begin{cases} \theta_0 = A0 \\ m' = \ln\left(\dfrac{\ln(0.9)}{\ln(0.1)}\right) \Big/ \ln\left(\dfrac{A10 - A0}{A90 - A0}\right) \\ a' = \ln(0.9) \Big/ (A10 - A0)^{m'} \end{cases} \qquad \text{Eq.54}$$

Heat release fraction is then calculated as:

$$\partial Q_{HR} = \eta_c \cdot m_f \cdot Q_{LHV} \cdot \left(x_{b,i+1} - x_{b,i}\right) \quad [J] \qquad \text{Eq.55}$$

where m_f is fuel mass present before combustion takes place and η_c is an assumed combustion efficiency. An example of the Wiebe heat release shape is showed in Figure 15.

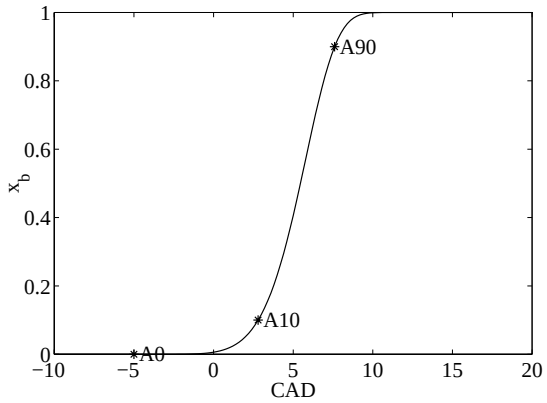

Figure 15 A typical Wiebe heat release shape representing HCCI combustion.

2.5.2 In-cylinder heat transfer model

Heat transfer is modeled with an expression derived by Woschni [104, see also reviews in 96, 101] The characteristic equation for the this model is:

$$Nu = 0.035 \cdot Re^{0.8} \qquad \text{Eq.56}$$

It relate the Nusselt number, $Nu = \alpha \cdot L_{ref} / \lambda$, – the dimensionless representation of the convective heat transfer coefficient, α, with the Reynolds number, $Re = \rho \cdot U_{ref} \cdot L_{ref} / \eta$, – the ratio between inertia forces and viscous forces. The Reynolds number is often used as a characterization of the flow, the degree of turbulence. The average cylinder gas velocity throughout the cycle is described by Eq.57 were indices "*ref*" denotes a reference state e.g. IVO or start of combustion:

$$\overline{w} = C_{adjust.1} \cdot 2.28 \cdot \overline{S}_p + C_{adjust.2} \cdot 3.24 \cdot 10^{-3} \cdot \frac{V_d \cdot T_{ref}}{p_{ref} \cdot V_{ref}} \cdot \left(p - p_{motored} \right) \qquad \text{Eq.57}^6$$

The original expression of Eq.57 used stroke dependant coefficients, the factor 2.28 was 6.18 during the exchange strokes and 3.24 was 0 for the exchange and compression strokes. In addition compensation factors ($C_{adjust.1}$, $C_{adjust.2}$) are introduced to give "tuning knobs" for better agreement with experiments. In this program the second term of the expression is used from start of combustion (*A0*) to EVO. Start of combustion is used as reference state and the motored pressure, $p_{motored}$ is estimated over the combustion and expansion period by an isentropic relation:

$$p_{motored}\left(A0 \ldots EVO\right) = p_{A0} \cdot \left(V_{A0} \Big/ V\left(A0 \ldots EVO\right) \right)^{\gamma_{A0}} \qquad \text{Eq.58}$$

The correlation between average in-cylinder gas properties and heat transfer coefficient is according to Woschni (please note the units):

$$h_c \left[W \Big/ m^2 K \right] = 3.26 \cdot B[m]^{-0.2} \cdot p[kPa]^{0.8} \cdot T[K]^{-0.55} \cdot \overline{w} \qquad [m/s]^{0.8} \qquad \text{Eq.59}$$

In cylinder surface is calculated from data about the actual engine's cylinder head and piston crown down to the first piston ring. The average wall temperature is assumed and kept constant, however it would be possible to insert cylinder wall temperature calculations based on the heat flux over the walls. The total heat transfer fraction is calculated as:

$$\partial Q_{HT} = \partial t \cdot \overline{A} \cdot h_c \cdot \left(T - \overline{T}_{wall} \right) \qquad [J] \qquad \text{Eq.60}$$

2.5.3 Exhaust port heat transfer model

In order to get a good estimation for the turbine conditions, especially the exhaust temperature, it becomes important to model the heat transfer in the exhaust ports. A model developed by Hires and Pochmara (1976, reviewed by Ferguson [101]) is used to calculate the instantaneous heat transfer in the exhaust port. The basic relation for this model is:

$$Nu = 0.158 \cdot Re^{0.8}$$

where Eq.61

$$Re = \left(\frac{\dot{m} \cdot D_p}{\eta \cdot A_p} \right)$$

---

[6] According to the original reference [104] the factor $3.24 \cdot 10^{-3}$ has the unit m/(s·°C) which means that T_r should be in °C. However, this seems strange since this part of the expression is in a way a calculation of the mass trapped inside the cylinder through the ideal gas equation of state. Therefore, it is believed that there is a misprint in the original reference and the unit should be m/(s·K).

The heat transfer coefficient is calculated as:

$$\alpha_p = \frac{C_{adjust.} \cdot Nu \cdot \lambda}{D_p} \qquad \text{Eq.62}$$

An adjustment factor $C_{adjust.}$ in Eq.62, initially set to 1, is can be used to fit the model to measurements. Note that there is about 4.5 times higher heat transfer in the exhaust port, than inside the cylinder, according to the basic equations, Eq.56 and Eq.61. One explanation can be that the flow becomes much more turbulent closer to the walls in the exhaust port, than in the cylinder, due to varying flow velocities and port geometry. This constantly disturbs and reduces the laminar boundary layers near the port walls, and hence increases heat transport to the walls.

The coolant side of the exhaust port wall is assumed to have a constant temperature, 100°C approximately equal to the boiling temperature of the coolant. The inner side temperature is calculated from a mean value of the heat flux over the exhaust wall which is calculated in iterative manner assuming that the wall can be described as a plate as shown in Figure 16. The thermal dynamics in the wall is not considered. That means that the mean wall temperature during an exhaust stroke is determined by the heat flux during that, and not previous exhaust strokes.

Different models for exhaust port heat transfer were compared to measurements by Caton and Heywood [105], both time-dependence and spatially at the exit of an engine port. The results indicated that the model selected here gave an ”approximate agreement” on the mean exit port temperature (so it suits the purpose here fairly well), the time-resolved temperature was less accurate.

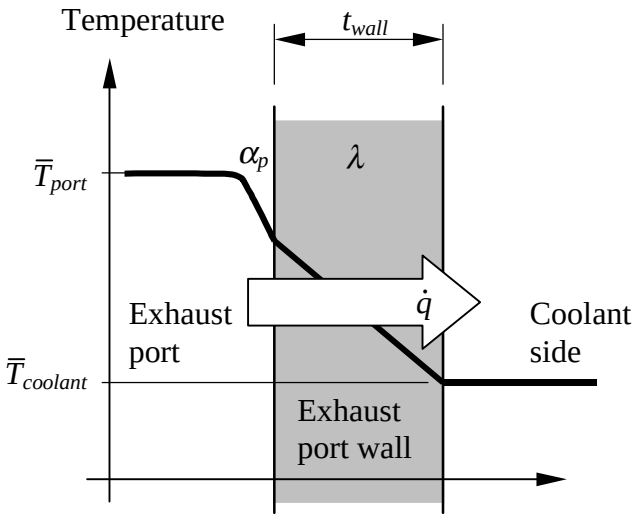

Figure 16 Scematic temperature distribution over exhaust port wall

2.5.4 Governing equations

Besides the energy conservation equation, mass conservation equations and equations governing species is needed.

Two things affect in-cylinder mixture; mass flow through the inlet valves and combustion. A mixture of fuel, air and EGR in the inlet manifold gives the gas composition of the mass flowing into the cylinder. An array of mole (N2, O2, Ar, CO2, H2O and fuel) represents the

mixture inside the cylinder. The flow into the cylinder is added to this array with respect of the mass flow rate and the inlet mixture.

The combustion is, as mentioned earlier, governed by the combustion shape function and combustion efficiency. With the specie set-up chosen here, it is assumed that if the combustion is not completed (less than 100% combustion efficiency), unburned fuel is the only emissions i.e. there are no CO emission or HC emission besides pure fuel, in order to reduce the specie set-up. The combustion is thereby only affecting the number of moles of fuel, O_2, CO_2 and H_2O. However, it is possible to expand the set of species, but it increases the computational time. The overall complete combustion equation for the involved species becomes:

$$\begin{aligned}&\left[C_aH_bO_c + dN_2 + eAr + fCO_2 + gH_2O\right]_{fuel} + \left(a + \frac{b}{4} - \frac{c}{2}\right)O_2 \longrightarrow \\ &dN_2 + eAr + (a+f)CO_2 + \left(\frac{b}{2} + g\right)H_2O\end{aligned} \qquad \text{Eq.63}$$

The total change in moles for combustion of one mole of fuel under lean mixtures ($\lambda \geq 1$) can be written as (please note the array notation):

$$\begin{aligned}&\Delta\mathbf{n}_{c,tot} = \Delta\left[n_{N_2} \quad n_{O_2} \quad n_{Ar} \quad n_{CO_2} \quad n_{H_2O} \quad n_{fuel}\right] = \\ &\eta_c \cdot \left[d \quad -\left(a + \frac{b}{4} - \frac{c}{2}\right) \quad e \quad (a+f) \quad \left(\frac{b}{2} + g\right) \quad -1\right]\end{aligned} \qquad \text{Eq.64}$$

Finally, the total change in cylinder gas moles and composition, due to valve flow and combustion, can be expressed by:

$$\mathbf{n}_{i+1} = \mathbf{n}_i + \partial t \cdot \frac{\overline{\dot{m}}_{inl}}{M_{inl}} \cdot \mathbf{x}_{inl} - \partial t \cdot \frac{\overline{\dot{m}}_{exh}}{M_{cylinder}} \cdot \overline{\mathbf{x}}_{cylinder} + \left(x_{b,i+1} - x_{b,i}\right) \cdot \Delta\mathbf{n}_{c,tot} \qquad \text{Eq.65}$$

In summary, Eq.65 combines the mass and atom conservation constraints.

2.5.5 Numerical problems

There is one numerical difficulty regarding the expressions for the valve flow. Consider the expression for non-choked flow in Eq.50. Lets simplify this function a little by setting $\gamma = 1.3$ and removing the dimensional part:

$$\dot{m}_0 = \left(\frac{1}{\pi}\right)^{0.769} \sqrt{8.67\left(1 - \left(\frac{1}{\pi}\right)^{0.231}\right)} \qquad \text{Eq.66}$$

When plotting this function close to a pressure ratio (π) 1, e.g. when flow switches direction, there will be a problem in finding a solution to the differential equation with the method that are selected here. This is visualized as in Figure 17. The first solution says that it flows into the cylinder, which means that the pressure increases inside the cylinder. Due to the length of the time-step, the pressure becomes too high and the new solution says that it flows backwards, and so on. The explanation of this behavior is that the slope of this curve goes to infinity close to 1 in pressure ratio. Another similar situation appears in the transition from non-choked to choked flow.

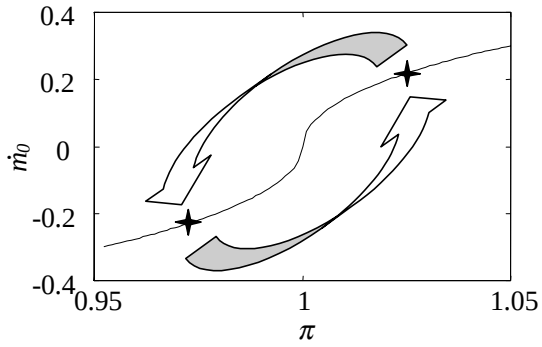

Figure 17 Numerical problem when flow changes direction

Two simple methods are used to solve these problems. The shape of the curve close to pressure ratio one is changed so the slope does not go to infinity. This is done by inserting a new function, a 2'nd degree polynomial function when the pressure ratio is about $0.99<\pi<1.01$. The same level and gradient is used at about $\pi=1.01$ as Eq.66, and the mass flow is zero at $\pi=1$. This modification has only effect when the pressure ratio is very close to one, which happens perhaps a few crank angles per cycle at higher engine speeds. Therefore, it does not have any noticeable effect on the results. The other method used is a damper inside the iterative loop. The mass flow is only allowed to change to a mean value of the previous (k) and new ($k+1$) calculated mass flow inside the iterative loop, as shown in Eq.67.

$$\dot{m}_{k+1} = \frac{1}{2}\left(\dot{m}_k + \dot{m}_{new}\right) \qquad \text{Eq.67}$$

2.5.6 Diesel engine combustion model

In order to verify calculations and models against measurements on a real engine, diesel combustion is modeled. Direct diesel injection and combustion is modeled as suggested by Egnell [106] which simply states that the heat release rate is proportional to the difference between injected fuel, in terms of heat and accumulated heat release:

$$\dot{Q}_{hr} = k_{hr} \cdot \left(Q_f - Q_{hr}\right) \qquad \text{Eq.68}$$

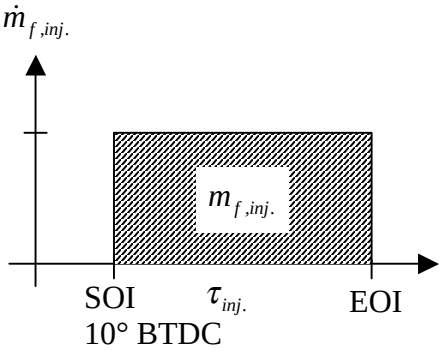

Figure 18 Assumed fuel injection, SOI - Start Of Injection, EOI - End Of Injection

With the assumption that fuel injection process can be described as shown in Figure 18, i.e. that the fuel flow through the injector nozzles are constant during the injection period, the differential equation Eq.68 can be solved analytically and the result is shown in Eq.69.

$$
\begin{aligned}
q_{hr}(t) &= \frac{1}{\tau_{inj.}}\left((t - t_{SOI}) + \frac{1}{k_{hr}}\left(\exp\left(-k_{hr}\cdot(t - t_{SOI})\right) - 1\right)\right) && t_{SOI} \le t \le t_{EOI} \\
q_{hr}(t) &= 1 + \left(q_{hr}(t_{EOI}) - 1\right)\cdot\exp\left(-k_{hr}\cdot(t - t_{EOI})\right) && t_{EOI} < t \\
\partial Q_{hr} &= \eta_c \cdot m_{f,inj} \cdot Q_{LHV} \cdot \left(q_{hr}(t_i) - q_{hr}(t_{i-1})\right) && [J]
\end{aligned}
\qquad \text{Eq.69}
$$

It is assumed that a fraction of the fuel that is injected, but has not burned, is in vapor phase. Vaporization has a cooling effect but is very small in comparison with the overall heat release. It can then be expressed as in Eq.70 and to illustrate this, heat release and vaporization are exemplified in Figure 19.

$$
\begin{aligned}
q_{VAP}(t) &= k_{VAP}\frac{(t - t_{SOI})}{\tau_{inj.}} + (1 - k_{VAP})\cdot q_{hr}(t) && t_{SOI} \le t \le t_{EOI} \\
q_{VAP}(t) &= k_{VAP} + (1 - k_{VAP})\cdot q_{hr}(t) && t_{EOI} < t \\
\partial Q_{VAP} &= m_{f,inj} \cdot Q_{VAP} \cdot \left(q_{VAP}(t_i) - q_{VAP}(t_{i-1})\right) && [J]
\end{aligned}
\qquad \text{Eq.70}
$$

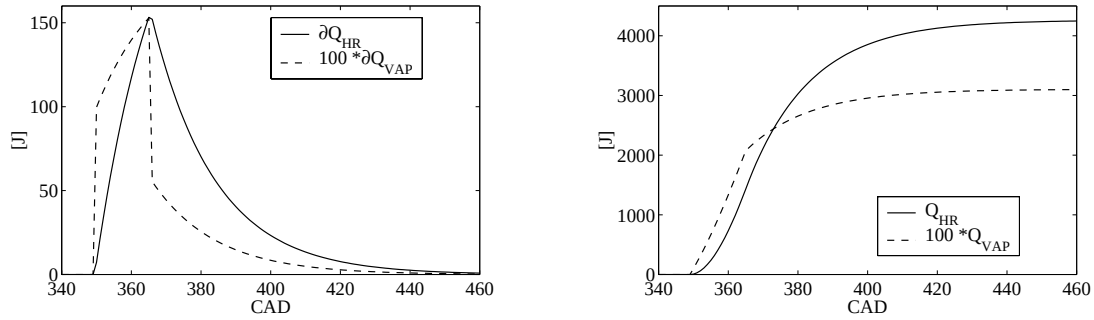

Figure 19 Example of diesel vaporization and heat release (Q_{HR}), note how small the vaporization part is compare to heat release (a magnification factor of 100 is used here!), k_{VAP} = 0.5 and step length is 1 CAD. The right plot shows accumulated values.

2.5.7 Engine friction model

There exist numerous of friction models, most of these give an estimate of the friction mean effective pressure (*FMEP*) as a function of mainly engine speed. A small comparison is made in Table 2 between different models. Experimental results from a SCANIA DSC 12 diesel engine running at 1500 rpm are used for comparison. Typically, IDI and small DI diesel engines give a higher degree of friction. The model selected for this study is for a direct injected diesel engine (Eq.71, reviewed by Heywood [96]). Despite the fact that it is stated that the last term in this model is pumping work it seems like to give a reasonable estimation of friction for the SCANIA DSC12 engine, when comparing to models for smaller TDI engines. Most simulation are made at 1500 rpm[7], so the speed dependence of the model is only used in some individual cases, *FMEP* of 1.71 bar seems to be a fair estimate at this speed.

[7] 1500rpm correspond to a synchronous speed of an electrical generator connected to 50Hz AC. Other synchronous speeds for 50Hz are e.g. 750, 1000 and 3000 rpm, and for 60Hz: 900, 1200 and 1800 rpm.

$$FMEP = 1000 \cdot \left(75 + 48 \cdot n/1000 + 0.4 \cdot \overline{S_p}^2\right) \qquad [Pa] \qquad \text{Eq.71}$$

Given this model a mechanical efficiency ($\eta_{M.e.}$, Eq.15) can be calculated from engine load (*BMEP*) and engine speed. The result is shown in Figure 20 and it clearly shows the importance of high load operation for efficiency.

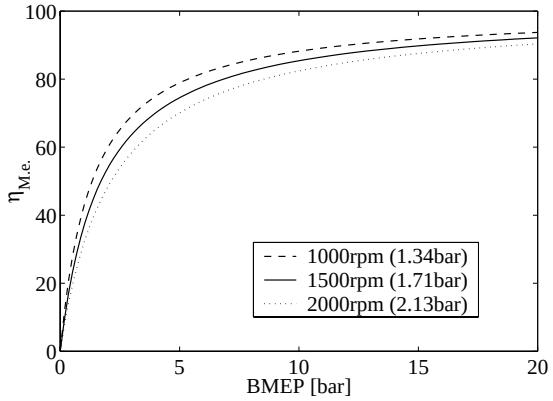

Figure 20 Speed and load dependence on mechanical efficiency. FMEP is noted in brackets.

Table 2 Friction models. The top one is used throughout this work (1 bar = 100 kPa).

Model [kPa]	FMEP [bar]	Description
$MEP_{Motored} = 75 + 48 \cdot n/1000 + 0.4 \cdot \overline{S_p}^2$	1.71	Reviewed by Heywood [96], last term stated to be pumping work. [8]
$MEP_{Motored} = 75 + 48 \cdot n/1000$	1.47	Same as above, but without last term.
$MEP_{Motored} = 110 + 48 \cdot n/1000 + 0.4 \cdot \overline{S_p}^2$	2.06	Same as top, but for large swirl chamber IDI engines.
$FMEP = 190 + 2.9 \cdot (n/60 - N_0)$ $N_0 = 30 \cdot \sqrt{3/(1000 \cdot V_{d,tot})}$ $[1/s]$	2.18	Model for Audi 1.9 liter TDI engine from 1990, Wu and Ross [107]
$FMEP = 183 + 2.3 \cdot (n/60 - N_0)$	2.06	Model for VW 2.46 liter TDI engine from 1992, Wu and Ross [107]
Experiment	1.5 - 1.9	Truck size TDI diesel engine

2.6 Turbocharger models

The HCCI engine is running on lean mixtures and has limited possibilities to use rich mixtures in even for short periods. It becomes critical to succeed in supercharge the HCCI engine in order to achieve acceptable specific power i.e. power output per engine size (weight or volume). The favored method is turbocharging since the power required for the compression of the inlet air is taken from the exhaust gas trough expansion. Other methods

[8] The friction was investigated on a motored engine. When using the model: FMEP = $MEP_{Motored}$, or more correct: (FMEP+PMEP) = $MEP_{Motored}$

are supercharging with a compressor, driven directly by the engine itself, however this directly costs energy and thereby efficiency. Another, quite advanced method is the Comprex-charger which uses the blow down - pulse of the exhaust gas to directly compress the inlet air, however this advanced solution has found very little acceptance on the market.

Turbocharging is selected here since it is the most dominating form of supercharging for heavy-duty engines. It exist several manufacturers, and dealers, that can provide complete turbochargers. The method that are used her to model the turbocharger should be applicable on various superchargers as well.

2.6.1 Performance data

The base for the turbocharger model is the performance map of the compressor and turbine respectively. Typically, these maps give a relation between:

- pressure ratio
- mass flow
- rotating speed
- isentropic efficiency

The speed and mass flow are often normalized with to certain standard states. For turbines a third approach is frequent and that is to model the turbine as a restriction with a varying effective flow area that depends on speed and pressure ratio. Depending on manufacturer and the standards they follow, different normalizing approaches are used; some typical examples are shown here.

$$\text{Compressor: } \pi_C = \frac{p_2}{p_1} \qquad \text{Turbine: } \pi_T = \frac{p_3}{p_4} \qquad \text{Eq.72}$$

The pressure ratio, π (Eq.72), is often given as *total to total* or *total to static*, probably due to what method that were used during the determination of the performance maps. The difference between the total and static pressure is in general quite small i.e. the dynamic pressure contribution is small. It is only at the short period of blowdown, the velocities become so high that there will be a difference and hence it becomes important when studying *pulse-loading turbocharging* (see below). In order to calculate from static to total and vice versa, information about flow velocities and density is needed. From now on all state variables are considered at stagnation state (total). The index numbers in Eq.72 indicate states at 1– before compressor, 2– after compressor, 3– before the turbine and 4– after the turbine.

For mass flow, there are two common types of normalization:

$$\text{Compressor: } CMF - \text{Corrected Mass Flow} = \dot{m}_{corr.} = \dot{m}\sqrt{\frac{T}{T_{ref.}}}\frac{p_{ref.}}{p} \qquad [g/s]$$

$$\text{Turbine: } MFP - \text{Mass Flow Parameter} = \dot{m}\frac{\sqrt{T}}{p} \qquad \left[\frac{g\cdot\sqrt{K}}{s\cdot Pa}\right] \qquad \text{Eq.73}$$

Examples of reference states are 1.013bar/288.15K for compressors and 2bar/773.15K for turbines and the states are upstream the compressor and turbine respectively. The parameter representation is simpler since there is no need for a reference state. However, it is easy to

convert between corrected- and parameter value representation. A third way to normalize mass flow is by calculate an effective flow area by rearranging equation Eq.50.

Speed is normalized in the same manner as mass flow but only against temperature:

$$\begin{aligned} &\text{Compressor:} \quad CSP - \text{Corrected speed} = N_{corr.} = N\sqrt{\frac{T_{ref.}}{T}} && [1/s] \\ &\text{Turbine:} \quad SPP - \text{Speed parameter} = \frac{N}{\sqrt{T}} && \left[\frac{1}{s\cdot\sqrt{K}}\right] \end{aligned} \qquad \text{Eq.74}$$

The isentropic efficiency is defined as:

$$\begin{aligned} &\text{Compressor:} \quad \eta_C = \frac{h_{2,s} - h_1}{h_2 - h_1} = \frac{\{\text{Isentropic}\}}{\{\text{Real}\}} \\ &\text{Turbine:} \quad \eta_T = \frac{h_3 - h_4}{h_3 - h_{4,s}} = \frac{\{\text{Real}\}}{\{\text{Isentropic}\}} \end{aligned} \qquad \text{Eq.75}$$

Index ”s” indicates isentropic states, which is calculated from pressure ratio and temperature before compressor and turbine respectively.

Typical schematic figures of performance maps are shown in Figure 21.

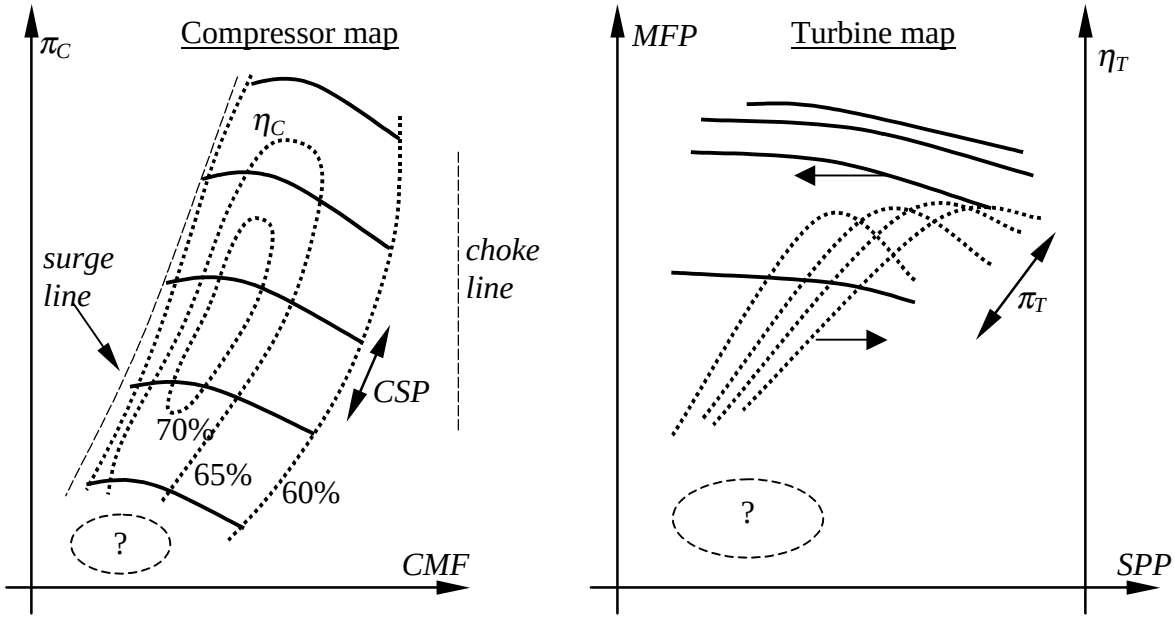

Figure 21 Schematic turbocharger performance maps, dotted lines are efficiency. The questionmarks indicate regions were interpolation is impossible without addition of data.

2.6.2 Performance data representation

A crude way to get the mass flow and efficiency of the compressor or turbine is to simply use some sort of interpolation method in the table representation of the maps. This has one major drawback, the performance maps are seldom complete and some operating situations are not covered, especially the region with low speed and pressure ratio as indicated in Figure 21. Some extrapolation is needed and this is very difficult, inefficient and often not very successful, which is a conclusion based on the experience of several attempts by the author. However, in the region where the data is provided from the maps, interpolation certainly is

possible. The problem is that it is not sure that the system reaches this region during startup for various reasons and it becomes critical that the extrapolation is correct. Models seem to be a more appropriate solution for handling performance data.

The following models are influenced by the work done by Müller et. al [108], however some models are modified, others are completely different. Müller has derived models from physical understanding and correlated this against performance maps and measurements for small turbochargers for spark ignition engines. However, when trying to directly use these expressions on turbochargers for a truck-size diesel engine, less accurate correlation was found here, so this model was modified.

2.6.3 Compressor mass flow model

This part of the model predicts the corrected mass flow (*CMF*) from the compressor given a certain pressure ratio (total-total, π) and a corrected speed (*CSP*). The model consists of first and second-degree polynomials that are connected. The model is fitted to performance data by looking at isolines in *CSP*, which is often the way the data is illustrated in the performance maps. Each isoline (*i*) is fitted to a second-degree polynomial with three coefficients:

$$\pi = C(i,1)\cdot CMF^2 + C(i,2)\cdot CMF + C(i,3) \qquad \text{Eq.76}$$

Given a certain isoline there is a maximum pressure ratio and this maximum is assumed to correspond to the surge[9] point at this speed. The surge point (CMF_S, π_S) together with the second-degree coefficient, A_π is simply another way to describe each isoline:

$$\begin{cases} CMF_S(i) = -C(i,2)/\left(2\cdot C(i,1)\right) \\ \pi_S(i) = C(i,1)\cdot CMF_S^2 + C(i,2)\cdot CMF_S + C(i,3) \\ A_\pi(i) = C(i,1) \end{cases} \qquad \text{Eq.77}$$

The surge point and the second-degree dependence for all isolines are then fitted against *CSP*. The pressure ratio and mass flow points of this surge line are assumed to depend on *CSP* only and the fit is done so that good extrapolation capabilities is achieved i.e. if the pressure ratio is 1 and the turbo shaft speed is zero, then the mass flow should become nil. The following equations are used to achieve this.

$$\begin{cases} CMF_S/CSP = C_{cmfS}(1)\cdot CSP + C_{cmfS}(2) \\ (\pi_S - 1)/CMF_S = C_{\pi S}(1)\cdot CMF_S + C_{\pi S}(2) \\ A_\pi = C_{\pi A}(1)\cdot CMF_S^{\,2} + C_{\pi A}(2)\cdot CMF_S + C_{\pi A}(3) \end{cases} \qquad \text{Eq.78}$$

This means that there are 7 coefficients that represent the mass flow model for the compressor. When the model is used in the simulations a certain *CSP* gives the surge point and the second-degree dependence from Eq.78. At this moment the isoline is determined at the given *CSP* and the polynomial coefficients to this isoline can be determined by solving the system of equations in Eq.77. The mass flow becomes the roots to Eq.76. The model behavior

[9] The surge line is the boundary to instable operation regimes at low mass flows. If the flow is restricted to left of the surge line there will initially be a reversed flow in some of the compressor flow area. This reduces the pressure upstream compressor (unless the inlet manifold volume are enormous), the pressure ratio drops suddenly. But after this drop it is possible that the resulting operation point becomes to the right of the surge line, in the stable regime, which means that the pressure can be built up again. We get an oscillating, surging, operation, which in the long run destroys the compressor.

in the extrapolation region of the map is exemplified in Table 3. Note that for zero speed, a pressure ratio higher than one gives a flow in the reverse direction.

Table 3 Extrapolation region in the compressor map. Last point is however covered by the map and added to show the transition from "extrapolation" to "interpolation".

π	*CSP [1/s]*	*CMF [g/s]* model	π	*CSP [1/s]*	*CMF [g/s]* model
1	0	0	0,9	0	51,7
1	100	30,7	1,1	0	-51,7
1	250	66,7	1,05	250	44,2
1	500	146,2	1,2	500	43,9
1	1000	441,8	1,6	1000	285,9*

*) Map value: 275,6

Normally it is the maximum root of Eq.76 that should be selected. However, if the pressure ratio becomes higher than the surge pressure, we assume that surging occur, in addition the roots to Eq.76 becomes imaginary. This surging situation is handled here quite simple by reducing the mass flow quite heavily according to the scheme illustrated in Figure 22 so the simulation of surging operation becomes quite realistic. The basic principle is that a virtual pressure ratio, π' is calculated that is below π_S as much as π is above π_S. Then, a virtual mass flow, *CMF´* is calculated from π' and *CSP* with the model as normal and this time there will be a real, maximum root to Eq.76 which is *CMF´*. The estimated mass flow, *CMF* is then assumed to be below CMF_S as much as *CMF´* is above CMF_S. Another way to look at it is that it is the minimum instead of the maximum root that is selected at π'.

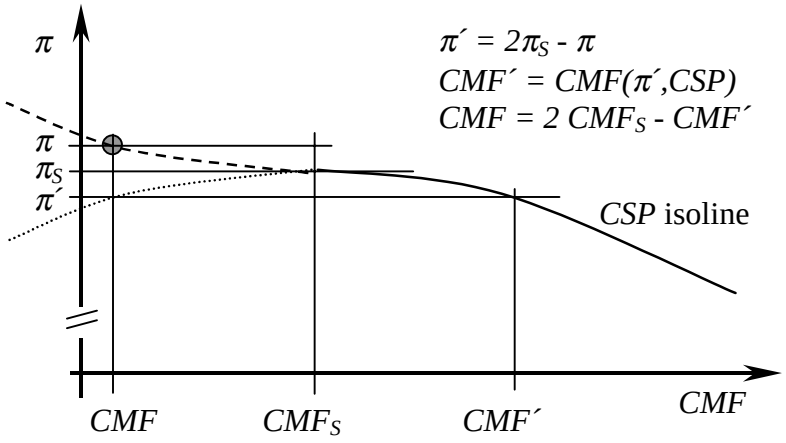

Figure 22 Handling surge operation (exaggerated figure). If the pressure ratio is higher than the surge pressure ratio, the estimated mass flow will become much lower than the surge mass flow, it can even become negative with this model. But it is more likely that when the mass flow drops heavily, so will also the pressure ratio, unless the inlet manifold volume is enormous.

2.6.4 Compressor efficiency model

The efficiency model works with a very similar principle and again, the isolines in corrected speed that are used for fitting the model to the data. The isentropic efficiency, η represent the

compressor effectiveness. Given an isoline in speed the efficiency is fitted to mass flow through a second-degree polynomial:

$$\eta = D(i,1)\cdot CMF^2 + D(i,2)\cdot CMF + D(i,3) \qquad \text{Eq.79}$$

The representation of this isoline is transformed to maximum efficiency, mass flow for maximum efficiency and the second-degree coefficient:

$$\begin{cases} CMF_{\eta Max}(i) = -D(i,2)/\left(2\cdot D(i,1)\right) \\ \eta_{Max}(i) = D(i,1)\cdot CMF_{\eta Max}(i)^2 + D(i,2)\cdot CMF_{\eta Max}(i) + D(i,3) \\ A_{\eta}(i) = D(i,1) \end{cases} \qquad \text{Eq.80}$$

These three coefficients are then fitted to three second-degree polynomials against corrected speed, this time without any extrapolation considerations since there is no obvious efficiency when pressure ratio is one and mass flow is zero. There are then 9 coefficients that define the efficiency model for the compressor. When using the model, the corrected speed gives the coefficients of the isoline through solving Eq.80 and the efficiency is the calculated directly by Eq.79, however efficiencies below 1% are not accepted. Note that the compressor can work like a turbine during speed up if the pressure ratio is below 1.

2.6.5 Turbine mass flow model

The turbine performance maps has also some sort of normalized or corrected parameters like the compressor. In this case mass flow parameter, MFP and speed parameter; SPP is selected as base for this model. Note that these parameters do not require any reference state[10]. This model is a little bit different than the compressor mass flow model, it requires no isolines and the fitting is done with the least square method of the following equation:

$$\pi = C(1)\cdot\left(MFP\cdot\pi\right)^2 + C(2)\cdot\left(MFP\cdot\pi\right) + C(3)\cdot SPP^2 + C(4)\cdot SPP + 1 \qquad \text{Eq.81}$$

The least square fit can be expressed in matrix terms as (n is the number of known points in the performance map):

$$\mathbf{y} = \pi(1\ldots n,1) - \mathbf{1}$$

$$\mathbf{A} = \begin{bmatrix} \left(MFP(1,1)\cdot\pi(1,1)\right)^2 & \left(MFP(1,1)\cdot\pi(1,1)\right) & SPP(1,1)^2 & SPP(1,1) \\ \left(MFP(2,1)\cdot\pi(2,1)\right)^2 & \left(MFP(2,1)\cdot\pi(2,1)\right) & SPP(2,1)^2 & SPP(2,1) \\ \vdots & \vdots & \vdots & \vdots \\ \left(MFP(n,1)\cdot\pi(n,1)\right)^2 & \left(MFP(n,1)\cdot\pi(n,1)\right) & SPP(n,1)^2 & SPP(n,1) \end{bmatrix} \qquad \text{Eq.82}$$

$$\mathbf{C}_{MFP} = \left(\mathbf{A}^T\times\mathbf{A}\right)^{-1}\times\mathbf{A}^T\times\mathbf{y} \quad [4 \text{ x } 1 \text{ matrix}]$$

$\mathbf{C}_{MFP}$ is the model representation; hence only 4 coefficients are required for the turbine mass flow model. Again, the model has good extrapolation qualities towards low mass flows as shown in Table 4. When using the model the mass flow parameter is the maximum real root to Eq.81.

[10] It seems strange that a reference state is ever required, even for the compressor maps. A reference state brings in unnecessary information into the performance data. There may be a historical or practical explanation.

Table 4 Extrapolation region in the turbine map. Last point is however covered by the map and added to show the transition from "extrapolation" to "interpolation". The first point with a pressure ratio below 1 is quite unrealistic for a turbine.

π	*SPP [1/(s·sqrt(K)]*	*10^3 · MFP model [g/s·sqrt(K)/Pa]*	π	*SPP [1/(s·sqrt(K)]*	*10^3 · MFP model [g/s·sqrt(K)/Pa]*
0,9	0	-23,7	1	10	13,3
1	0	0	1,1	15	28,6
1,1	0	15,2	1,2	20	38,3
1,2	0	25,7	1,3	25	44,6
1,3	0	33,3	1,4	30	48,8*

*) Map value: 48,2

2.6.6 Turbine efficiency model

The efficiency model is similar to the compressor efficiency model but more care is taken to the extrapolation problem. Isolines for different constant pressure ratios are used to fit the data. Given a constant pressure ratio, efficiency are fitted against *SPP* in the following equation, which can be done through a linear fit against η/SPP:

$$\eta = SPP \cdot \left(D(i,1) \cdot SPP + D(i,2) \right) \qquad \text{Eq.83}$$

This also means that if the speed is zero then the efficiency also becomes zero regardless of the D-coefficients, which seems to comply with the performance maps as well. Again this isoline representation is transformed by calculating the maximum efficiency and the corresponding speed parameter:

$$\begin{cases} SPP_{\eta Max}(i) = -D(i,2) \big/ \left(2 \cdot D(i,1) \right) \\ \eta_{Max}(i) = SPP_{\eta Max}(i) \cdot \left(D(i,1) \cdot SPP_{\eta Max}(i) + D(i,2) \right) \end{cases} \qquad \text{Eq.84}$$

These "coordinates", $SPP_{\eta Max}$ and η_{Max} are then fitted against pressure ratio through second-degree polynomials, which means that there are 6 coefficients that define the efficiency model for the turbine.

2.6.7 Model accuracy

When using the model, the pressure ratios, the upstream gas temperature and rotational speed are used to calculate the mass flow through the device (turbine and compressor respectively) and the resulting shaft work, or shaft power. In addition the isentropic enthalpy is required to calculate the temperature downstream the device. This resulting work then accelerates the turbo shaft according to the total inertia (assumed) of the shaft. This inertia has a great effect on the response of the system. So when determine lack of fit it is important to make the comparison as the model is supposed to be used i.e. from speed and pressure ratio determines mass flow and efficiency.

There exist numerous of factors that limit the turbocharger model from giving a correct description of a real turbocharger. First of all, the performance data itself who often are determined from very few individual compressors and turbines, perhaps not even in engine like operation. Then we have a lack of fit of the model and its limitation of handling some phenomena, in this case there has not been taken any special measures to handle choking on either compressor or turbine, although some is already handled in the model itself. Choking

means that the flow reaches sonic velocities and the flow will not depend on the pressure ratio.

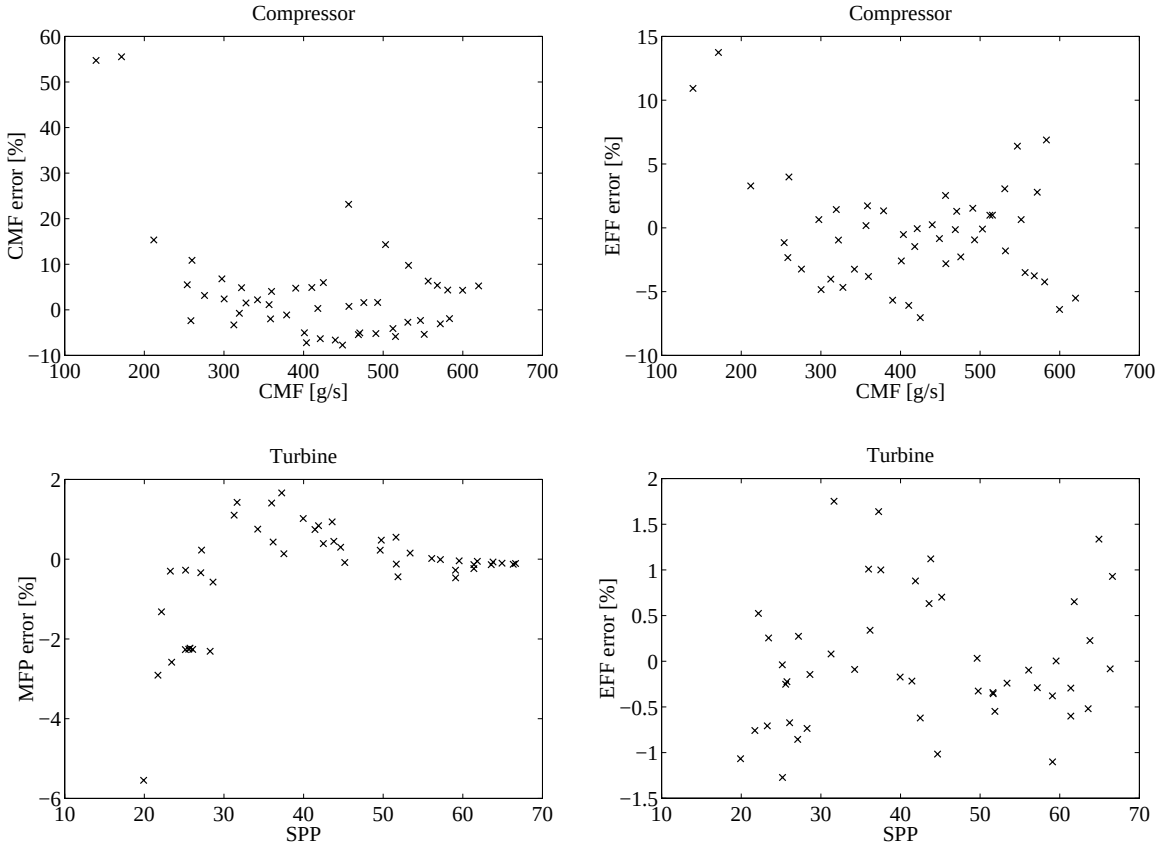

Figure 23 Turbo model fit to performance maps. Mass flow – left, efficiency – right, compressor – top and turbine – below.

At this stage, the lack of fit is the only possible error to study. Measurements could have been useful if turbine speed was measured. In Figure 23 is a fit to a compressor and turbine for a truck-size diesel engine shown with lack of fit plots. The turbine model show excellent agreement, the compressor model does not show that good agreement. It must be pointed out that close to surge a small deviation in pressure ratio will lead to big change in mass flow and that can explain the poor agreement in some points, unfortunately the points with the poorest agreement are in the low load region.

2.6.8 Improved model using interpolation and extrapolation techniques

Despite the great effort of searching for a proper and general model for the turbocharger an exact fit of the map data is not possible as seen earlier. There will be better fit in some operating regions than in others. To overcome some of this error a combination of interpolation techniques and modeling is tested. Given the corrected speed value, *CSP*, the speed-isoline at this speed is first determined by finding the closest isolines from the map at speeds over, CSP_2 and below, CSP_1 the actual speed. These are fit by 3´rd degree polynomials:

$$\pi_C\big|_{CSP1} = p_3(CMF) \qquad \pi_C\big|_{CSP2} = p_3(CMF)$$
$$\eta_C\big|_{CSP1} = p_3(CMF) \qquad \eta_C\big|_{CSP2} = p_3(CMF) \qquad \text{Eq.85}$$

The coefficients for each isoline are then weighed together against speed according to a factor:

$$x = \frac{CSP - CSP_1}{CSP_2 - CSP_1} \qquad \text{Eq.86}$$

Once the new isoline is determined, the problem is to select the correct root of the polynomial. Here it is assumed that it is the maximum root that is the correct one, which makes it important that the isoline really decreases at higher mass flows.

In order to handle surge operation it is assumed that the point with lowest mass flow in each isoline corresponds to the surge point. This point is weight against CSP in the same manner as the coefficients. (Surging is treated as previous model as seen in Figure 22.) Given the new mass flow, the efficiency can be calculated directly.

When moving into the low load regions (indicated by question marks in Figure 21) the isoline with the lowest speed is shifted parabolic in the y direction and linear in the x direction by moving the surge point according to:

$$\begin{cases} CMF_S = CMF_{S,1} \cdot \dfrac{CSP}{CSP_1} \\ \pi_S = 1 + C_S \cdot CSP^2 \qquad C_S = \dfrac{\pi_{S,1} - 1}{CSP_1^2} \\ \eta_{C,S} = \eta_{C,\min} + CSP \cdot \dfrac{\eta_{C,S,1} - \eta_{C,\min}}{CSP_1} \end{cases} \qquad \text{Eq.87}$$

The isolines (pressure ratio and efficiency) is moved and interpolated again to a 3'rd degree polynomial that is used in the same way as the interpolated line. A figure explaining the interpolation and extrapolation scheme is shown for an arbitrary compressor in Figure 24.

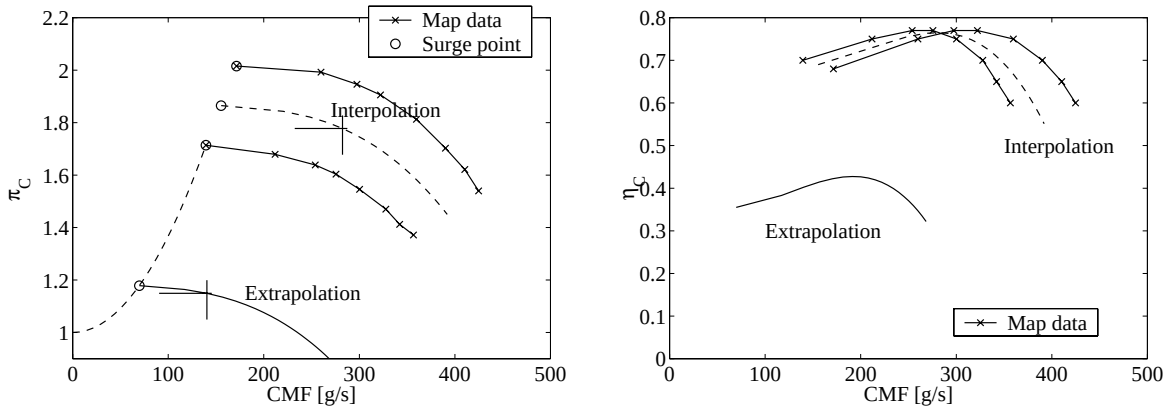

Figure 24 Improved compressor model. Interpolation and extrapolation of mass flow (left) and efficiency (right). The isolines with the two lowest speeds of the map data are shown.

The turbine model is improved in a similar way but it is more straightforward to use. Given a certain pressure ratio the isolines in pressure ratio above and below the actual isoline is determined and these isolines are fitted to 2'nd degree polynomials (turbine data is usually less complex than for compressors):

$$\begin{aligned} MFP\big|_{\pi T,1} &= p_2(SPP) & MFP\big|_{\pi T,2} &= p_2(SPP) \\ \eta_T\big|_{\pi T,1} &= p_2(SPP) & \eta_T\big|_{\pi T,2} &= p_2(SPP) \end{aligned} \qquad \text{Eq.88}$$

These isolines are then weighed together according to a factor *x*:

$$x = \frac{\pi - \pi_{T,1}}{\pi_{T,2} - \pi_{T,1}} \qquad \text{Eq.89}$$

The speed the directly give the mass flow. If extrapolation is required, the two isolines with the lowest pressure ratio are used to calculate mass flow at zero speed (SPP = 0), MFP_{01} and MFP_{02} respectively. Together with the point were the turbine is in rest, (SPP = 0, MFP = 0, π_T =1), a 2'nd degree polynomial can be fitted for zero speed. Given the actual pressure ratio a new mass flow at zero speed can be calculated, MFP_0 . The isoline with the lowest pressure ratio is then moved in the y-direction according to this value. The efficiency for this isoline is shifted in a linear manner simply by scaling against the pressure ratio. It is assumed that the efficiency is corresponding to a small value ($\eta_{T,min}$ = 1%) when the turbine is at rest. The geometrical interpretation in the performance map is shown in Figure 25.

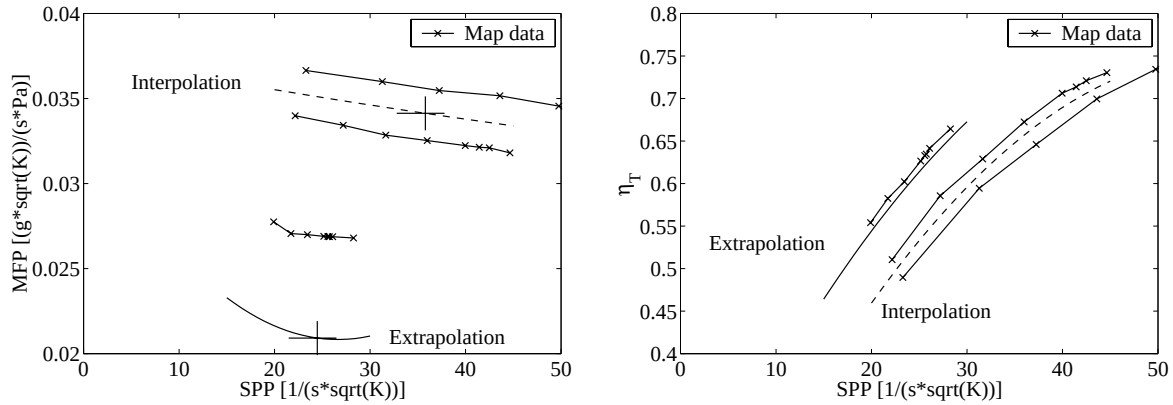

Figure 25 Interpolation and extrapolation of the turbine performance map, mass flow parameter (left) and efficiency (right).

This improved model show much better agreement to the map data due to the interpolation technique, as seen in Figure 26 and Figure 27. There is still some points in the compressor map that has a quite high error, it should be pointed out that it will be difficult to predict the mass flow close to the surge line; a small deviation in pressure ratio give a big change in mass flow.

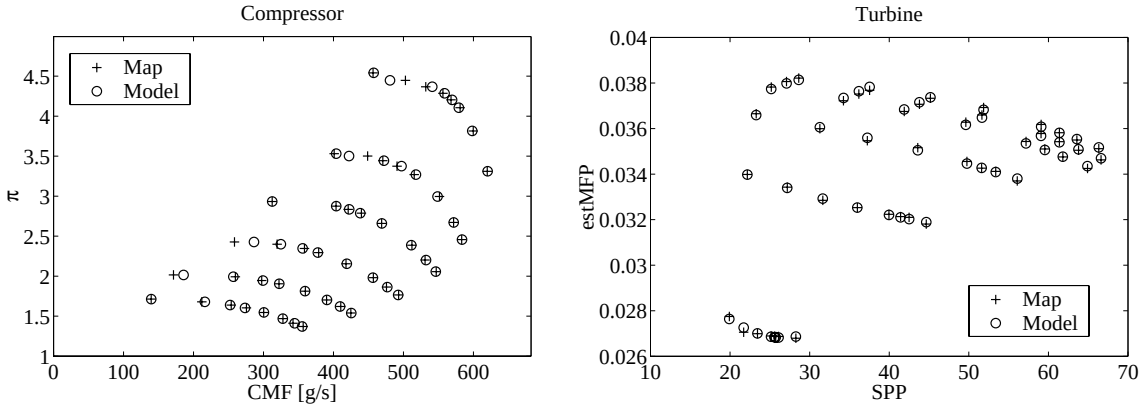

Figure 26 Improved model, fit to performance data

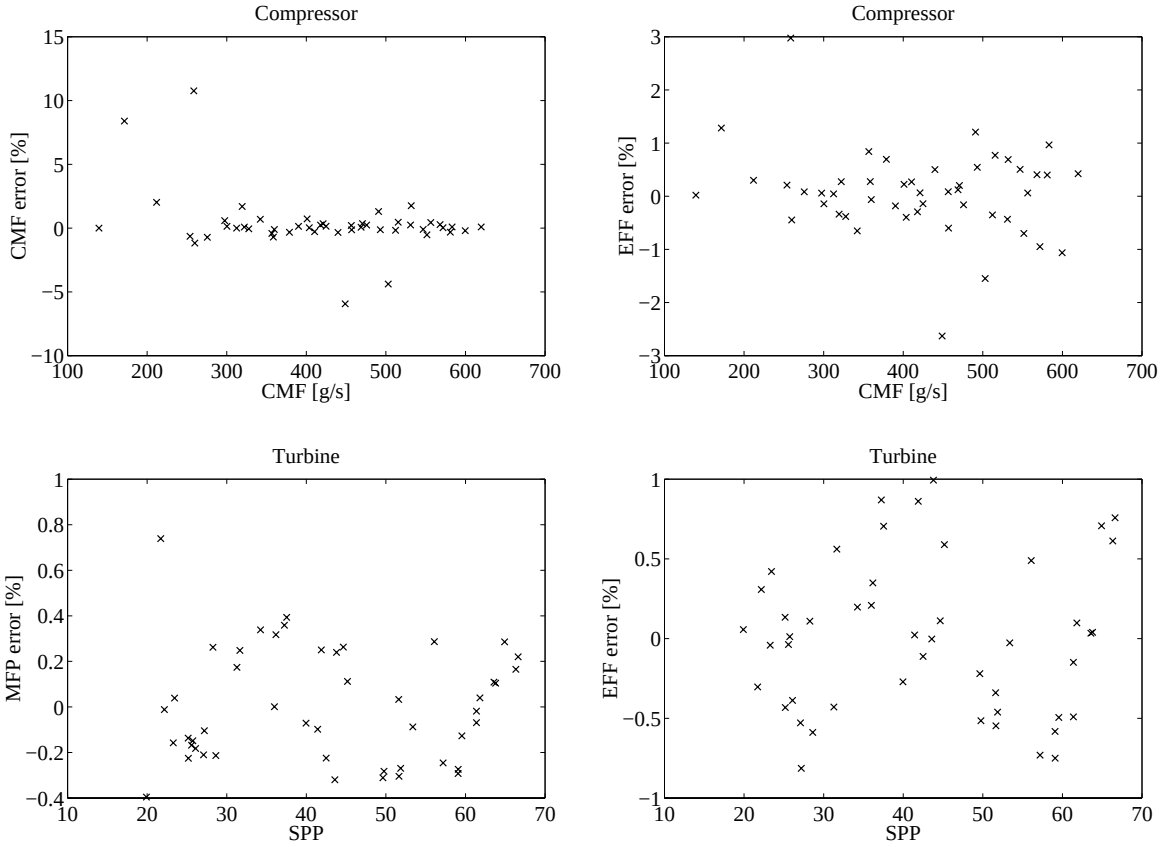

Figure 27 Improved turbo model, fit to performance maps. Mass flow – left, efficiency – right, compressor – top and turbine – below.

2.6.9 Governing equations

In the system calculation the mass flow and efficiency is determined from pressure ratio and speed. The mass flows and efficiencies is then used to calculate the power transformed in the turbine and compressor:

$$\dot{W}_C = -\dot{n}_C \cdot (h_2 - h_1)$$
$$\dot{W}_T = \dot{n}_T \cdot (h_3 - h_4) \qquad \text{Eq.90}$$

The resulting (accelerating) work on the turbocharger axis is then calculated and it results in a changed kinetic energy and hence a rotating speed:

$$\partial W = \left(\eta_{mech.} \cdot \dot{W}_T + \dot{W}_C\right) \cdot \partial t$$
$$\omega_2 = \sqrt{\omega_1^2 + \frac{2 \cdot \partial W}{J_{TC}}} \qquad \text{Eq.91}$$

The calculation proceeds as follows:

1. Given a pressure ratio and a speed the mass flow and efficiency is determined, either from interpolation in maps or through a model.
2. The pressure ratio and the temperature before the compressor/turbine are used to calculate isentropic temperature after the compressor/turbine, which also gives the isentropic enthalpy.

3. The efficiency then gives the real enthalpy and together with the mass flow the work needed/developed in the compressor/turbine is calculated.
4. The difference in work between compressor and turbine then gives an accelerating work, torque or power.
5. Depending on the inertia of the turbo-shaft, the new rotating speed can be calculated.

With the numerical method described earlier, it is appropriate to use mean state values of pressures, temperatures, sped and mass flow over one time-step.

2.6.10 Comments

Despite the good behavior of the turbocharger models, the low-mass flow, or low load, region there has to be some caution when using the models for the turbocharger. Especially since it is not clear what happens with the efficiency when extrapolating in this region. The more the maps are covering; the better the model become. The low load region should also be given special attention because it set the possibilities to reach higher loads. Depending on turbocharger performance and what is possible to achieve in exhaust temperature and mass from the engine, the performance in the low load region determine if the speed and thereby the boost pressure become higher or not. It is like a threshold. In some engines or applications, the engine operating range is limited, then the mass flow and energy of the exhaust gas is limited, and perhaps not sufficient to accelerate the turbo so that boost pressure increases. An example of this can be found in the experimental work by Olsson [68], where the air-fuel ratio cannot be reduced due to fast combustion and thereby limits the exhaust temperature. The inlet pressure does not exceed 1.05 bar in this case.

The reason why the models are not tested on a variety of compressors and turbines is that there is very few of these are distributed freely. The manufactures are not willing to give everyone free access to these, probably due to several reasons. The major one is probably to protect the manufactures own consultant activity.

In this work, *constant-pressure turbocharging* is considered, compared to the *pulse-loading turbocharging*. The geometrical difference is shown schematically in Figure 28. In constant pressure turbo-charging, an exhaust manifold with significant volume is inserted between the engine and turbine collecting the exhaust gas from all cylinders. It has one exit to the turbine that then will work with a constant upstream pressure (constant pressure ratio). In the pulse loading system, this volume is very small, the turbine is mounted very close to the exhaust port so that the pulse from blow-down is directly transferred to the turbine. It becomes important to design the manifold properly on a multi-cylinder engine; turbines with two entries are often used on 6-cylinder engines with pulse loading system.

Watson and Janota [109] and Heywood [96] state that there will be a loss of kinetic energy when high velocity gas from the blow-down, mixes with low velocity gas in a constant-pressure system. However, the kinetic energy from the pulses are not lost completely, this energy must be, at least to some extent, transformed via turbulence to heat, increasing the overall temperature in the exhaust manifold, providing more energy to be transformed in the turbine. The part that remains in turbulence through the turbine is the real loss. In pulse-loading turbocharging, the high kinetic energy of the blowdown pulse is directly transferred to the turbine. The idea is that the high pressure at EVO is transferred to the turbine through a small exhaust manifold with very small losses. However, it is not clear that a pulsating but higher energy level is of benefit; the turbine and turbine entry must be designed properly to handle this flow.

There are two other good reasons why pulse-loading system is better. The response of the system is faster, because of the fast acting of each pulse into the turbine (compare with *pressure wave supercharging*, the *Comprex* charger, with even faster response). The heat transfer in the exhaust manifold is probably smaller due to the smaller volume and surface area of the exhaust. However, these advantages depend on the success of the design of the turbocharger system, how well the turbine is designed for this pulsating flow from a multi-cylinder engine and how well the exhaust pipes are designed with respect of the number of cylinders and firing order.

If a pulse-loading system should be simulated, the dynamics of the exhaust pipes should be handled as well. It also requires that the performance data for the turbine is determined under similar pulsating flow. This is often not the case. The constant-pressure model is used here regardless of what the real system is, due to its simplicity and that the turbine performance data is determined under steady state flow, but it is important to remember the limitations of this approach.

Turbocharger related phenomena like surging and choking is quite difficult to correctly handle in this type of simulations. A simple method of handling surging operation is employed, however far from validated. Choking occur when the velocities become sonic, then the mass flow will more or less depend on the pressure ratio only, choking are normally treated in the performance maps. Compressor choking is not treated at all.

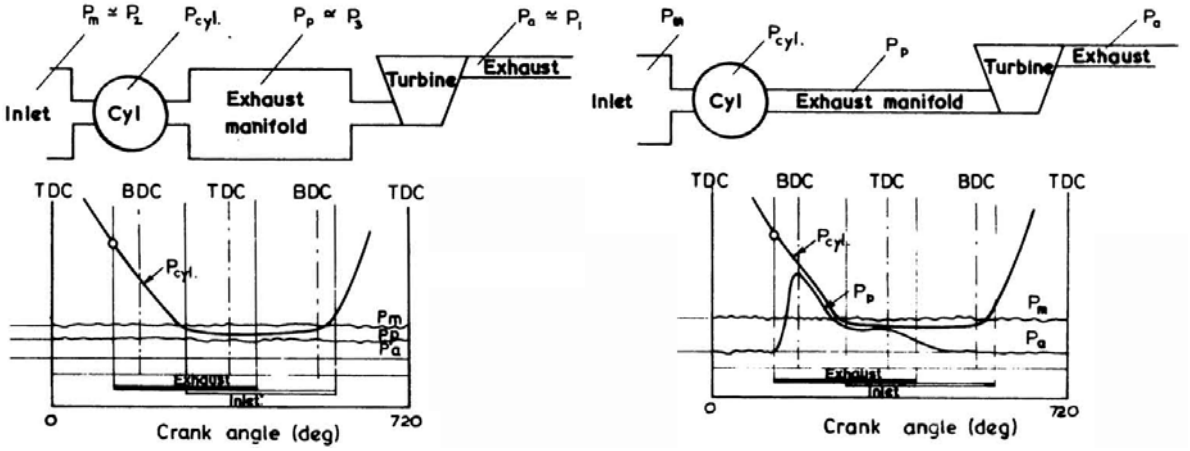

Figure 28 Constant pressure turbocharging (left) and pulse-loading system (right). From Watson and Janota [109].

2.7 Manifold models

The inlet and exhaust manifolds are volumes where different components are connected. These volumes provide pressures, temperatures and mixtures for the other components e.g. the inlet manifold has a certain pressure that affects the mass flows trough the compressor and engine. The manifolds are assumed well-stirred volumes and the thermodynamics of the manifolds are assumed to follow the first law and the ideal gas law according to the general assumptions described earlier. The modeling determines a new pressure and temperature after a period (time-step), given the mass flow to and from the volumes. Both the mixture and temperature of the flowing media has to be considered. With the numerical method used here, the mass flow trough other components are calculated under mean value assumptions and it becomes the role of the manifold model to provide the points that are used for these mean values.

Eq.44 become:

$$\partial Q\left(\overline{T},\overline{p},...\right)+\sum \partial n_{IN}\cdot \overline{h}_{IN}+\sum \partial n_{OUT}\cdot \overline{h}_{OUT}\approx H\left(T_{i+1}\right)-H\left(T_i\right)-V\cdot\left(p_{i+1}-p_i\right) \qquad \text{Eq.92}$$

Again, the new enthalpy is calculated and the ideal gas law Eq.18 is then used to calculate the pressure in the (i+1) point.

If the numerical method described earlier for solving differential equations is used, then some numerical damping of the calculations are often required in order to obtain convergence. The easiest way to this is only allowing, for example, 1/10 of change in manifold pressure and temperature, compared to what the direct calculation give. This damping does not affect the results since the system is calculated in an iterative way, however it increases computational time. This damping should also be set with respect of what time resolution that is chosen. This affects the resolution in time for the simulations. Higher resolution (smaller steps in time) requires smaller damping in general. If dynamic processes are of interest, then of course, the resolution should be set quite high. A good start value to test with is 0.1s steps, which is sufficient if some dynamics should be treated as well, another more general solution is to vary the resolution depending on the number of iterations needed.

2.7.1 Inlet manifold

Into the inlet manifold flows in general pure air from e.g. compressor, fuel from fuel injectors and EGR from exhaust via an EGR valve. In this work, it is assumed that all liquid fuel vaporization takes place in the inlet manifold if port fuel injection is used. Heat transfer is neglected but it is quite easy to insert heat transfer if needed (e.g. as shown in Exhaust manifold below). The cooling effect of vaporizing fuel is simply calculated as:

$$\partial Q=-\dot{n}_{fuel}\cdot M_{w,fuel}\cdot Q_{vap,fuel}\cdot \partial t \qquad \text{Eq.93}$$

2.7.2 Exhaust manifold

The exhaust manifold connects the exhaust ports of the engine (see section 2.5.3) with turbine and waste gate valve, if one is used. In addition, the EGR gases are taken from the exhaust manifold. A heat transfer model for the exhaust manifold is used developed by Malchow, Sorenson, and Buckius (1976, as reviewed by Ferguson [101]) and the basic equation for this model is:

$$Nu=0.0483\,\mathrm{Re}^{0.783} \qquad \text{Eq.94}$$

This model is actually derived for straight tubes with D/L = 0.3 only but are used here as a general model anyway in order to limit input data. A constant convective heat transfer coefficient is applied on the outside of the manifold and is set to 15W/(m^2K). Mean values of mass flow are used when calculating Reynolds number. The surface areas of exhaust ports and manifolds are set to a value that seems to represent the real engine. The temperature distribution over the exhaust manifold wall is illustrated in Figure 29. The temperatures both inside and outside the manifold walls and the heat flux are calculated under the assumption that the manifold wall is described as a plate. The heat transfer relation's ends up with a system of equations with three unknowns, which is quite easy to solve.

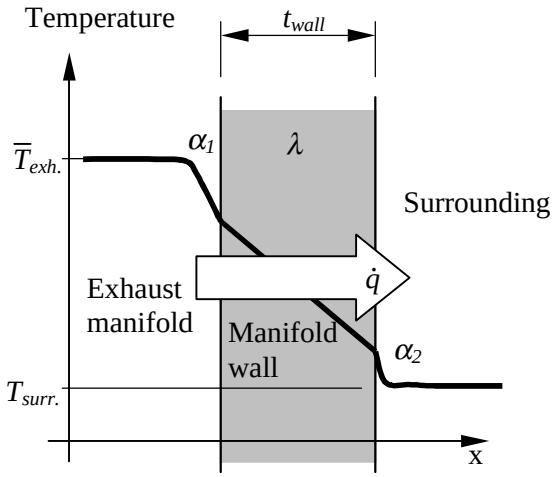

Figure 29 Schematic temperature distribution over exhaust manifold wall

2.8 Charge air cooler (Intercooler) model

A model for charge air coolers (CAC) is developed, however verified against very limited data. The model is based on weighing two different models, first the simplest possible relation for an optimum, ideal heat exchanger:

$$T_{2,CAC,ideal} = T_{0,CAC} \qquad \text{Eq.95}$$

$T_{2,CAC}$ is the exit temperature of the air that is to be cooled and $T_{0,CAC}$ is the coolant temperature (surrounding air temperature) before entering the coolant side of the charge air cooler.

The other model is based on a residence-time view, the longer the gas stays in the CAC, the closer it comes to the CAC coolant temperature. Consider a portion of air, a virtual control volume or its mole representation, n [mol], equal to the flow times the residence time, τ [s], as illustrated in Figure 30.

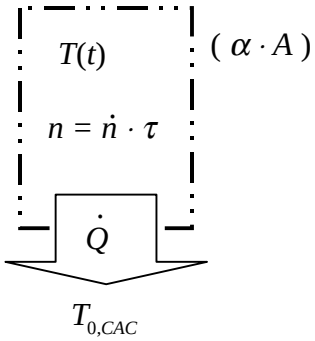

Figure 30 Virtual control volume for residence time dependant CAC model

Assume also that this volume has a certain heat transfer coefficient (αA) [W/K], which is determined for different charge air coolers, by fitting the model to data. Heat balance for the control volume then gives a differential equation for the temperature development during the residence time:

$$-\dot{T} \cdot \overline{C_p} \cdot \dot{n} \cdot \tau = (\alpha \cdot A) \cdot \left(T(t) - T_{0,CAC}\right) \qquad \text{Eq.96}$$

This can easily be solved with the boundary conditions of inlet and exit temperatures, corresponding to t = 0 and t = τ respectively, and with steady state assumptions, resulting the following expression for exit temperature:

$$T_{2,CAC,\tau} = T_{0,CAC} + \left(T_{1,CAC} - T_{0,CAC}\right) \cdot \exp\left(-\frac{(\alpha \cdot A)}{\overline{C_p} \cdot \dot{n}}\right) \qquad \text{Eq.97}$$

The two expressions Eq.95 and Eq.97 are weighed together with a constant, *K*, and the resulting CAC model become:

$$T_{2,CAC} = K \cdot T_{2,CAC,ideal} + (1-K) \cdot T_{2,CAC,\tau}$$

$$T_{2,CAC} = T_{0,CAC} + (1-K) \cdot \left(T_{1,CAC} - T_{0,CAC}\right) \cdot \exp\left(-\frac{(\alpha \cdot A)}{\overline{C_p} \cdot \dot{n}}\right) \qquad \text{Eq.98}$$

When the mass flow is very large, then Eq.98 becomes:

$$T_{2,CAC} \approx T_{1,CAC} - K \cdot \left(T_{1,CAC} - T_{0,CAC}\right) \qquad \text{Eq.99}$$

This relation indicates that *K* can be seen upon as minimum heat exchanger efficiency at high flows. When the flow is very small, then Eq.98 become close to the ideal heat exchanger:

$$T_{2,CAC,ideal} \approx T_{0,CAC} \qquad \text{Eq.100}$$

An example where *K* and (αA) is fitted to measured CAC data are shown in Figure 31 where also the pressure drop are fitted against corrected mass flow, representing a very simple model for the pressure drop over the charge air cooler.

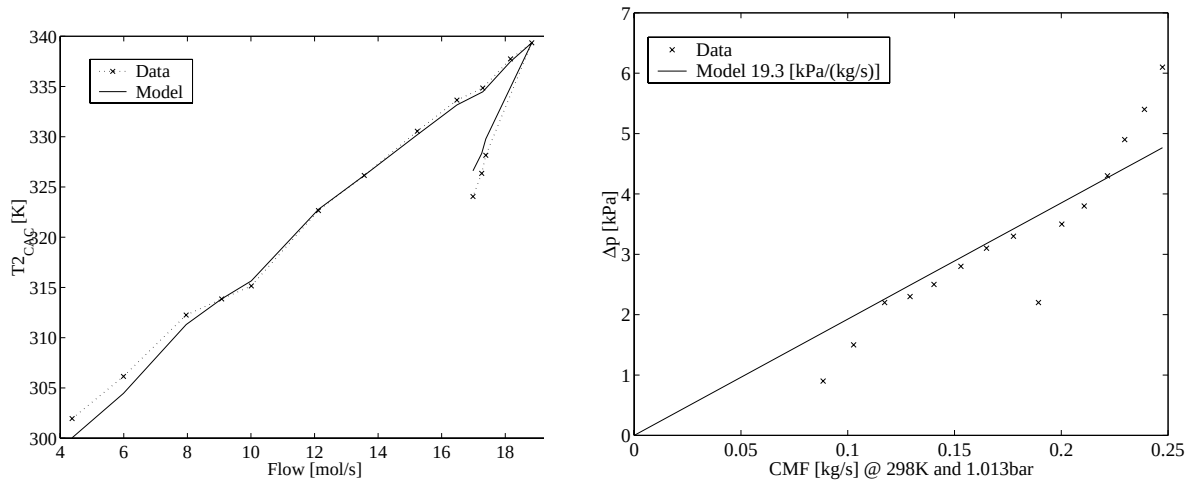

Figure 31 Example of CAC model in comparison with measured data, note that temperature varies before the charge air cooler ($T_{1,CAC}$.). Measurements are made on a charge air cooler for a SCANIA DSC12 diesel engine.

2.9 Humidifier

In order to simulate the Humid Air Motor concept a humidifier has to be modeled. The humidifier adds water to the inlet air after the compressor. This air has an elevated pressure and temperature so it has a capability to can carry substantive amount of water vapor (steam). Liquid water is pumped to the top of a humidification tower as illustrated in Figure 32, before it enters the humidifier it is heated (if necessary) through a heat exchanger, heat can be taken from either the coolant system of the engine or the engine exhaust. The purpose of this preheating is to get above the saturation temperature in the humidifier entry. Depending on this heating, the temperature and water content will change in the humidifier exit. The pumping work for the liquid water become more or less insignificant compared to engine delivered power. In the humidifier, the air is cooled down and the water content increases due to the vaporization. Some of the liquid water passes down through the humidifier (against the direction of the airflow) is not vaporized and is collected in the bottom of the humidifier. This water is then recirculated. The air after the humidifier will have a high relative humidity, close to 100%.

The purpose of the humidifier model is to predict the water content and the temperature of the air leaving the humidifier. The required input are the airflow, temperature and composition in the entry, the liquid water temperature and the pressure (assumed uniform in the humidifier). Further more, an estimation of the relative humidity on the humidifier exit is required, i.e. an estimation of how "good" the humidifier is.

The humidifier layout is simplified a little bit, as shown in Figure 32, by removing the heat exchanger and use only a single entry for the water i.e. the water flow correspond to the vaporization rate. This gives maximum cooling of the air. If circulation and higher water flow is used, like in the original design, the temperature on the exit will increase corresponding to a heating of the media, and more water will be vaporized due to this temperature increase.

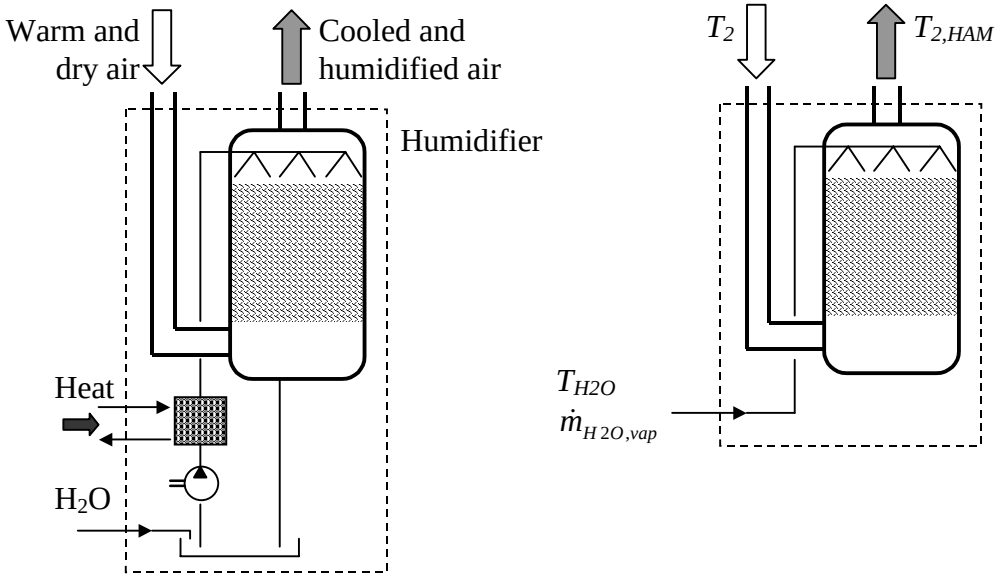

Figure 32 Schematic layout of the humidifier (left) and simplified representation (right)

It is quite clear that an iterative approach is required since both the water content and temperature is to be predicted, and they are dependent on each other. The thermodynamic properties are again calculated with the NASA-polynomials. The data for liquid water is only valid up to 500K, but this limit is above what we expect from the compressor (about 450K at

2 bar boost pressure). In addition, the liquid – vapor saturation curve is required. The Antoine equation used to calculate the vapor pressure given the temperature. The parameters, coefficients *A*, *B* and *C*, are taken from data reviewed by NIST Chemistry Webbook [110] (selection: Bridgeman and Aldrich, 1964).

$$\log_{10}\left(p_{sat.}\right) = A - \left(\frac{B}{T + C}\right) \qquad \text{Eq.101}$$

The water molar fraction is calculated trough:

$$x_{H2O} = \frac{p_{sat.}}{p} \cdot \varphi \qquad \text{Eq.102}$$

The calculation procedure for the humidifier follows:

1. Determine the enthalpies for the air in the humidifier entry and the liquid water. Note that the enthalpy representation must include heat of vaporization.
2. Guess an exit temperature, $T_{2,HAM}$ (previously value)
3. From the assumed relative humidity, φ, pressure, p, and (guessed) temperature, in the exit of the humidifier, calculate the water content through Eq.101 and Eq.102.
4. The mass flow of air and calculated water content on the exit gives the water vaporization rate (mass balance) and the exit mixture.
5. Given the enthalpy and mass flow of air and the enthalpy and vaporization rate of the liquid water, the enthalpy of the humidified air can be calculated (energy balance).
6. The mixture and enthalpy of the humidified air give a new exit temperature through Eq.24.
7. The steps 3 to 6 are iterated until stable exit temperature. Numerical damping is used, the newly calculated temperature is not allowed to change too much after each iteration (does not affect the results).

After this iterative process the temperatures, mass flows and gas mixtures are known for the humidifier.

2.10 Other components

2.10.1 Heater

When simulating HCCI engine system it is sometimes necessary to include an inlet air heater in the system. This can be done by inserting a heat-source and a pressure drop. The pressure drop can be modeled as in the charge air cooler described earlier. Input to this model would then be the mass flow and the heating power. The exit temperature, $T_{2,HTR}$ is calculated from the exit enthalpy as shown in Eq.103.

$$h\left(T_{2,HTR}\right) = h\left(T_{1,HTR}\right) + \frac{\dot{Q}_{HTR}}{\dot{n}} \quad \left[J/mol\right] \qquad \text{Eq.103}$$

$\dot{Q}_{HTR}$ [W] is the power of the heater (electrical power) and $\dot{n}$ is the flow [mol/s].

2.10.2 Wastegate

A waste gate valve is a component used for controlling boost pressure by affecting the pressure ratio over the turbine. The waste gate is simply modeled as a restriction with variable throat area and a constant discharge coefficient. The poppet-valve geometry (Figure 13) can be used and the mass flow is calculated trough equations Eq.50. Input to the model is valve opening (valve lift) and pressure ratio.

2.10.3 Engine control

This part is the least developed part in this work and is now only used to calculate fuel and EGR flow from desired values. I addition various heat release models are adjusted here e.g. when direct injected diesel engine are simulated, then the fuel injection duration has to be set.

3 Simple heat release

In this first step a simple heat release function (see sections 2.5.1 and 2.5.6) was adopted and fitted to measurements made on a single cylinder and on a 6-cylinder HCCI engine. The purpose was to validate the simulation software.

3.1 Validation of HCCI Cycle Simulation

This validation is a first step that is used to see if the cycle simulation can fit measured cycles. In this case, measurements on a single cylinder TD100 engine were used as reference. Comparison is made on pressure trace, and resulting parameters like exhaust temperature, indicated mean effective pressure and efficiency. Regarding measured pressure traces it must be pointed out that the measurements gave a relative pressure, which means that the pressure trace has to be calibrated so that if the measurement were made at atmospheric pressure the reading should be 1.023 bar. However, the pressure transducer has very good linearity, which means that indicated work could be calculated directly without knowing the absolute pressure since:

$$W_C = \oint_{cycle} p_{abs.} \cdot dV = \oint_{cycle} \left(p_{rel.} + p_{ref.} \right) \cdot dV = \oint_{cycle} p_{rel.} \cdot dV + \oint_{cycle} p_{ref.} \cdot dV = \oint_{cycle} p_{rel.} \cdot dV + 0 \qquad \text{Eq.104}$$

For comparison it is much more desirable if the absolute pressure is known but this is a little bit tricky to do, at least if a good agreement with reality is desired. There are several ways to do this:

- Assume a pressure at a certain CAD
- Assume an average intake stroke pressure
- From "simulation" of a part of compression stroke with a assumed $\gamma = C_p/C_v$ value

Here an average intake pressure, determined from transducer measurements (absolute pressure) in the intake manifold is assumed between 20 and 160 CAD ATDC during intake stroke. Mathematical expressed:

$$p_{abs.} = p_{rel.} - \overline{p_{rel.}\big|_{20-160CAD}} + \overline{p_{inlet}} \qquad \text{Eq.105}$$

The inlet pressure in the simulations are shifted a little bit to get a good agreement at the beginning of the compression stroke.

Below is a comparison of pressure trace expressed as pressure – CAD diagrams. As input to the simulation the heat release determined from measured traces are used through angles for 0, 10 and 90% burned fraction. The 0% burned fraction is estimated through angle for 1%, minus 1 CAD (the angle for 0% burned fraction is very difficult to determine experimentally). In addition, the combustion efficiency determined from exhaust gas

emission analysis is also used as input to the simulation. A question mark is the heat transfer and compression ratio. From analyzing pressure traces without firing the engine, the compression ratio was determined to be about 17.7:1 which is used in the simulations. Engine geometry is shown in Table 5. In this case, the heat transfer correlation of Woschni [104] is used straight off without any compensation. There seems to be only a small difference indicating that the compression ratio and heat transfer is properly estimated.

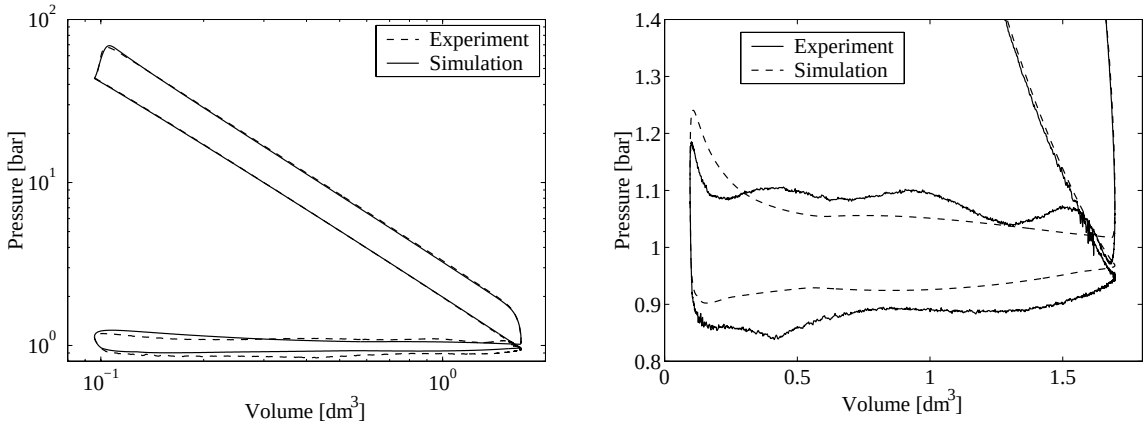

Figure 33 Comparison between simulation and measurement. Left - In-cylinder pressure against volume in log-log scale. Right – Gas exchange linear scale, note especially the difference during the intake stroke. Volvo TD-100 engine with HCCI combustion at approx. 1000rpm, $\lambda = 3$ with isooctane.

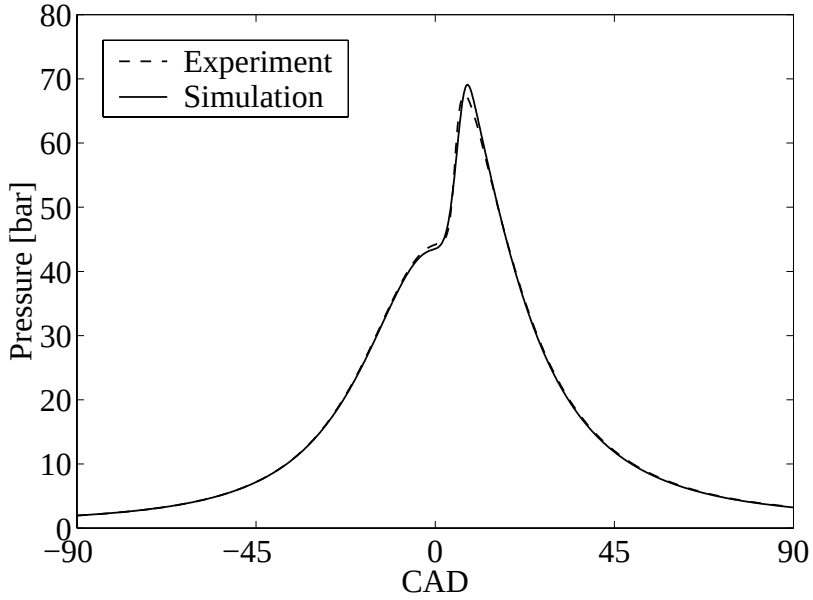

Figure 34 Comparison between measured and simulated in-cylinder pressure during late compression, combustion and early expansion.

Very good fit can be seen during compression and expansion stroke but the agreement is less during intake and exhaust stroke which is not that surprising since there is nothing in the simulated model that handles flow dynamics inside and outside the cylinder. Adding dynamics to the model would probably give much better agreement, but also longer computational time. It is always a compromise between levels of detail in the model and execution time; if more detail is to be considered it usually also requires more computational time.

It is also interesting to look at resulting parameters like indicated efficiency and indicated mean effective pressure (Table 6). Both indicated pressure, and especially efficiency, is overestimated. The difference in efficiency can be explained by the lower pump work required in the simulations despite the lower inlet pressure. The pressure inside the cylinder during the intake stroke is lower in the real engine compared to the simulated one. During the exhaust stroke there is no clear difference; the flow produces pressure oscillations in the experiments as shown in Figure 33. In summary, the difference is quite small and mostly dependant on the poor intake and exhaust stroke prediction.

Table 5 Engine geometry for the Volvo TD-100 engine used for HCCI experiments in Lund. The reference point (0°) for valve timings (zero lift) refers to combustion-TDC.

Bore	120.65mm	Camshaft	NG-SI
Stroke	140mm	EVC	-350
Conrod length	260mm	IVC	-140
Compression	varied	EVO	120
Cylinders	1	IVO	340

Table 6 Parameters and results

Input:	Measurement	Simulation	Results:	Measurement	Simulation
r_C	17.7:1	17.4:1	p_{inlet} [bar]	0.989	0.970
Speed [rpm]	994	994	$IMEP_{net}$ [bar]	3.201	3.226
λ	3.04	3.04	$IMEP_{gross}$ [bar]	3.395	3.355
T_{inlet} [K]	369	369	*PMEP* [bar]	0.194	0.130
$p_{exhaust}$ [bar]	1.015	1.015	$\eta_{i,net}$	37.5%	38.9%
η_c	91%	91%	$\eta_{i,gross}$	39.8%	40.5%

3.2 Validation of System Simulation – Diesel operation

A direct injected, six-cylinder SCANIA DSC12 turbocharged diesel engine with a displaced volume of 11.7 liter is simulated under varying speed and load (see Figure 35). In the simulations, speed and fuel injection time are adjusted linear during 4 seconds, then kept constant during 8 seconds and so on. The results from the simulations are then compared to stationary measurements on a real engine. Engine speed is set to be equal to the real engine and the fuel injection time is set to result in a fuel flow equal to the fuel flow measurements.

The simulation is made without any knowledge about the specifications of the real engine regarding injection strategy (injection timing is set to 10°BTDC in the simulations) or fuel injector characteristics (fuel rate is set to 30g/s per injector). Another difficulty is absence of heat release knowledge (the heat release factor k_{HR} is set to 300). However, some simulations were made first to set these parameters to realistic values, before presenting the results here.

The real engine uses pulse-loading turbocharging, which has not been possible to simulate correctly, due to model and data limitations, as discussed earlier. Instead, a constant pressure system is simulated.

In Figure 36 $IMEP_{net}$ and maximum pressure are shown. $IMEP_{net}$ shows quite good agreement, whereas the maximum pressure has become too high, which probably can be explained by somewhat early or fast heat release.

In the last point (at 72s), the boost pressure becomes too low, which can be a result of the difference in turbocharging technique, constant-pressure turbocharging in the simulations and pulse-loading turbocharging in the real engine. In this low speed, high load regime the pulse-loading technique probably results in higher turbine efficiency and thus higher boost pressure.

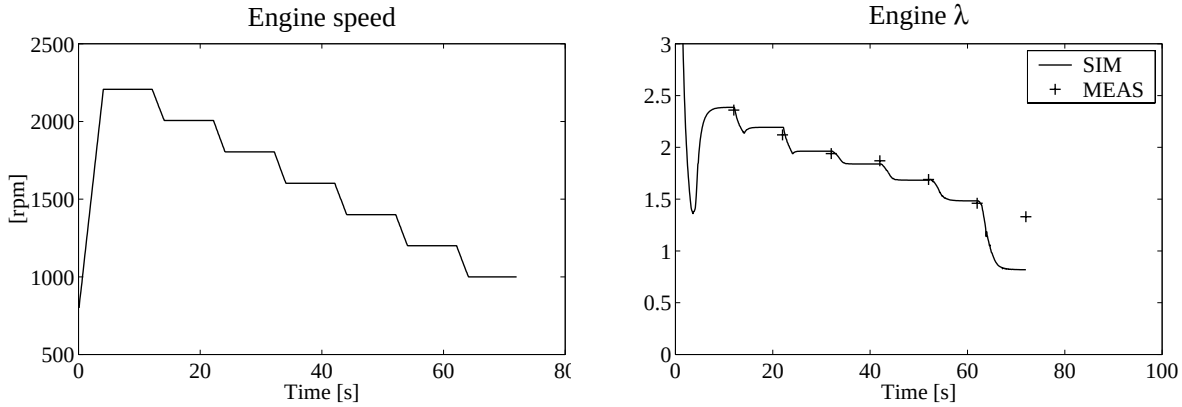

Figure 35 Engine speed (left) and calculated air-fuel equivalence ratio, λ (right). Note the good agreement in λ, indicating correct air and total mass flow to the engine. Notation: MEA (crosses)- experiments, and SIM (lines)- simulations.

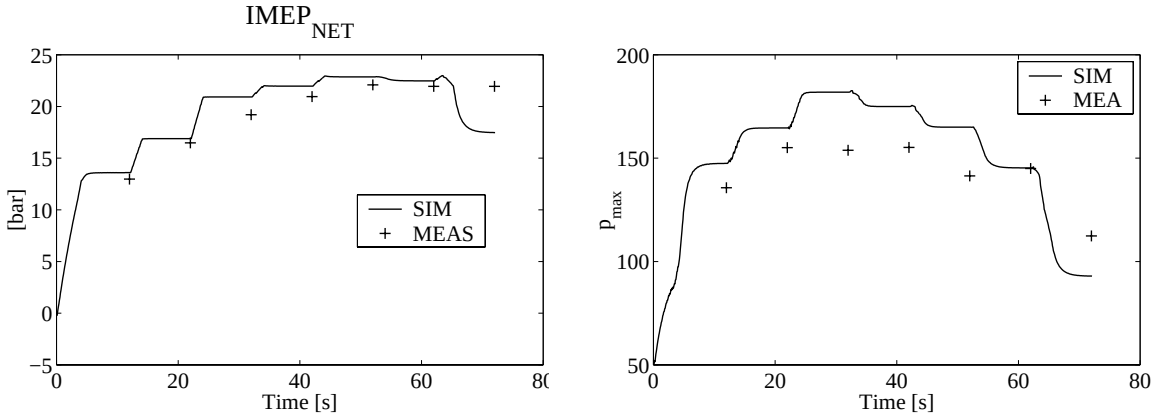

Figure 36 IMEP$_{net}$ (left) and maximum cylinder pressure (right).

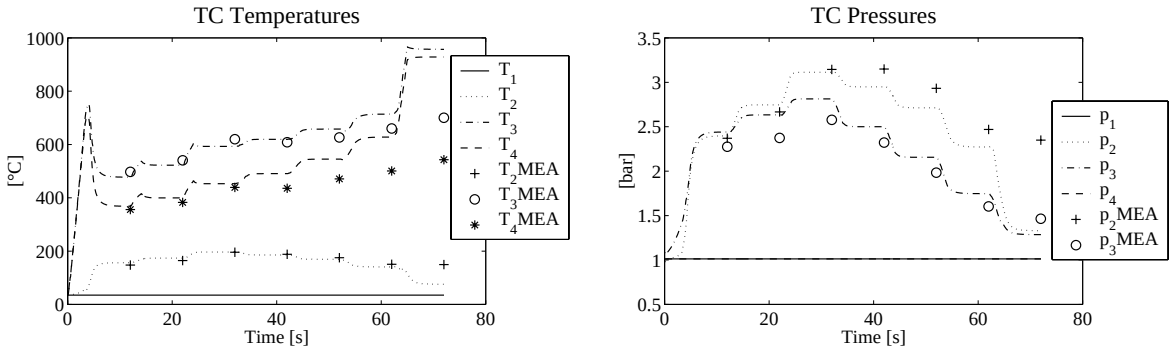

Figure 37 Temperatures (left) and pressures (right) around the turbocharger.
Notation: 1- before compressor, 2- after compressor, 3- before turbine and 4- after turbine.

In figure Figure 37, the temperatures and pressures before and after the turbocharger are shown. The temperatures show quite good agreement in the beginning of the simulation (high engine speeds). Later in the simulations, the temperature after the turbine becomes much

lower, and in the last point, the boost pressure becomes too low resulting in lower airflow into the engine and higher exhaust temperature. Please note that the measured pressures are static. Total pressure is a little higher depending on where the static pressures are measured. In the simulations, all pressures are total pressures. The difference in pressures cannot fully be explained by the difference between static and total pressure, especially on the inlet side (p_2), which is quite surprising since temperatures, air-fuel ratio and IMEP shows better agreement.

3.3 Validation of System Simulation – HCCI operation

The experimental work and the validation below were published at the SAE Fuel and Lubricants Conference in Baltimore 2000 [68]. The primary purpose was to demonstrate a working full-size multi-cylinder HCCI engine and to verify the calculations in the simulation software (ESIM). The experimental efforts were made by Jan-Ola Olsson and were sponsored through other channels.

A 6-cylinder turbocharged diesel engine (SCANIA DSC12, normally used in trucks) was modified to be operated as a HCCI engine by removing the diesel injectors and inserting low-pressure fuel injectors in the inlet manifold. The engine had 4 valves per cylinder so each cylinder had 2 inlet ports in which a fuel injector was mounted. Since each cylinder was fed with 2 fuel injectors it was possible to use two different fuels. The engine control system then handled the fuel injection individually for each cylinder and each fuel. All fuel injectors were mounted in a spacer between the cylinder heads and the original inlet manifold. In addition, an electrical inlet air heater (maximum power of 37kW) was used in some points to ensure ignition. The system is schematically shown in Figure 38. Iso-octane and n-heptane were used as fuel which makes it possible to run the engine on different research octane numbers, RON between 0 (n-heptane only) and 100 (iso-octane only), the mass percentage of iso-octane gives the RON number.

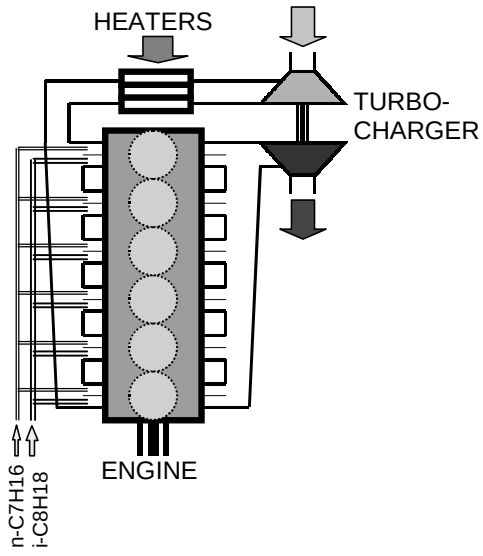

Figure 38 Engine system

Pressure transducers replaced the original fuel injectors in the cylinder heads, which gave an opportunity to monitor cylinder pressure during operation. These in-cylinder pressure traces were then evaluated by heat release analysis in order to find ignition timing and combustion duration. No other changes were made to the engine i.e. pistons, cylinder head, engine block were left unchanged. The properties of the engine are summarized in Table 7.

Validation was first made to find out how well cycle and system simulations fitted with experiments. The simulation software was fitted with a simple heat release shape function, Eq.106 originally developed by Wiebe (see section 2.5.1). This function gives an accumulated heat release expressed as burned fraction. The total amount of energy released (100%) depends on the amount of fuel present, the lower heating value of the fuel and the combustion efficiency.

$$x_b = 1 - \exp\left(a'\left(\theta - \theta_0\right)^{m'}\right) \qquad \text{Eq.106}$$

Table 7 Basic geometry of the SCANIA DSC 12 engine. Valve timings refer to zero lift.

Cylinders	6
Swept Volume, total	11 705 cm3
Compression Ratio	18:1
Bore	127 mm
Stroke	154 mm
Connection Rod	255 mm
Exhaust Valve Open	96° BBDC
Exhaust Valve Close	52° ATDC
Inlet Valve Open	54° BTDC
Inlet Valve Close	78° ABDC

This shape function was fitted to the experimental data from the heat release analysis, however not individually but as an average for each cylinder. It is possible to do simulation for each cylinder individually but that required longer computational time and also demands better models of inlet and exhaust manifold in order to become valuable. The crank angles for 10, 50 and 90% burned fraction (x_b) are used to fit the function and an example of such fit are shown in Figure 39.

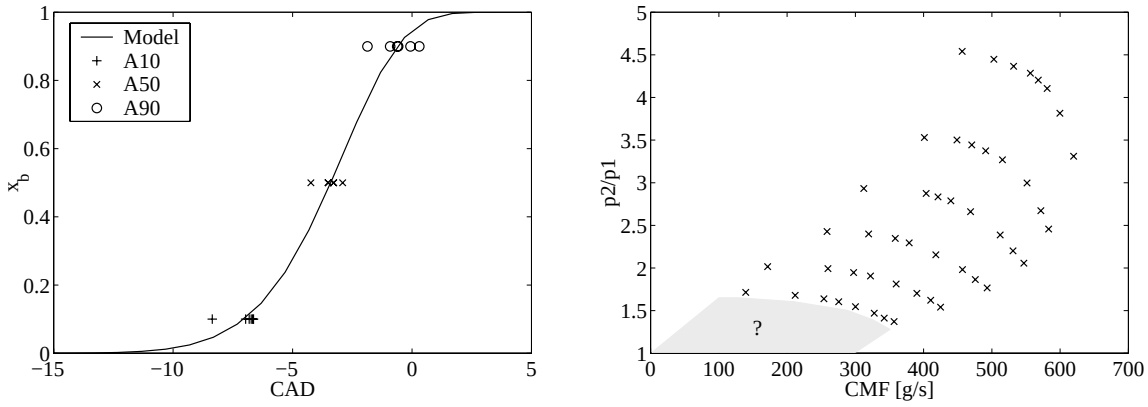

Figure 39 Left - Example of heat release fit at one operating point. Right - Compressor performance map that illustrates the problem at low mass-flow and pressure ratios. The "x" signs indicate isolines in turbine speed.

The engine was fitted with the original turbocharger (Holset HX50), which can be considered as well matched for diesel engine operation. In HCCI operation, the turbine was found too big. The compressor (map shown in Figure 39) was acceptable since the airflow should be about the same as in a diesel operation.

The turbocharger is an important engine component that has a great influence of the maximum power output of an engine. What it does is simply increasing the mass flow trough the engine and thereby increases the power output. The performance maps of a specific turbocharger relate pressure ratio, turbine speed, mass flow and isentropic efficiency, and cubic interpolation from tabled maps are used. Some extrapolation is needed at low mass flows and low-pressure ratios since the maps lack data in this region. This extrapolation becomes quite difficult and has to be done very precautious since this region directly sets the possibility to reach higher engine loads. It becomes even more important in the HCCI case since rich mixtures cannot be used in order to increase exhaust temperature and hence energy levels upstream turbine. It would be possible to gain information from the experiments in order to fill this blank area in the maps but that requires measurements of the turbine speed, which at the time of the experiments was unavailable. This turbocharger map-problem was later dealt with, see following section. Here is the extrapolation done manually by adding points in the unknown region resulting in a smooth interpolation "surface". A similar approach was used for the turbine.

Besides engine and turbocharger data and heat release shape some measured values was used as input in order to compare simulations with measurements as seen in Table 8. The surrounding temperature was set to 35°C, and the surrounding pressure (upstream compressor and downstream turbine) to 1.023bar.

Table 8 Input data for the simulation, P_H – heating power, η_c – combustion efficiency.

Case	Speed	λ	RON	P_H	*A10*	*A50*	*A90*	η_c
	[rpm]			[kW]	[CAD]			[%]
1	1510	5,82	0	0,0	-20,8	-9,3	-0,6	77,7
	1510	5,16	19	6,0	-20,9	-10,8	-3,9	94,1
	1502	3,78	69	0,0	-7,0	-3,5	-0,6	95,2
	1495	3,26	89	0,0	1,8	4,6	7,1	94,8
	1477	2,87	93	0,0	5,9	9,1	12,8	94,2
	1501	2,34	94	0,0	4,1	5,9	15,1	96,7
2	1991	3,51	86	0,0	1,6	5,4	8,9	90,2
3	1202	2,20	98	0,0	8,1	10,3	16,3	96,2

Simulated net indicated mean effective pressure, *IMEP* and exhaust manifold temperature shows very good agreement with measurements as shown in Figure 40. *IMEP* depends heavily on the heat release, both timing and the amount (accumulated) heat released, and in-cylinder heat transfer. The timing and shape is set to correspond to measurements and hence the good agreement should indicate a proper heat transfer and fuel flow, the latter gives the accumulated heat release. The exhaust temperature depend mostly on air-fuel ratio, heat transfer in-cylinder and heat transfer in the exhaust port (the thermocouples were mounted in the exhaust manifold close to the cylinder head). Again, air fuel ratio was set to the same as measured (from exhaust emissions) value so the good agreement should indicate that the valve-flow and heat transfer models (at least together) seem to simulate the reality (represented here by measurements) fairly well.

There is a much bigger difference if we look at the inlet and exhaust pressures as seen in Figure 41, and this difference is believed to be connected to the poor turbocharger model. Another factor is that the simulated systems do not have any model for an air-cleaner, which normally reduces the inlet pressure somewhat. The intake air heater has also some unknown

resistance that would cause a pressure drop on the intake side. Altogether, it is not surprising that there is a difference in intake pressure. The same goes for the exhaust side, although in this case it's probably the model alone that has to be blamed. A possible contribution can be that the heavy oscillating pressure due to the blow down pulses may cause inaccurate pressure registrations. The exhaust pressure transducers were mounted on approx 0.5 m long tubes with 4mm bore directly on the two exhaust channels (from cylinder 1-3 and 4-6 respectively) entering the turbine, which should give a reading of *total* pressure. The average pressure reading of the two channels is shown here.

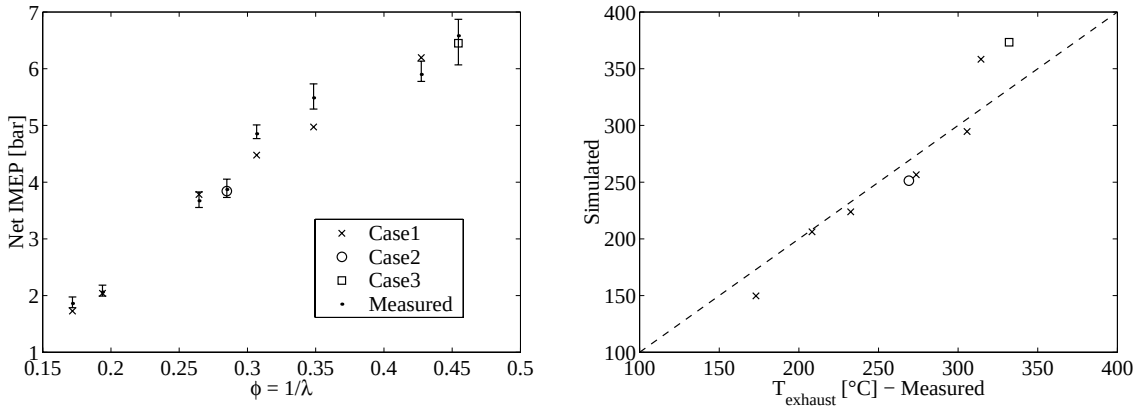

Figure 40 Left – Net indicated mean effective pressure. The measured points (dots) are surrounded by bars that indicate maximum and minimum of the 6 cylinders. Comparison between measurements and simulations is possible by looking at a specific ϕ (=1/λ) value for which two points exist, one measured and one simulated. Right – Exhaust temperature comparison between experiment and simulation

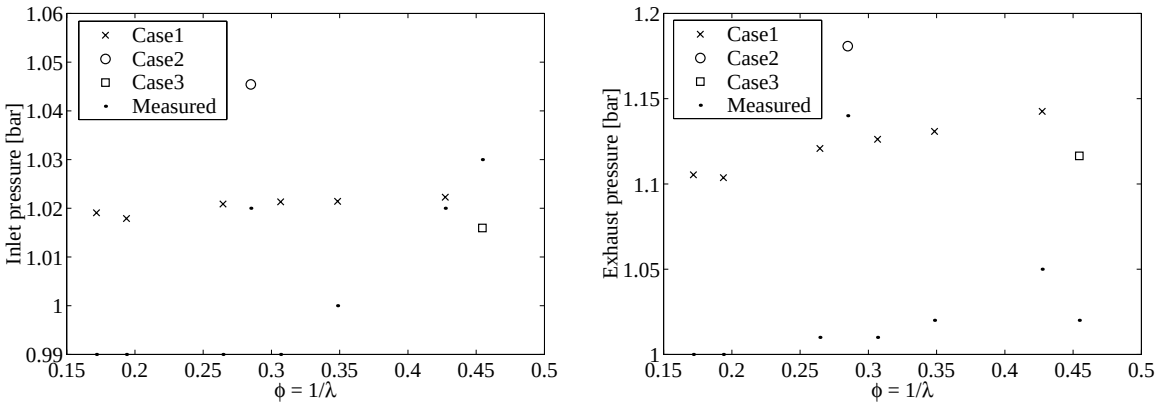

Figure 41 Inlet pressure (left) and exhaust pressure (right) over fuel-air equivalence ratio.

The inlet temperatures (Figure 42) are over estimated about 5 – 10 degrees, which can be explained by the absence of a heat transfer model for the inlet manifold, the cylinder heads transfer heat to the intake manifold and in its turn to the intake air. Deviations in inlet pressure should render in a similar difference in mass flow as seen in Figure 43, but the measured mass flow is *higher* than the simulated values, which is quite contradictable. A further analysis reveals that the mass flow measurements probably somewhat erroneous since the volumetric efficiency (Eq.107) become higher than 100% in several cases.

$$\eta_V = \frac{60 \cdot \dot{m} \cdot R \cdot T_{inlet} \cdot n_R}{M_{A+F} \cdot p_{inlet} \cdot V_d \cdot n} \qquad \text{Eq.107}$$

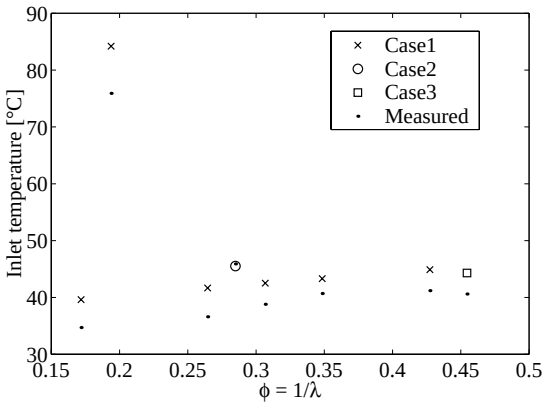

Figure 42 Inlet temperature over fuel-air equivalence ratio

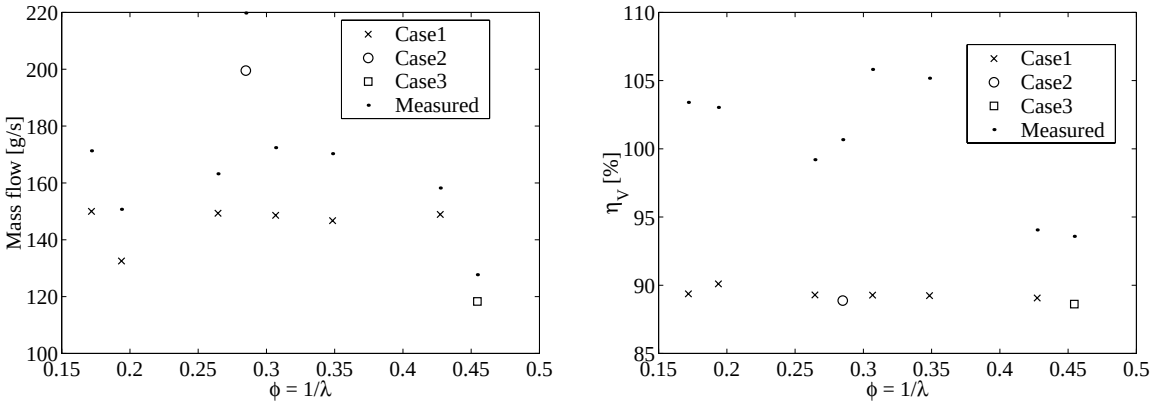

Figure 43 Total mass flow over fuel-air equivalence ratio (left) and volumetric efficiency over fuel-air ratio (right).

Before this simulation tool is used to study different engine systems or to match turbochargers, some improvements have to be made, e.g. regarding the heat release calculations and extrapolation of the turbo maps. The heat release calculations are to be made based on empirical knowledge or by looking into the chemical kinetics. The extrapolation of the turbo maps has to be improved in order to handle e.g. start up situations where the original maps are not sufficient. Other than that, the calculations seem to represent the measurements quite well.

3.4 Turbocharger considerations

As mentioned in the previous section the turbocharger performance heavily affects the performance of the engine system. By forcing higher mass flows through the system higher engine loads is possible i.e. it becomes more economical since a smaller engine can produce the same amount of power as a bigger one. In addition, frictional losses are not that load dependant; higher brake output of an engine usually makes frictional losses less significant and brake efficiency increase.

The requirements for increased load is that the mass flow and exhaust gas energy upstream the turbine of the turbocharger is high enough to first accelerate the turbo shaft into regions were the compressor becomes useful and then provide boost pressure. In spark-ignited (SI) engines, this is usually not a problem since they can be operated with rich or stoichiometric mixtures that give high exhaust temperature. In addition, the compression ratio of

turbocharged SI engines is around 9 to 10 in order to avoid knocking combustion and too high peak pressures but this limits the efficiency of the engine so the exhaust temperature and hence the energy levels always becomes high enough. Lean-burn SI stationary engines can use a temporary richer mixture and late ignition in order to gain boost pressure and then lean out to a desired operational level when boost is enough. The same goes for diesel engines where the slow combustion process and low heat transfer also contribute to high exhaust temperatures. In a HCCI engine, too rich mixtures cannot be used due to too fast knocking-like combustion that gives heavy sound emissions and is believed too cause engine damage. Because of this operational mixture limit of HCCI engines, it becomes important to simulate the boost build-up period in order to find out if the engine can reach desired operating load. Since the turbo performance maps has limited information in the low mass flow and low pressure ratio regions a turbocharger model with good extrapolation qualities in this region are desired. As shown earlier (section 2.6), the turbocharger model used in this work has been subject to stepwise improvement, in this case the models described in sections 2.6.3 - 2.6.6 are used which is basically a system of polynomials fitted to performance map data.

When matching the turbocharger to the engine the first step is to select a proper compressor that will provide the desired boost pressure and mass flow to the engine in the desired engine operating speed. It also is important to minimize the necessary compressor work, which is essentially the same as maximizing the efficiency of the compressor. For a truck size engine radial compressor this efficiency is typically between 75 and 80% in the best point.

The size of the turbine determine the pressure ratio given a certain speed and mass flow. A small turbine brings up the pressure ratio at lower speeds. The size of the turbine is usually classified by A/R-ratio, which is the inlet area of the turbine divided by radius of turbine housing. A basic turbine geometry or type can often be delivered with various A/R-ratios. Without becoming an expert on turbo-charging, it is possible to model and simulate different sizes of compressors and turbines and an example is used for the discussion here.

Three different turbine sizes were compared through simulation of a load sweep at 2000 rpm. TC-1 corresponds to the diesel engine's original turbine size (geometrical flow area: 25 cm^2) while the two smaller ones, TC-2 and TC-3 produce higher pressure ratios since they have smaller flow area (16 and 13 cm^2 respectively). A photo of two of the turbines is shown in Figure 44. The simple heat release function was used with fixed parameters (A0 = -5, A10 = 0 and A90 = 10 CAD ATDC) and the results were compared against indicated mean effective pressure and indicated efficiency i.e. engine friction was not considered. It was also assumed that HCCI combustion was the case in each operating point, which perhaps is not the case in the reality, at least not with a single fuel. Isooctane was used as a single substitute of a mixture of n-heptane and isooctane.

The simulation was made so that the engine was started from idle speed with fuel injection off, then during the first 24 seconds a 2-step ramp was used to bring up the speed to 2000 rpm and a fuel injection corresponding to 10g/s into the inlet manifold. Thereafter followed a reduction to 4g/s and then a stepwise increase in fuel rate ending at 16g/s as illustrated in Figure 45. It is this last stepwise increase that is studied here. The first peak is to ensure boost pressure buildup since there is a possibility that there can be two operating modes given a certain fuel flow in some cases, especially low load. The varying fuel flow results in varying load, boost pressure and hence air-fuel ratio and resulting efficiency. Air-fuel equivalence ratio (Figure 45) depend heavily on how much boost pressure the turbocharger can provide since this directly affects the airflow to the engine.

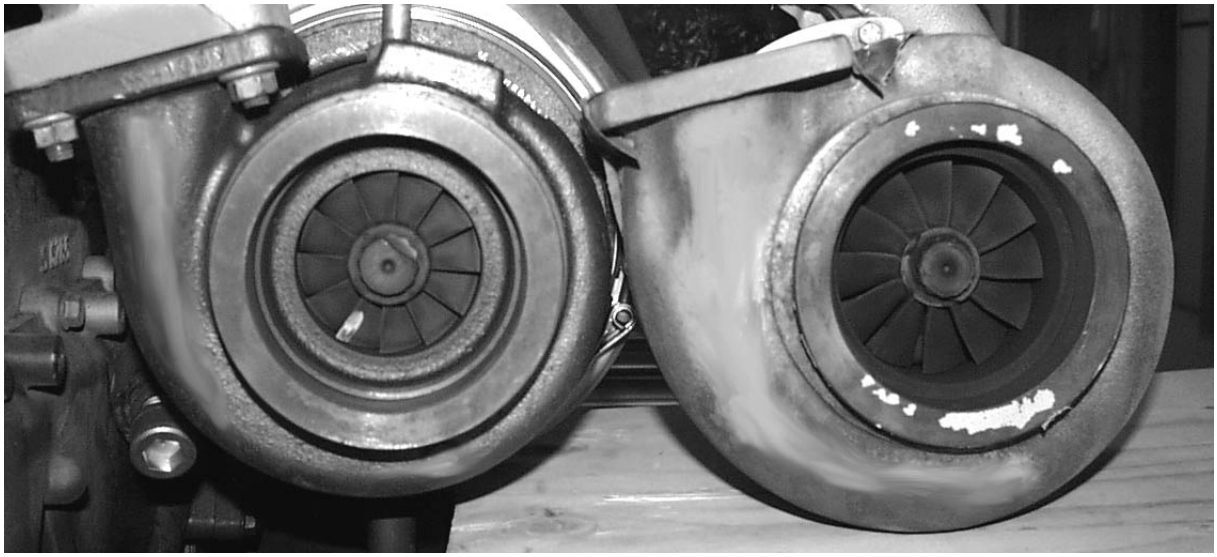

Figure 44 Photo (by J.-O. Olsson) showing the exit of the smallest (TC-3, left) and the largest (TC-1, right) of the three turbines.

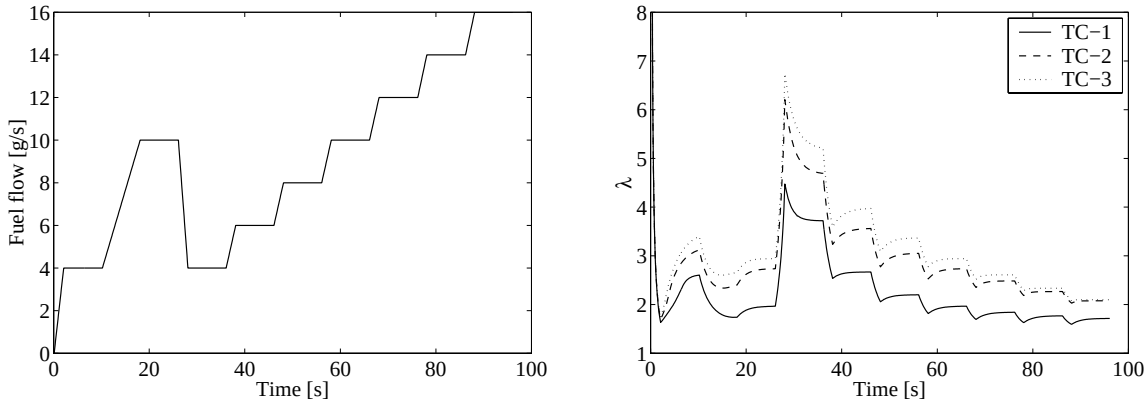

Figure 45 Fuel rate for simulation (left) and resulting air-fuel ratio (right)

A smaller turbine forces the backpressure (exhaust manifold pressure) to increase due to smaller flow area put it also bring up the pressure level (energy level) on the exhaust side which means that more work for the compressor work can be delivered, resulting in higher air-flow and higher air-fuel ratio. However, the increased backpressure also gives high pumping losses on the engine itself, which reduces the overall efficiency of the engine. A too large turbine on the other hand has difficulty to extract the exhaust energy but gives lower pumping losses. A difficulty that is connected to the HCCI combustion is the λ-dependence on heat release rate. If λ becomes to rich, a too fast combustion occur that bring fourth oscillating pressure waves inside the cylinder. In spark-ignited engines, this is usually the result of knocking i.e. self-ignition of the air-fuel mixture outside the flame-front. In a SI engine, this can be devastating if the phenomenon prevails for a long time with structural damage on the piston as result. The normal mixture in SI engines are stoichiometric which means that the energy released per mass mixture is obviously higher than in a lean burn HCCI engine so structural damage due to too fast combustion seems a less unlikely in a HCCI engine. However, the noise-emission increases heavily. From experiments it is reported to be "painful" to run the engine with richer mixtures than about λ = 2.1 (isooctane) and lets assume that this is the limit for HCCI in this case then the resulting operating range with the different chargers can be seen in Figure 46. Turbocharger 2 and 3 (medium and small size) gives the highest mean effective pressures without getting lower than λ = 2.1.

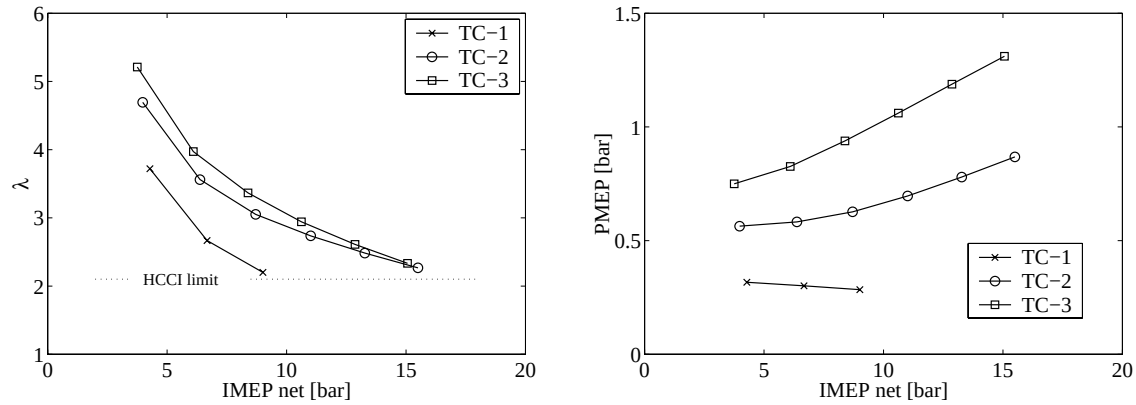

Figure 46 Operating range at 2000 rpm, in simulation (left) and simulated pump mean effective pressure (right)

As explained above a smaller turbine also brings up pump losses that reduces efficiency, which is clearly seen in Figure 46. Now, indicated efficiency is not quite what is interesting in a car, truck or power plant. The brake efficiency is more interesting and with the friction model described earlier (section 2.5.7), we get lower efficiency (Figure 46) at with low loads. Friction has a crucial effect at low loads as shown earlier in Figure 20.

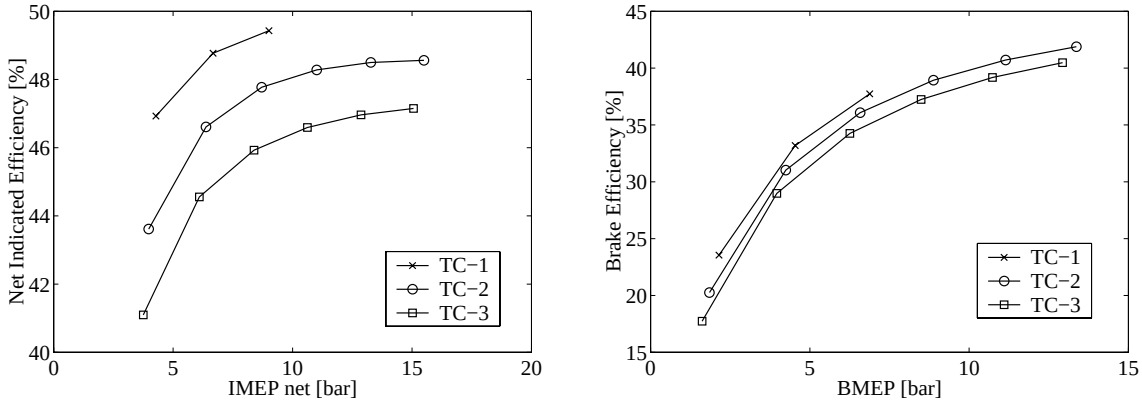

Figure 47 Net indicated - (left) and brake - (right) simulated efficiencies over mean effective pressures at 2000rpm.

It is quite clear that it is the medium size turbine, TC-2 that should be selected in this case, it seems like a good compromise between efficiency and performance. If more advanced turbo technology were accepted, like the variable vane turbine, this may be a way to keep the larger turbine without loosing to much pumping work at high loads. A variable vane turbine is a way to extend the optimum operating range of a certain turbine by adjusting the flow field in the turbine and hence optimize it for different mass-flows.

3.5 Lean-burn spark ignition

A small validation was made by simulating a whole engine system working with lean-burn spark ignition and compare the results with experiments. The purpose was to illustrate what we can expect from a lean burn natural gas engine, in terms of NOx emissions and efficiency, and to check the validity of the system simulation software.

The experiment was made on a 10 liter Volvo TG103 natural gas engine which has basically the same design as the TD100 engine mentioned earlier, however, it has a lower compression ratio of 11.2. In the simulation the compression ratio of the DSC12 engine was reduced to 10:1, the medium size turbine (TC-2) was selected and a simple wastegate model was inserted to control inlet pressure. A much longer combustion duration (25 CAD) was used to simulate the SI combustion. Although the engine simulated was not the same as the experimental one (due to lack of information about the turbocharger), the efficiency estimates were accurate as shown in Figure 48. One explanation for the difference between simulated and experimental results can be the friction model used in the simulations. At 1200 rpm the friction mean effective pressure (FMEP) became 1.48 bar compared to about 1.2 bar for the experiments (the mean value of net IMEP for the 6 cylinders was used to calculate FMEP). Note the high NOx emissions, around 20g/kWh.

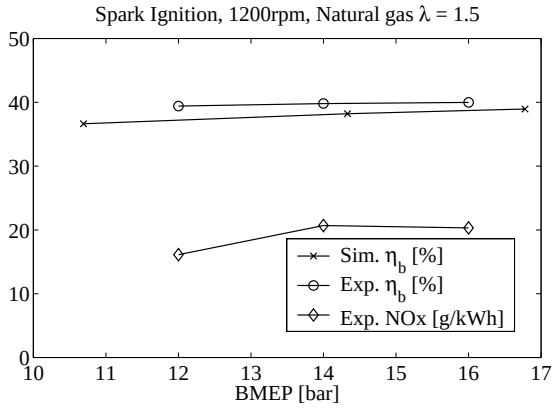

Figure 48 SI operation. Experimental results with the TG103 engine, compared with simulations of a spark ignition (SI) converted DSC12 engine.

Lean burn spark ignited engines, especially those with 3-way catalysts, is the main competitive solution to HCCI regarding both efficiency and NOx. Regardless of technology, current and future engines must comply with the legislations. Table 9 shows some examples of legislations for stationary natural gas engines in Europe (reviewed by Nellen and Boulouchos [111]).

Table 9 Legislations is Germany and Switzerland for stationary natural gas engines. Emissions in mg/Nm^3 at 5% O_2 (except for NMHC). 250 mg/Nm^3 correspond to about 0.76 g/kWh for a lean burn SI engine [111].

Legislation	NOx	CO	NMHC
TA-Luft 92, Germany	500	650	150
Switzerland	250	650	-
Zurich - city	50	650	-

3.6 The effect of ignition timing on efficiency

As in SI engines, the ignition timing in HCCI engines is possible to set to a desired value if a suitable control system is used. The ignition timing affects not only the emissions but also the efficiency of the engine. In the following simulation, the ignition timing is varied keeping constant combustion duration ($D_{0\text{-}10}$ = 8 CAD and $D_{10\text{-}90}$ = 5 CAD) and combustion efficiency (92%). The case correspond to the simulation in section 3.1 and the resulting indicated efficiency is shown in Figure 49. Note that it is the angle of 0% burned mass fraction, *A0* on the X-axis. The angle of 50% burned mass fraction, *A50*, is about 8 + (8-5)/2 = 9.5 CAD later than *A0*.

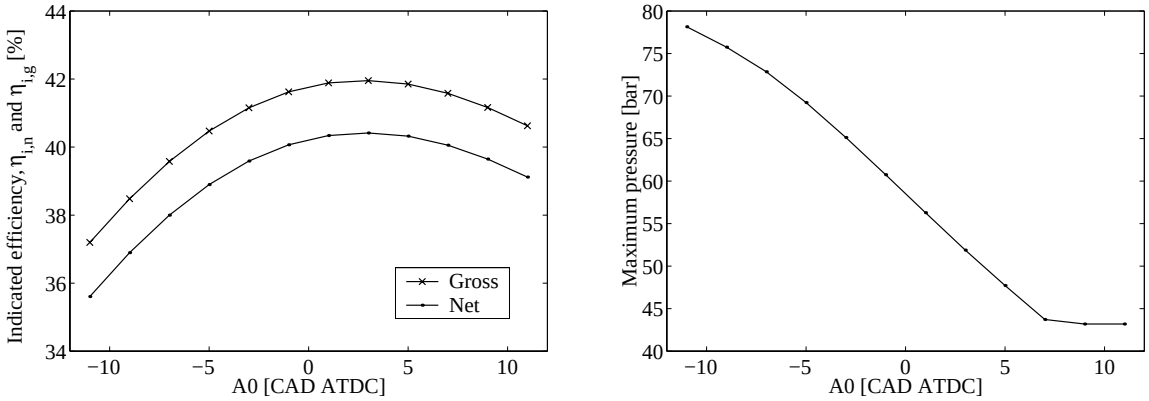

Figure 49 Ignition timing and its effect on indicated efficiency (left) and maximum pressure (right). At A0 > 7 CAD ATDC, the maximum pressure is limited by the pressure after compression.

With fixed combustion duration, a later ignition timing (from optimum efficiency) reduce the maximum pressure and hence the indicated work from the cycle and the efficiency goes down. An earlier timing brings up the maximum pressure and thereby the maximum temperature. This increases the time at high temperatures and thus the heat transfer. A lot of heat transfer in the beginning of the expansion stroke reduces the pressure during expansion stroke and thereby the indicated work. When the indicated work goes down, the efficiency goes down if the fuel flow is constant.

It appears that the indicated efficiency does not change that much with ignition timing, but it is important to remember that in reality, there is an influence of combustion duration and heat transfer, both factors change when changing ignition timing.

4 Single zone chemical kinetic model

Since ignition in HCCI engines is affected by numerous parameters, a proper prediction of ignition timing is required in order to simulate if, and when, ignition occur. Using chemical kinetics calculations seems like a reasonable solution. Since the HCCI process is similar to the knocking phenomena in SI engines, software developed for studying these phenomena seems appropriate to use. Development of that type of software is made at several combustion research groups around the world and among them is the group lead by professor Fabian Mauss at the Combustion Physics Division, department of Physics at Lund Institute of Technology.

Their software has been linked into the cycle calculation developed here. This link provides an estimate of air-fuel-residual mixture, temperature and pressure at a fixed CAD during the compression stroke. Then the chemical kinetics calculations take over, including the same heat transfer model as for the cycle simulation described in section 2.5. The chemical kinetics program calculates pressure and temperature in a desired CAD-interval, as long as the intake and exhaust valves are closed.

However, the program has some limitations. In order to save computational time only one zone is considered which means that the ignition process does not consider any distribution of fuel or in-cylinder temperature. It has possibilities to do so but that is not used in this work, if used, it brings up the computational time even more depending on the number of species and reactions are used. Fuels like isooctane require longer time than fuels like methane since more species and reactions are needed to describe the combustion process. Each reaction has a rate that depends on pressure, temperature and specie concentration. All these reactions and the thermo dynamical calculations can be expressed in a system of equations that has to be solved for each time step and this is what the program does. Since the reactions depend exponential against temperature (see the Ahrenius expression) and some reactions are very fast the system becomes very stiff which puts large demands on the solver of the system. It all becomes even more complex because negative concentrations cannot be allowed. Deeper description of this program will not be made here since the author would like to identify himself as end-user of this software.

4.1 Mathematical model

The mathematical model used for calculating the chemical reactions in the combustion process is based upon a set of zero-dimensional time dependent differential equations: One balance equation for the conservation of energy, and one mass conservation equation for each chemical species in the reaction mechanism. The differential equations are solved using Newton's method and the time is resolved with higher order backward differential functions. The main characteristics of the chemical kinetics program have been discussed in previous publications [65], more detailed information is given by Amneus [112].

The conservation equation for the chemical species is given by Eq.108. Y_j is the mass fraction of the species, ρ is the density, M_j the molar mass, $\nu_{j,k}$ the stoichiometric coefficient and ω_k the reaction rate.

$$\frac{dY_j}{dt} = \frac{M_j}{\rho} \sum_{k=1}^{N_r} \nu_{j,k} \omega_k \qquad \text{Eq.108}$$

The energy conservation equation is given by Eq.109. The first term is the contribution from chemical reactions, the second is the work, and the third term is the change in internal energy of all mass within the engine cylinder. The fourth term is the convective heat transfer from walls. m is the total mass, u_j the specific internal energy of species j, p pressure, V volume, t time, C_v the heat capacity and T the temperature. α is the heat transfer coefficient attained from the heat transfer model, A_w is the wall surface area and T_w is the average wall temperature.

The use of internal energy and constant volume heat capacity in the energy equation is justified by the fact that for HCCI ignition and combustion, the peak values of normalized pressure derivative are higher than the normalized values of maximum temperature derivative - Eq.110. Using the constant volume specific heat minimizes the error in each time step and convergence is reached faster. Using constant pressure specific heat for gas property representation give the same results, but require more iteration. In each time step, the volume is set constant.

$$m \sum_{j=1}^{N_s} \left(u_j \frac{M_j}{\rho} \sum_{k=1}^{N_r} \nu_{j,k} \omega_k \right) + p \frac{dV}{dt} + m C_v \frac{dT}{dt} + \alpha A_w \left(T_w - T \right) = 0 \qquad \text{Eq.109}$$

$$\frac{\max\left|\frac{dp}{dt}\right|}{\overline{p}} >> \frac{\max\left|\frac{dV}{dt}\right|}{\overline{V}} \qquad \text{Eq.110}$$

The volume decrease and consequently the pressure increase due to the piston movement can easily be calculated. Thus, the total pressure is calculated as the sum of inlet pressure, the pressure increase caused by piston movement, and the pressure increase due to chemical reactions. The instantaneous volume is calculated from Eq.111 (note the absence of piston pin – cylinder – crankshaft offset, compare with Eq.46) and the pressure is calculated from the ideal-gas equation of state (Eq.17).

$$V = V_c + \pi \cdot B^2/4 \cdot \left(l + a - a \cdot \cos(\Theta) + \sqrt{l^2 - a^2 \sin^2(\Theta)} \right) \qquad \text{Eq.111}$$

The ESIM package uses 6 species to describe the gas inside the cylinder (and in the rest of the system as well): N_2, O_2 Ar, CO_2, H_2O and "Fuel". The chemical kinetics program handles about 60 to 100 (or more) different species depending on mechanism, which means that the linkage has to handle this difference in a logical sense. The 6 species are split into air, fuel and residuals simply by looking at the fuel and CO_2 fraction. The CO_2 fraction gives the amount of burned gases since the amount of CO_2 in the air is known and set constant. If water injection is used the amount of steam also has to be determined. The fraction of fuel is given directly and the rest is then air, and perhaps steam. Then the specie setup for the kinetics can be set up, air and fuel is simple, residual gas is assumed by using the mixture from the previous cycle, when the exhaust valve opens. This is sometimes not a correct assumption if

there are many residuals left at this point. Radicals may play an important role and could affect the combustion timing. Since there is no chemical kinetic calculation during the gas exchange period, several of the radicals in the residual gas become over estimated. It is quite simple to study at the other extreme by setting all radical mole fractions to zero in the residual gas.

The linking process is done quite simple, at 60 CAD BTDC a series of input files (text files) is created and then the chemical kinetics program is called. When the execution of this program is completed, the output files are read and interpreted by ESIM. The results are interpolated to CAD resolution so the representation of the cycle in the ESIM program becomes correct. Using only a little interval with kinetics, give less interpolation time when doing the connection.

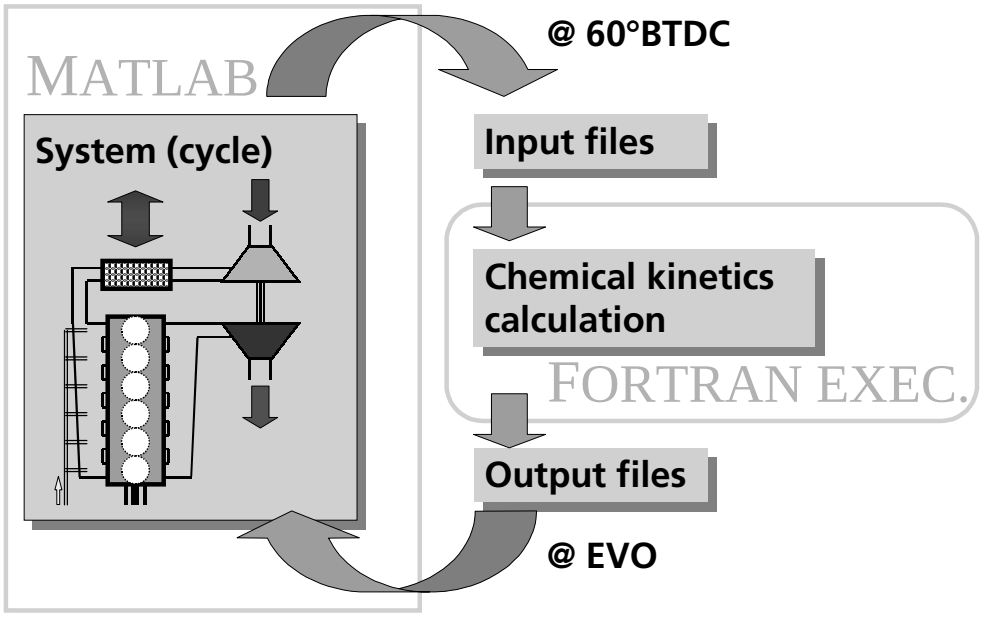

Figure 50 Linking between ESIM and the chemical kinetics program

When interpreting the output files the identification of N_2, O_2, Ar, CO_2, H_2O is simple and straightforward. The rest of the species is transformed to "Fuel" by looking at the mass equivalent. This brings in a small error since some of these species is carrying some O-atoms that do not originate from the fuel, which means that the mass of fuel is somewhat overestimated. The effect of this error is very small since there is very little left of these species and the amount of residual gas is in general very small, usually 5 – 10% of the total mass when inlet valve closes.

It is obvious that the lack of chemical reactions during the gas exchange period may bring some degree of uncertainty. So to illustrate the effect simulations are made with two different starting conditions of kinetic calculation, and also termination of some important radicals; H, O, OH, HO_2, CH and CH_3 in order to simulate the effect gas exchange has on these radicals. The results are shown in Figure 51. Starting the kinetics earlier give only a minor change in combustion timing, about 0.2 degrees later timing, termination of remaining radicals does not give any noticeable change in the timing. The conclusion is also that any remaining radicals seem not to affect ignition timing in any major way, at least not in low speed (1000 rpm) 4-stroke HCCI engines.

Another limitation is the use of a zero dimensional model with chemical kinetics, since heat, transfer is affecting the overall (average) in-cylinder temperature. Therefore, if the software is used to find i.e. inlet temperatures, this temperature will probably be overestimated. In a real

engine, the temperature of the gas in the bulk should become somewhat higher than the mean temperature, T_{mean}, since it is not exposed to any heat transfer (the temperature in boundary layer is then lower than T_{mean}). To illustrate this difference an "adiabatic bulk temperature", T_{bulk} is calculated given a simulated pressure trace. From a initial state at IVC where the temperature is assumed to be uniform all over the combustion chamber the gas is compressed. Heat transfer reduces the pressure at the end of the compression stroke compared to adiabatic conditions. Given the initial state and the pressure trace it is possible to calculate an adiabatic temperature trace using an adiabatic assumption. First law (Eq.43, Eq.44) become:

$$0 - \bar{p} \cdot \partial V = \left(H\left(T_{a,i+1}\right) - p_{i+1}V_{i+1}\right) - \left(H\left(T_{a,i}\right) - p_i V_i\right) \Rightarrow$$
$$H\left(T_{a,i+1}\right) = p_{i+1}V_{i+1} + \left(H\left(T_{a,i}\right) - p_i V_i\right) - \bar{p} \cdot \partial V \qquad \text{Eq.112}$$

(Correspond to an isentropic relation, $\Delta s = 0$ in Eq.25) . Given the enthalpy $H(T_{a,i+1})$ the adiabatic temperature $T_{a,i+1}$ can be calculated through Eq.24 and this temperature is the estimation of the bulk temperature, seen in Figure 51. The difference is about 35 degrees at the end of the compression stroke. In reality, we would have a distribution of temperature ranging from below the calculated T_{mean} and above the T_{bulk} estimation. If the inlet temperature is trimmed to give the same temperature at the end of the compression stroke, the inlet temperature should be about 15 degrees lower (if the compression ratio is about 18:1). This means that the inlet temperature is overestimated by about 15 degrees. However, in this work different kinetic mechanisms are studied and compared with experiments and a proper mechanism that agrees with the experiments are selected for the further studies. It would perhaps be an idea to select a mechanism that would have required 15 degrees higher inlet temperatures; in order to get a proper prediction of ignition timing. So the simulations over-estimate the inlet temperature, however, the absence of heat transfer models for inlet manifold and inlet port compensates this "error" to some degree.

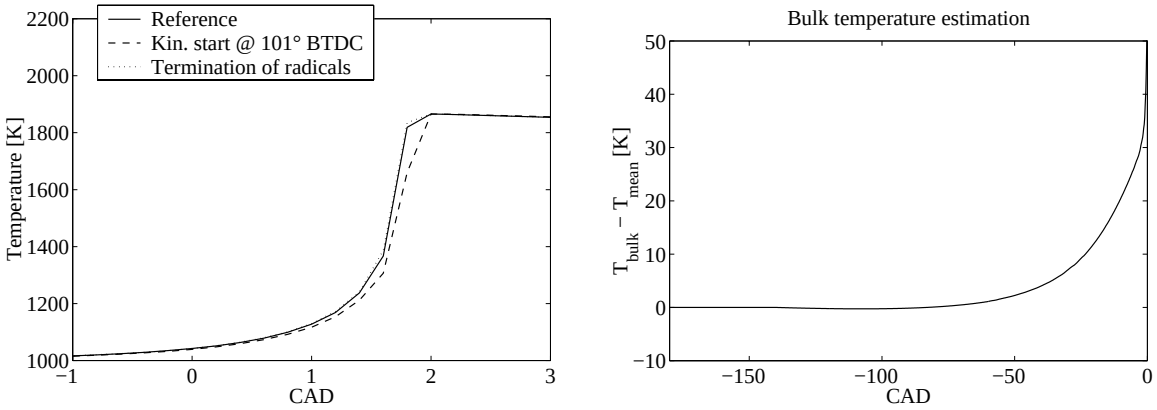

Figure 51 Left –The effect of different start angles and the effect of termination of some radicals. "Reference" – calculation starts at 60° BTDC (plot resolution: 0.2 CAD). Right - Estimation of the difference between a mean temperature and an adiabatic bulk temperature.

As with other numerical methods of solving differential equations, iteration limits may affect the results. One mechanism is used to study the effect of changing tolerances. The heat release rate is plotted and compared with measurement, note that the experimental result is an average of 200 cycles. Medium and fine (more accurate) tolerances provide approximately the same results. Coarse give a fair prediction of ignition timing but start to oscillate during the main combustion. "Medium" tolerances are used as basic setting and correspond to absolute tolerance of 1E-10 and relative tolerance of 1E-7. "Coarse" correspond to 5E-10 absolute, 5E-7 relative and "Fine" to 0.5E-10 absolute, 0.5E-7 relative tolerances.

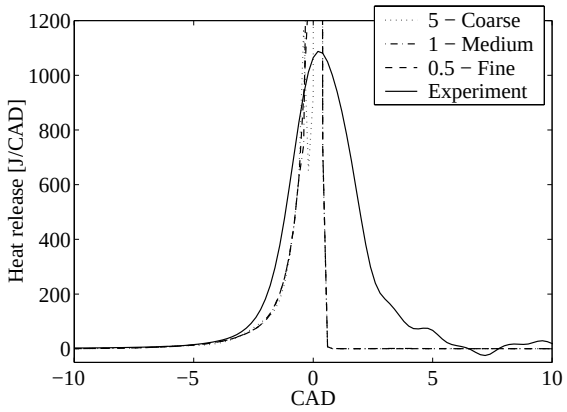

Figure 52 The results of different tolerances on heat release prediction. Simulation peaks at about 12000J/CAD.

4.2 Validation of chemical kinetics

To find out how good the zero dimensional chemical kinetics are to predict ignition timing some comparisons are made with experiments. First some comparisons are made with several kinetic mechanisms (set of species and reactions) developed for natural gas and then also mechanisms for iso-octane, however most of these are still under development.

4.2.1 Natural gas

Several natural gas mechanisms have been tested and in Figure 53 a comparison is made between simulations with two different mechanisms and with experimental results. The fuel (natural gas from Denmark) composition is shown in Table 10. The experiments are made by Christensen [65] on the Volvo TD-100 engine under supercharged conditions. Engine data is shown earlier in Table 5 although the compression ratio were about 17.4:1 in this case. The measured pressure trace is an average of 100 cycles.

Table 10 Fuel composition and energy content, average of 3´rd quarter 1998.

Specie	Mole fraction
CH_4	88.11%
C_2H_6	6.35%
C_3H_8	2.89%
$N\text{-}C_4H_{10}$	0.57%
$I\text{-}C_4H_{10}$	0.43%
C_5H_{12}	0.18%
C_6 +	520ppm
N_2	0.34%
CO_2	1.07%

$(A/F)_S$	16.58
Q_{LHV} [MJ/kg]	47.8
$Q_{stoich.\ mix}$ [MJ/kg]	2.72

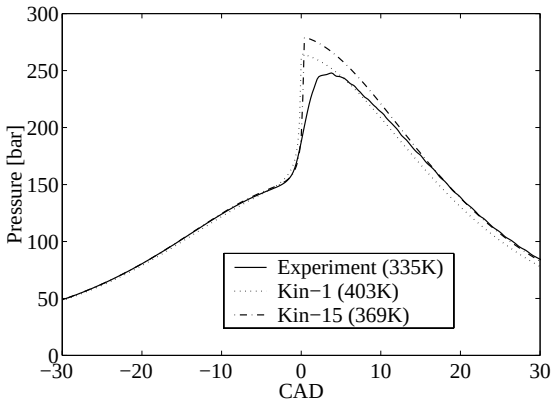

Figure 53 Natural gas cycle simulations with different chemical kinetic mechanisms compared to experiments. Inlet temperature is shown within brackets.

The simulations are made with the same compression ratio as the experiment in which compression ratio is determined from heat-release analysis on motored (non-firing) cycle. The same average inlet pressure and exhaust pressure; engine speed and air-fuel ratio is use as measured during the experiments. The simulation requires much higher inlet temperature than measured on the real engine. The difference is about 34 degrees between the experiment and "Kin-15". Some of this difference, perhaps 10 – 15 degrees or so, can be explained by the difference discussed earlier about zero dimensional modeling. The rest has to be explained by the absence of a proper inlet port heat transfer model and perhaps limitation in the chemical kinetics. "Kin-1" uses 58 species and 668 reaction while "Kin-15" uses 62 species and 711 reactions. Further description will be left out here.

4.2.2 Isooctane

It is possible to create mechanisms for heavier hydrocarbons as well, however these are still limited to well defined fuels like n-heptane (N-C_7H_{16}) and isooctane and not like commercial fuels, i.e. gasoline and diesel that is composed of a broad, almost infinite, spectrum of different hydrocarbons. Again, several different chemical kinetic mechanisms have been studied and some are illustrated in Figure 54. I this case the same compression ratio (evaluated from heat-release analysis), inlet and exhaust pressure and the same inlet temperature was used in the simulations as measured during the experiment. In this case, the engine was operated at 1000 rpm and under naturally aspirated conditions. Pure isooctane (I-C_8H_{18}) was used as fuel. (The experiments are described further in [67].) Based on the knowledge earlier about the zero dimensional modeling the conclusion is that this mechanism ignites slightly to early, however it is still quite impressive how close the ignition timing is to the experiment.

When looking at the heat release rate, Figure 55, a first peak occurs at about 25 degrees BTDC. It is possible that this peak occur in the real engine as well, if so, it may have drowned in the smoothing effect of in-homogeneities or by the averaging process during heat release analysis. However, Christensen [65] reported such 2-stage combustion when operating with isooctane with inlet pressure of 3 bar and low inlet temperature, and not during naturally aspirated conditions. What happens is that a "cool flame", or two-stage combustion appears. During this process there is a small temperature increase as seen in Figure 55 and this first peak causes some backward reactions to temporarily dominate and the ignition is halted [113].

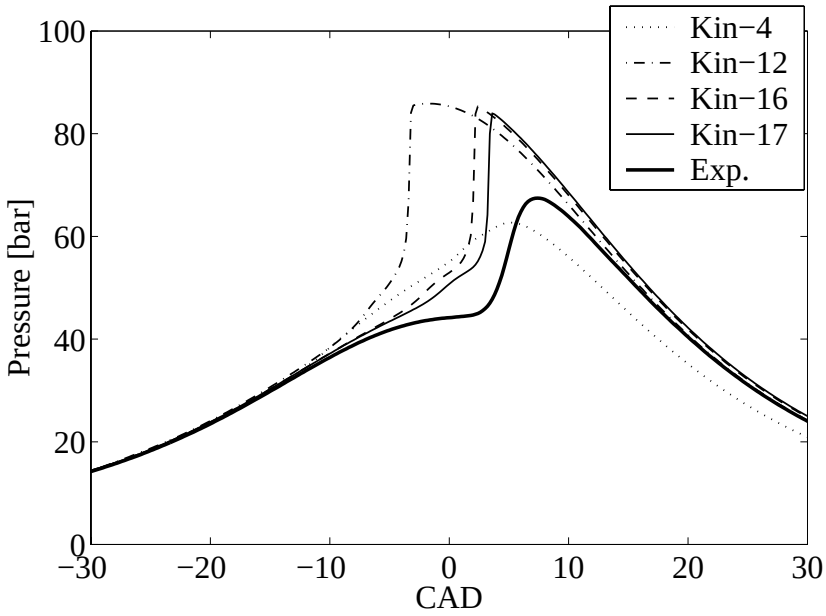

Figure 54 Cycle simulations with different chemical kinetic mechanisms for iso-octane compared to experiments ("Exp."). The experimental pressure trace is an average of 201 cycles. Naturally aspirated conditions on the Volvo TD100 engine, inlet temperature of 370K, engine speed 1000rpm and compression ratio is about 18:1 (17.7:1 was used in the simulations).

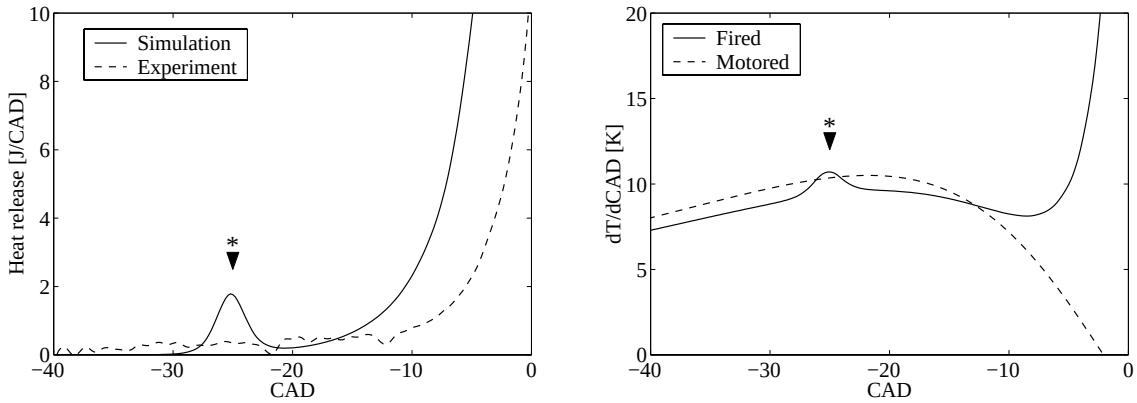

Figure 55 Left – Heat release rate with isooctane. There is a small first peak at 25 degrees BTDC, marked with "". Maximum heat release rate: Simulation: 2937J/CAD, Experiment: 315J/CAD. Right – Simulated temperature rate (K/CAD) trace during first peak, compared with motored cycle.*

4.3 Cycle simulations with chemical kinetics

The chemical kinetics provides an estimation of ignition timing and is therefore useful to study some interesting phenomena and new control techniques for HCCI. It must be pointed out that that the zero dimensional models are a limitation because some concepts may have a completely different effect if the degree of homogeneity is considered. The chemical effect will on the other hand be predicted fairly correct; however some wall effects may produce local variations in both concentrations and reaction pathways due to the temperature difference.

4.3.1 The effect of various engine operating parameters

Since the ignition process of HCCI rely totally on the auto-ignition chemistry, any factor that affect the chemical reactions during this process will affect ignition timing and hence the combustion process. To illustrate some of these parameters a cycle is simulated repeatedly varying one parameter at the time from a reference case summarized in Table 11. Again the Volvo TD100 geometry is used (Table 5) with compression ratio of 17.4:1 running with natural gas (Table 10) at naturally aspirated conditions. The result is illustrated in Figure 56 by the change of combustion timing, A50 (angle for 50% of accumulated heat release), from the reference case.

- Changing the compression ratio (r_C) has a great influence on combustion timing and this makes engines with variable compression ratio very suitable for HCCI operation. Higher compression ratio increases both temperature and concentrations at the end of the compression stroke. Generally, this promotes chemical reactions.
- Engine speed determines directly how long time the chemical reaction has to start, higher speed mean less time and hence later timing.
- The lambda value (λ) determines the fuel/oxidizer concentration ratio and lower lambda means more fuel per amount of oxidizer, this also increases the overall reaction rate as long as the mixtures are lean, λ well over 1.
- Increasing the inlet temperature ($T_{inl.}$), increases the overall cycle temperature and higher temperature promote reactions in general.
- Higher inlet pressure ($p_{inl.}$) simply increases both fuel and oxidizer concentrations and hence the reaction rates.
- Increasing the exhaust pressure ($p_{exh.}$) force more residual gas to be trapped inside the cylinder when the exhaust valve closes. In this case the residual gas fraction goes from 5.2% to 7.4%, but it causes a more important thermal effect; the temperature at IVC rise about 2 degrees. Increasing the residual gas fraction even further give a chemical effect, e.g. exhaust gas recycling - EGR.
- Adding 20% EGR reduces the oxidizer concentration (the mass of fuel per cycle is maintained by reducing λ to 2.4), which reduces the overall reaction rate, combustion is delayed.
- Natural gas composition changes over time and a more up-to-date blend, as shown in Table 12, give a slightly earlier timing. The explanation is the higher amount of heavier hydrocarbons like ethane and propane that ignites more easily than methane (compare with Table 10). Note that iso-butane and heavier hydrocarbons ends up as n-butane in the kinetic mechanism used here. Fiveland et al has investigated a variety of natural gas compositions [114], showing the importance of higher order hydrocarbons; ethane, propane and butane.

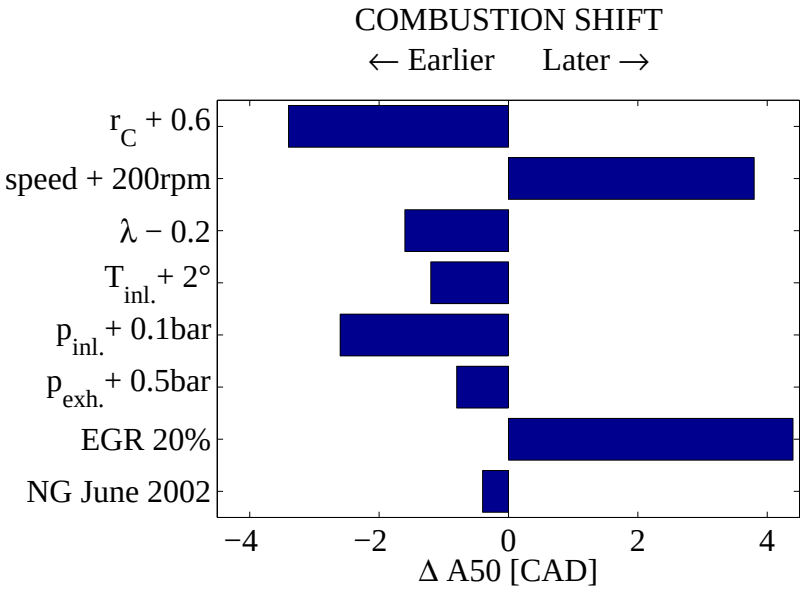

Figure 56 Shift of combustion timing when some operating parameters are changed.

Table 11 Reference case

Input:		Results:	
r_C	17.4:1	$IMEP_{net}$ [bar]	3.22
Speed [rpm]	1000	$IMEP_{gross}$ [bar]	3.30
λ	3	*PMEP* [bar]	0.08
p_{inlet} [bar]	1	$\eta_{i,net}$ [%]	41.84
$p_{exhaust}$ [bar]	1	*A50* [CAD ATDC]	7.4
T_{inlet} [K]	405		

Table 12 Fuel composition and energy content of natural gas from Denmark (North See), average during June 2002 [115].

Specie	Mole fraction
CH_4	87.15%
C_2H_6	6.93%
C_3H_8	3.11%
$N\text{-}C_4H_{10}$	0.63%
$I\text{-}C_4H_{10}$	0.44%
C_5H_{12}	800ppm
C_6 +	500ppm
N_2	0.32%
CO_2	1.19%

$(A/F)_S$	16.53
Q_{LHV} [MJ/kg]	47.7

4.3.2 Stability and late ignition phenomena

In general, the HCCI combustion is very stable in its nature; the cycle-to-cycle variations are in general very low and this fact was one of the early discovers by Onishi [4]. One interesting question is what makes HCCI so stable. From HCCI experiments, we know that there are operating regimes where the combustion become instable and typically this occur at very late ignition timing. To study the stability of HCCI cycle simulation of several consecutive cycles is made during a startup procedure. This approach reveals much of the stabilizing feature about HCCI.

Consider a warm, non-firing HCCI engine running at 1000rpm with the fuel injection and inlet air preheating turned off. Suddenly fuel injection and preheating is turned on and we start to monitor the in-cylinder pressure during the first 10 cycles as seen in Figure 57. The first cycle (C1) will not fire since the mixture is pure and cold air as seen in Figure 58. Fuel is present during the second cycle (C2), however, the residual gas from the first cycle is pure air and the low temperatures of this gas limit the fuel fraction. So there is not enough fuel and the temperature is too low for ignition. During the third cycle (C3), the residual gas is fuel rich since there was no combustion in the previous cycle. The gas temperature at IVC is also higher due to the preheating of the inlet air. Ignition occurs early and combustion timing[11] is about 6 degrees ATDC. In the 4'th cycle, the residual gas is hot and the temperature at IVC is even higher but there is no fuel present in the residual gas, combustion timing is later than the third cycle. In the following cycles, C5 – C10, combustion timing stables to about 9 degrees ATDC. The amount of fuel present corresponds to the injected fuel. In this simulation, the combustion efficiency is about 100% so there are no HC or CO emissions in the residual gas. The residual gas fraction is 5.4% for C10.

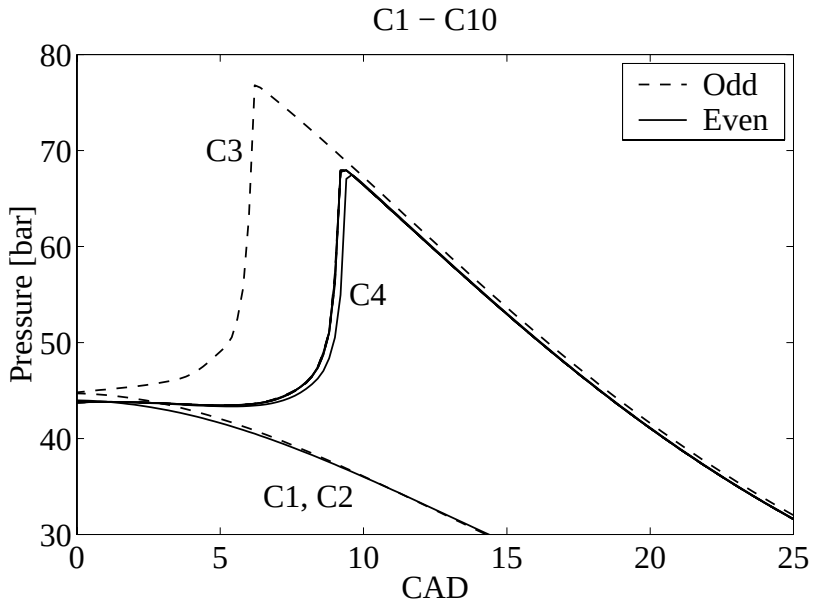

Figure 57 Inlet temperature of 130°C result in stable combustion with late timing after less than 10 cycles. Odd cycle numbers indicated by dashed lines and even cycles with solid lines. Cycle C5 – C10 is fairly the similar and cannot be separated here. (Naturally aspirated conditions, natural gas at $\lambda = 3$, compression ratio of 17.4:1 .

[11] Crank angle for 50% heat release, A50 is used here as a measure of combustion timing.

If a lower inlet temperature is selected, in this case 124°C, oscillating combustion timing may occur as seen in Figure 59. In this case, the timing does not get stable as previously, modal behaviors occur. A cycle with slightly earlier combustion timing produces residual gas that is slightly colder due to increased heat transfer and efficiency. So, the temperature at IVC for the following cycle becomes slightly lower as seen in Figure 60. The difference in temperature is very small but since the combustion is very late, even this small change will delay combustion timing. This later timing will bring up the residual gas temperature and the following cycle gets earlier combustion timing. Note that the amount of fuel does not change. Therefore, this tiny oscillation depends on small variations in initial temperature and the late combustion timing. If we continue the simulation to 50 cycles, we see that the oscillation is still there, however phase shifted 1 cycle, indicating that stability will not be reached. Modal behavior similar to this is also known from the 2-stroke self-ignited (ATAC/AR) engines, see Ishibashi and Asai [5].

Reducing the inlet temperature even further, to 122°C, the oscillation becomes bigger and the cycles alternate, as seen in Figure 61, between 100% combustion efficiency and about 10% combustion efficiency. In this case, it is not the temperature that is of importance but the amount of fuel that is present: If combustion is poor, there will be lots of fuel and other hydrocarbons in the residual gas (hydrocarbons and CO ends up also ends up here in "Fuel" fraction) and this will act as ignition improvement. Ignitions occur early despite the fact that the initial temperature is lower, as seen in Figure 62.

It would be possible that some of the effects shown previously may be to the radicals and some intermediates that are allowed to survive from the previous cycle. So in order to investigate this, termination of some species is made. Besides the species in the fuel and air, only H_2O_2, CH_2O, CH_3OH, C_2H_2, CO and H_2 are allowed to survive to the next cycle. The result is basically the same as shown in Figure 63, both regarding oscillating and alternating combustion. However, in the oscillating case the magnitude of the oscillation is bigger and eventually occur a misfire, a cycle with poor efficiency (C8). The following cycle (C9) ignites earlier. Note that the inlet temperatures are the same as earlier.

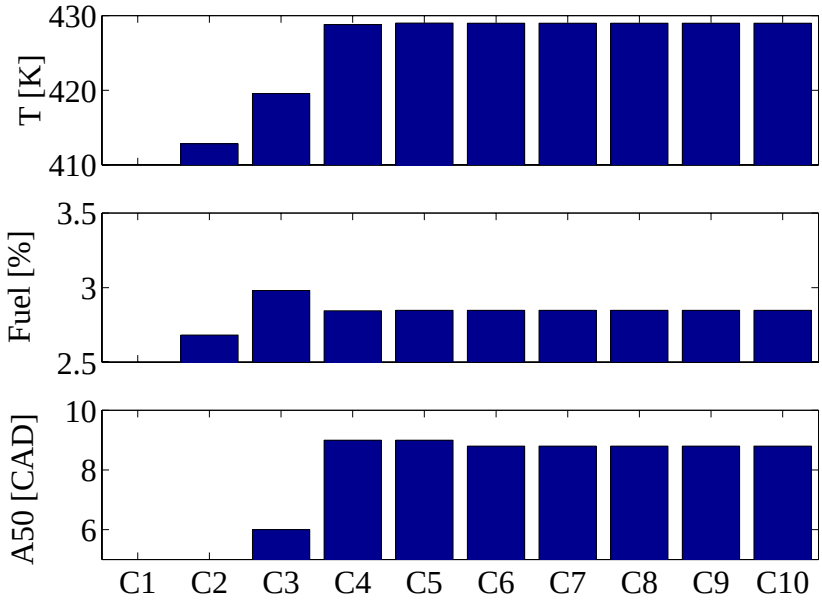

Figure 58 Stable combustion. Temperature ("T") - top, and fuel mole fraction ("Fuel") - middle, at IVC. Combustion timing expressed as crank angle for 50% heat released ("A50") - bottom.

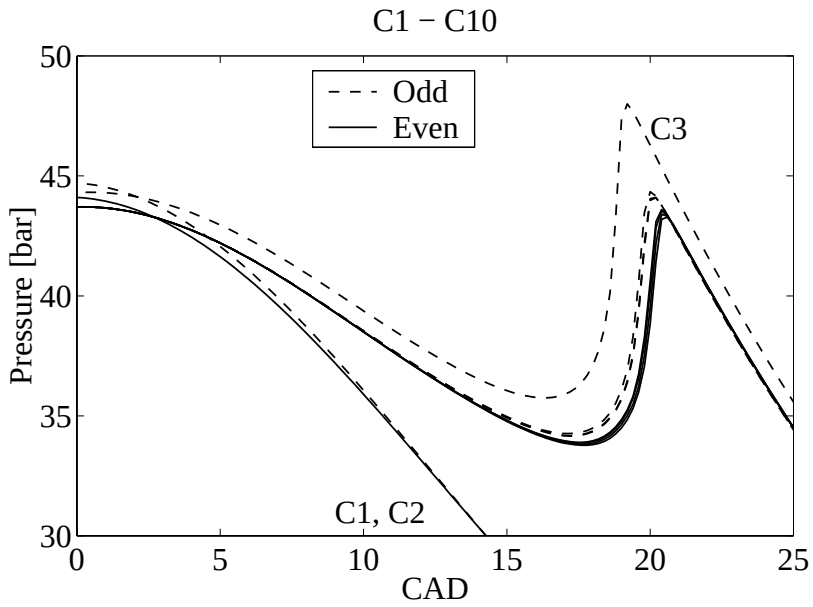

Figure 59 Lower inlet temperature, 124°C, result in a oscillating combustion timing after three cycles. C5, C7, C9 has about 0.2 degrees earlier timing than C4, C6, C8 and C10.

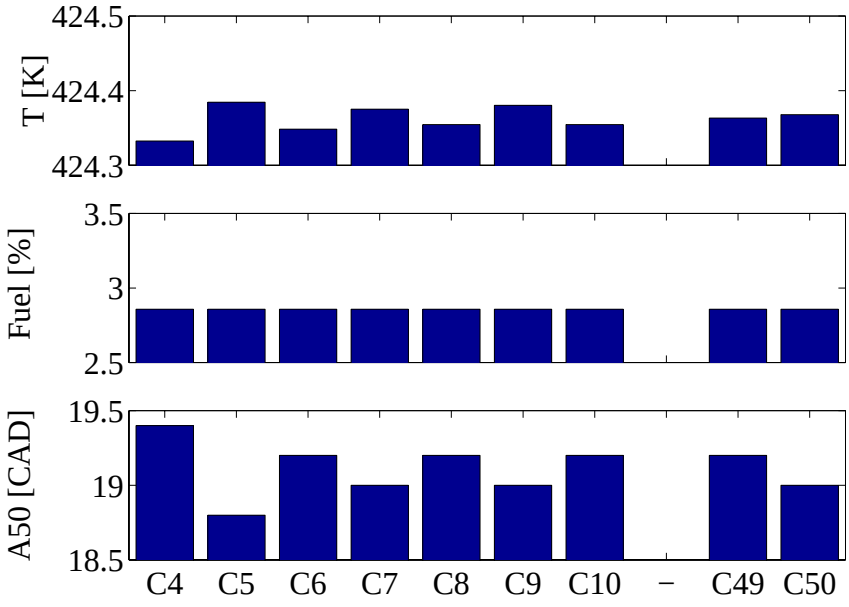

Figure 60 Oscillating combustion. The combustion oscillates around 19 degrees ATDC after 10 cycles. The cycles with earlier ignition (odd numbers) has higher temperature at IVC. After 50 cycles the oscillation is still there, however the order is shifted, odd cycle number has a late ignition due to a lower temperature. (Note that the resolution of A50 is 0.2 degrees).

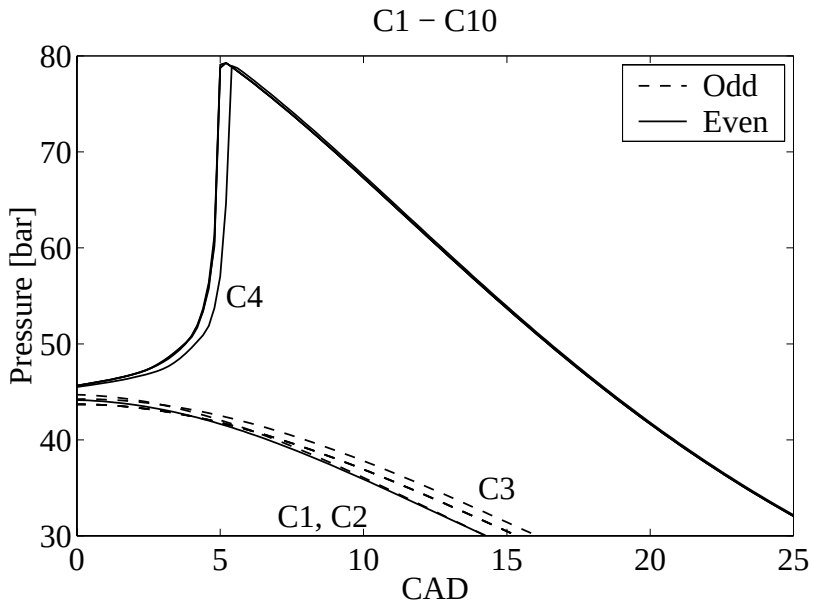

Figure 61 Even lower inlet temperature, 122°C, result in an alternating combustion with either a high combustion efficiency, ~100%, and early timing (C4, C6, C8, C10), or poor combustion efficiency, ~10%, and late timing (C5, C7, C9).

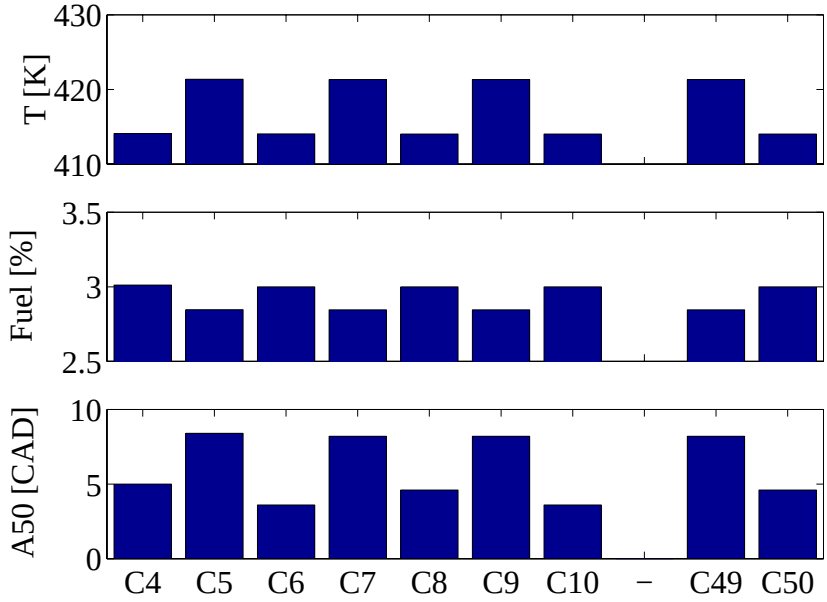

Figure 62 Alternating combustion with either high or low combustion efficiency. Due to the poor combustion efficiency of the cycles with odd numbers, there will be "fuel" in the residual gas that brings up the fuel fraction for the following, even number, cycles.

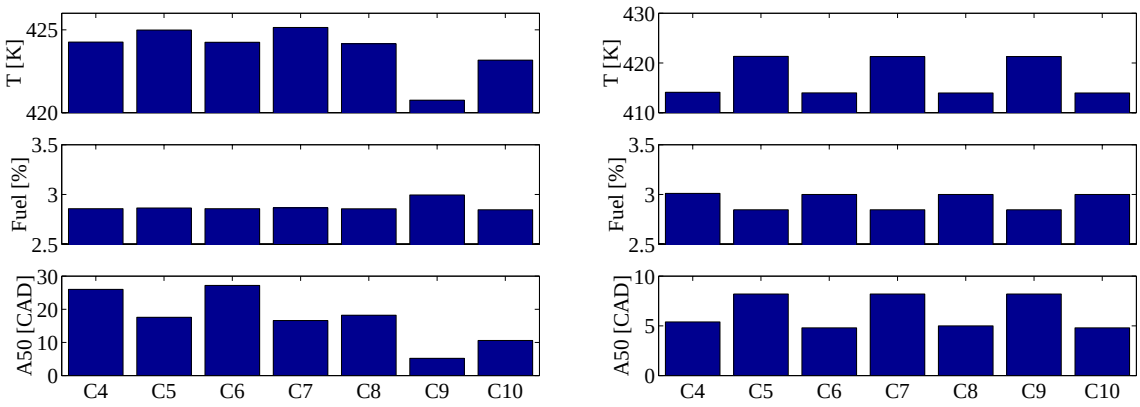

Figure 63 With termination of radicals. With inlet temperature that provided oscillating combustion timing earlier, 124°C, the oscillation become heavier and C8 become even a misfire with poor combustion efficiency (left). With lower inlet temperature, 124°C, alternating combustion occur, as in Figure 62 (right).

Given the stable operation, (as seen in Figure 57 and Figure 58) it is possible to suddenly insert a disturbance in terms of a cycle with slightly later ignition timing (C11*, without chemical kinetics) and see what happens in the following cycles. The result is shown in Figure 64 and it is clear that the initial temperature can explain the response again. To further investigate this affects the temperature at EVO, IVO and 60 degrees BTDC (i.e. when the chemical kinetic calculation start) is shown in Figure 64. It clearly shows that later combustion timing first brings up the EVO temperature (due to less heat transfer and lower efficiency), this also increases the residual gas temperature, here illustrated by the temperature when the intake valve opens (IVO). Finally, the temperature at the end of the compression stroke in the following cycle (C12) is also increased and if this temperature is increased it will give the same effect as if the inlet temperature would be higher, ignition occur earlier.

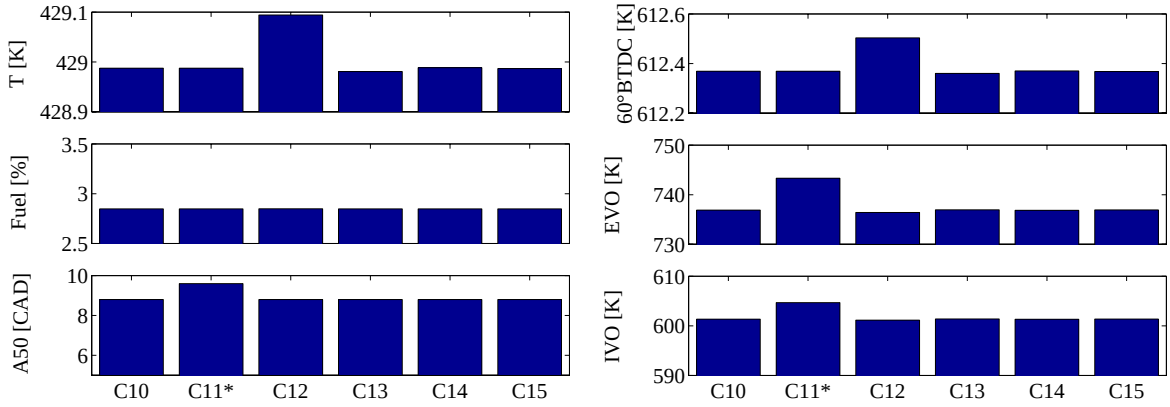

Figure 64 The response after a "disturbance cycle" with later ignition timing, C11. The following cycle will experience a higher initial temperature at IVC (T) and hence also at 60 degrees BTDC. Note that each cycle starts and stops at IVC so that the EVO and IVO temperatures will refer to the result of each cycle respectively.*

From the results above it is clear that there are one stabilizing effect due to the temperature of the residual gas. Another stabling, or "rescuing", effect activates if combustion is poor, the residual gas become fuel rich (or rich of other hydrocarbons, CO or any other combustible specie) the following cycle may occur earlier and give better combustion. Any radicals surviving have little or no effect on the stability.

There is other stabilizing or destabilizing effects that also have importance e.g. heat transfer, which is thoroughly studied by Olsson et al [116]. This has an important role at high load operation where earlier ignition timing may cause the wall temperature to increase, causing less heat transfer and higher temperatures at the end of the compression stroke. The ignition timing gets earlier and earlier and it becomes critical for the control system to detect and stop such development. At high load supercharged or turbocharged operation, this may cause too high peak pressures and eventually engine damage.

4.3.3 The effect of valve timing

As seen earlier, the residual gas temperature plays an important role when it comes to HCCI timing control. Therefore, it is obviously interesting to use methods of controlling the amount of residual gas inside the cylinder. Koopmans and Denbratt [117] has recently reviewed and investigated this experimentally in a camless gasoline engine using mostly negative valve-overlap (increasing positive overlaps too much may cause the valves to interfere with the piston), meaning that EVC is moved earlier and IVO later than usual. He also showed that this concept could be used during a transition from spark ignition to HCCI operation. This concept force significant residual gas to stay in the cylinder during exhaust stroke and the gas will actually be compressed during the late end of the exhaust stroke. They also showed and explained cycle-to-cycle variations in this engine by variations in the initial temperature [118].

A simple simulation is used here to study this concept simply by using the reference case described in Table 11 as a start point, and then shift EVC earlier and IVO later up to 90 degrees. Valvelifts for 60 degrees shift is shown in Figure 65. An iterative approach is used so that the amount of injected fuel per cycle (into the engine inlet port) is the same, about 26 mg/cycle, hence the engine load may change only due to the effect of variation in combustion timing and pumping work and not how much air-fuel mixture is entrapped in the cylinder.

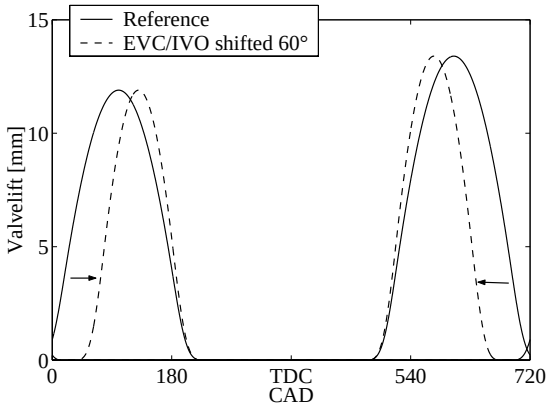

Figure 65 Valve lift curves without (Reference) and with 60 degrees shift of EVC and IVO

This concept allow a lot of residual gas to stay inside the cylinder, over 50% is possible as seen in Figure 66, and with a constant amount of fuel per cycle this means that the λ-value goes down towards 1, i.e. stoichiometric mixture. Despite this heavy amount of residual gas, the combustion timing becomes earlier and earlier as also seen in Figure 66. Lot of hot residual gas increases the temperature prior ignition here illustrated by the temperature 60 CAD BTDC and this explains the earlier timing. The increasing amount of residual gas and temperature explain this concepts capability of handling a transition from spark ignition to HCCI.

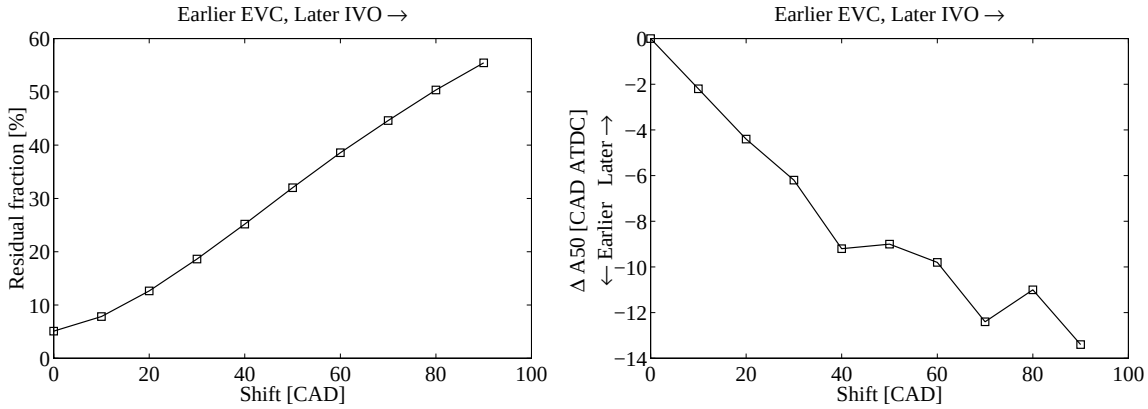

Figure 66 Earlier EVC, later IVO shift and its influence on residual gas fraction and combustion timing.

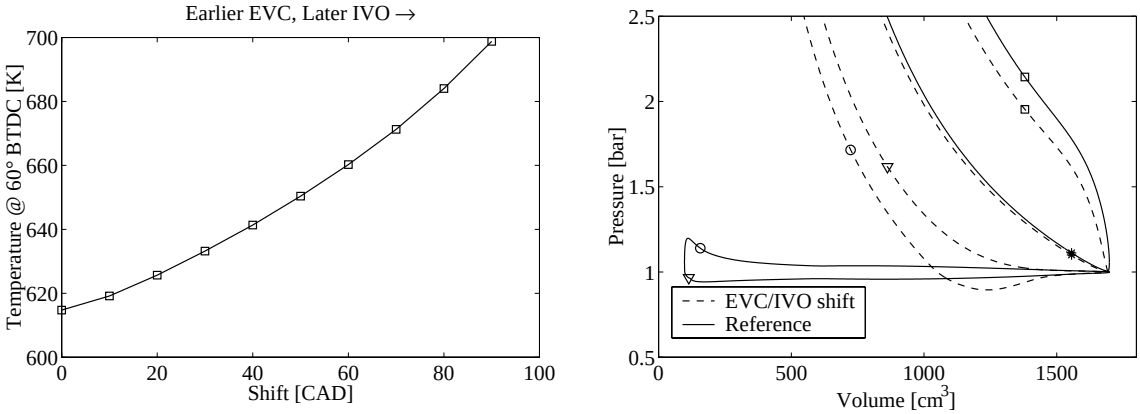

Figure 67 Earlier EVC, later IVO shift and its influence on temperature at 60 CAD BTDC (left) and pressure over volume during intake and exhaust stroke (right). □ indicate EVO, ▽ - EVC, ○ - IVO and ✱ indicate IVC.

Another way to control residual gas is to use inlet cam phasing, and move both IVO and IVC earlier (increasing overlap) and thereby affect the valve flow process e.g. the backflow over the intake valve. This backflow of burned gas will then increase the residual gas fraction. To study this effect the reference case described in Table 11 is used again and the cam timing is phased +/- 35 degrees. In addition, moving only the IVO timing is investigated as well. The Volvo TD100 geometry is used however calculated valve lift (from timing and maximum lift) is used instead of measured lift in order to modify valve timing more freely. It should be pointed out that the model does not include any heat transfer model for the inlet manifold; the heat loss of this hot residual gas is one factor of uncertainty.

If the inlet valve timing is moved earlier by using either IVO/IVC shift (cam phasing) or IVO shift, the residual gas fraction is increased but the combustion timing changes depending on what method is used as seen in Figure 68. Using cam phasing give first an earlier timing, then at about 20 degrees shift, the trend alter an we get later and later timing. This behavior can be explained by the temperature and pressure during the compression, here showed at 60 degrees BTDC in Figure 69. With early cam-phase shift down to –20 CAD, the amount of residual gas increase and cause an increase in temperature that move combustion timing earlier. With more cam-shift, the effective compression is reduced since IVC has become too early and this limits both temperature and pressure. The temperature ends up at approximately at the same level as with zero shift but the pressure is much lower and combustion timing becomes later.

Shifting only IVO earlier does not affect the pressure during the compression stroke; the temperature increase with more residual gas and combustion timing become earlier.

Slightly later cam phasing reduces the amount of residual gas and the temperature at 60 CAD BTDC is reduced, combustion is delayed. With more shift, the amount of residual gas does not change, instead is the temperature of the residual gas affected. Later cam phasing effectively reduces the trapped amount of air in the cylinder; the λ-value is reduced (Figure 70), from 3.0 down to about 2.6, and this brings up the temperature after combustion and hence the residual gas temperature. Despite the lower pressure, reduced by late intake valve closing, again the temperature has the greatest influence and combustion timing become earlier.

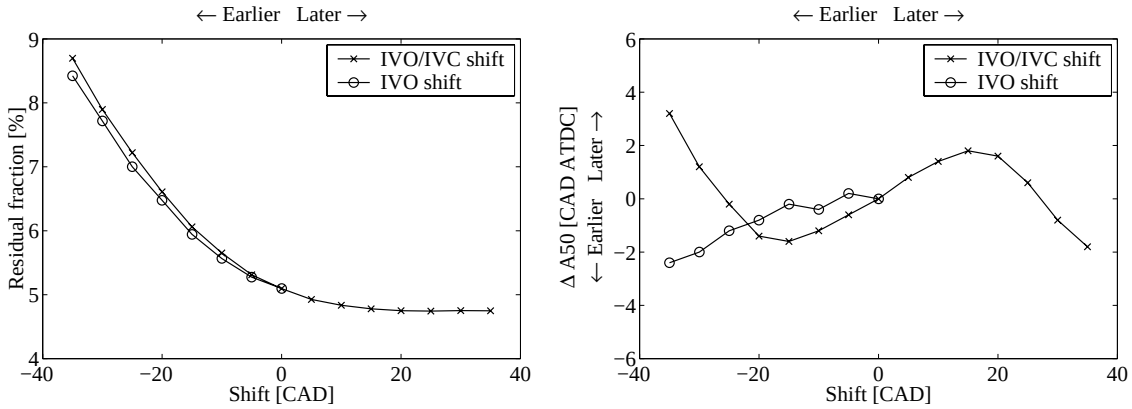

Figure 68 The effect of inlet valve timing on residual gas fraction (left) and combustion timing (right).

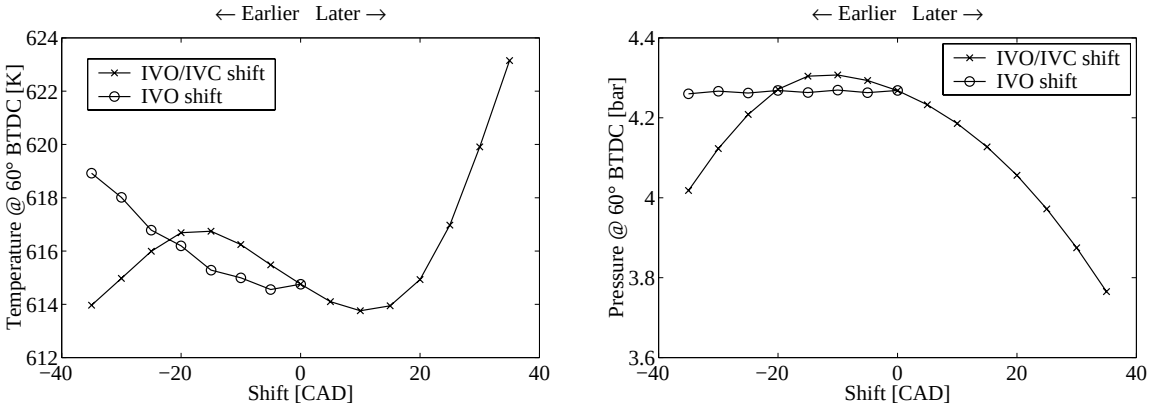

Figure 69 The effect of inlet valve timing on temperature (left) and pressure (right) at 60 degrees BTDC.

In summary, using inlet cam phasing has very little influence on combustion timing; it is not a suitable as a single method to control HCCI combustion. Shifting EVC/IVO or using late inlet cam phasing also introduce pumping work illustrated by the p-V diagrams in Figure 67 and Figure 70. The resulting pump mean effective pressure for the different solutions is showed in Figure 71. Shifting EVC/IVO causes an "extra" compression phase. Heat transfer during this phase causes a loss of energy that results in increased pumping work. It should be pointed out that this extra heat transfer may be overestimated due to model limitations and the wall temperature may become higher due to the extra heat transfer. Using late inlet cam-phasing give a huge pumping loop since enough valve flow area is not allowed to be high enough in time. Maximum valve lift occurs too late in the intake stroke.

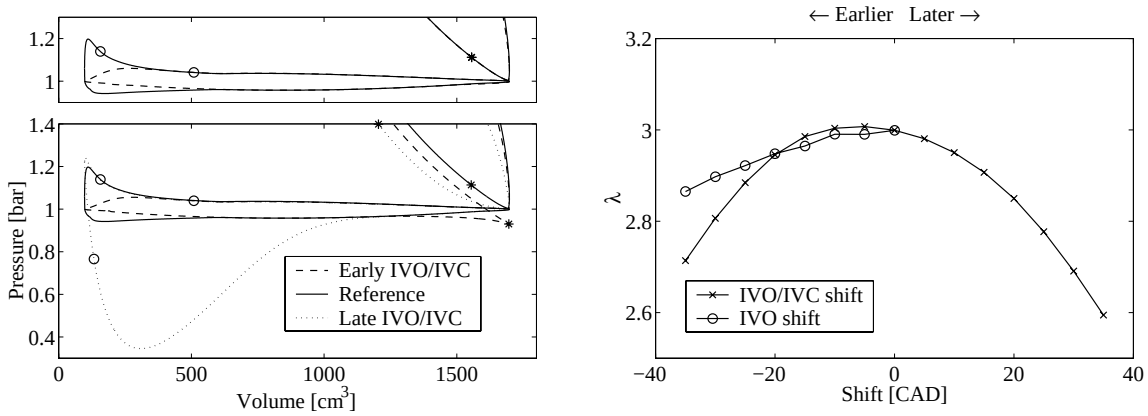

Figure 70 Pressure over volume (left) for 35 degrees earlier IVO (top) and +/- 35 degrees cam phasing (bottom). ○ indicate IVO and ✱ indicate IVC. The resulting λ-value (right).

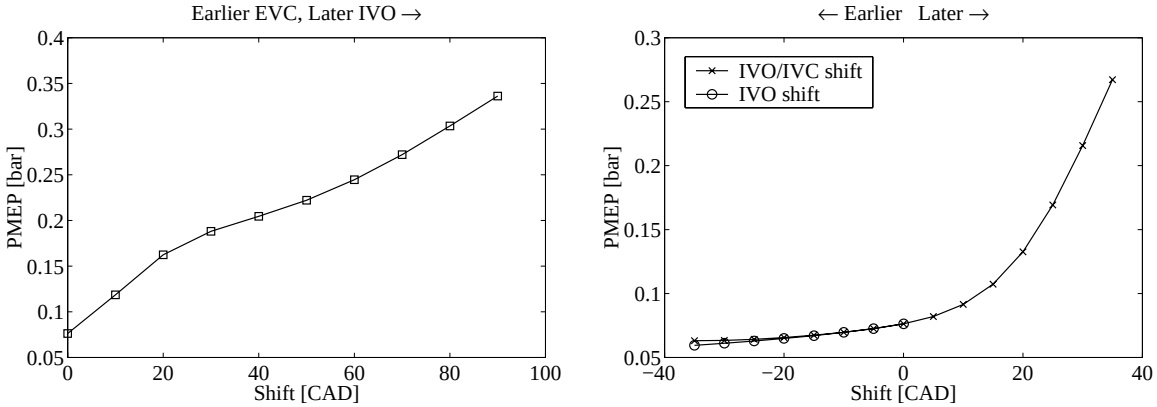

Figure 71 Pump mean effective pressure, PMEP for EVC/IVO shift (left), IVO/IVC (cam-shift) and IVO shift (right).

4.3.4 The effect of exhaust gas recirculation - EGR

Exhaust gas recirculation, EGR, has been used successfully in spark-ignited engines and lately also in diesel engines to reduce NOx formation. It affects the specific NOx emissions (g/kWh) in two ways; chemically by reducing the oxygen concentration, and hence NOx formation rate at high temperatures, and by substitute air with EGR reduces the mass flow through the system and hence the mass of NOx leaving the system.

In HCCI engines the same result is shown for most fuels, however EGR also affect the combustion timing through the ignition temperature. Christensen [38] showed that for natural gas and EGR higher inlet temperature were required and this actually increased the volume fraction of NOx, the specific NOx emissions were quite un-changed. The specific emissions of HC, and to some degree CO emissions also, went down due the lower mass flow leaving the system. The volume fraction of HC and CO was quite constant. Using EGR with a fuel like natural gas may not give any significant benefits but it is perhaps necessary if the combustion become to fast, or if knocking appear at high load operation. The zero dimensional models used here cannot handle the oscillating pressure from knocking combustion and is not very suitable for studying combustion duration. Instead are the work focused on understanding the influence of EGR on inlet conditions and the gas properties, and what consequence it has on performance and efficiency.

In this simulation, the amount of fuel is kept constant at 25.79±0.01 mg/cycle corresponding to the reference case (Table 11, $\lambda = 3$ without EGR). The amount of EGR is increased is steps of 10% up to 50% and the inlet temperature is adjusted so that 50% burned fraction (A50) occur at 8 degrees ATDC. The required inlet temperatures and the resulting indicated efficiencies are shown in Figure 72.

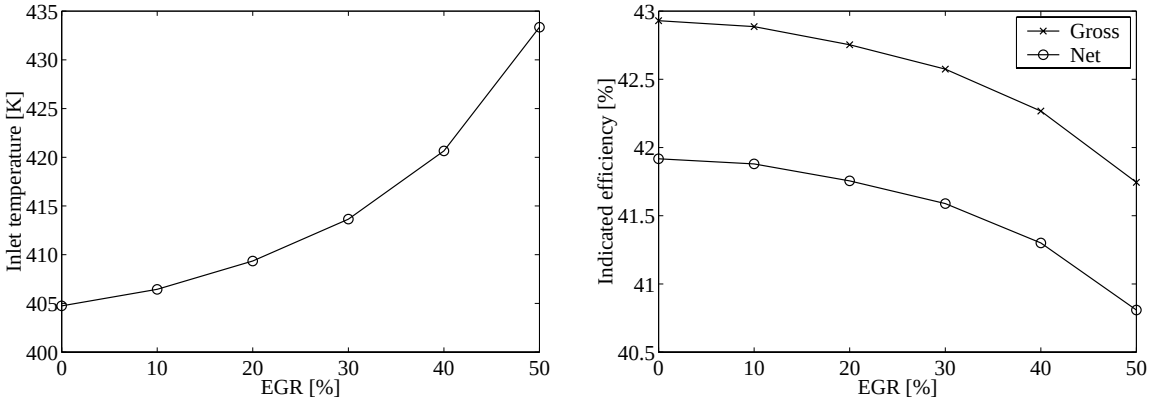

Figure 72 Required inlet temperature (left) and resulting indicate efficiencies (right) with EGR. "Gross" = compression and expansion stroke and "Net" = whole cycle.

Higher inlet temperatures are required with EGR due to altered thermal properties of the working gas and higher ignition temperatures. With EGR, the specific heat of the inlet mixture is higher (Figure 73) due to higher specific heat of the burned gas compared to the fresh charge. During the compression stroke, only a limited amount of energy (work) can be added to the gas trapped in the cylinder due to a fix compression ratio, which means that both the pressure and temperature is limited at the end of the compression stroke and after the combustion, due to the higher specific heat. Therefore, a higher inlet temperature is required to reach the ignition temperature. The ignition temperature is quite constant at low amounts of EGR, but increases significantly with EGR levels above 20%, as seen in Figure 74. At high levels of EGR the O2 concentration degreases since air is replaced with burned gases. In addition, all concentrations are slightly reduced due to lower pressure and hence density.

Higher specific heat limits the maximum temperature after combustion, which limits the heat transfer to some degree. Therefore, if the simulation is made without heat transfer, the efficiency drops even more, as seen in Figure 75. In total, the lower pressure levels give a slight reduction in efficiency. At higher amount of EGR there is a significant increase in ignition temperature and even higher inlet temperatures are required. The overall temperature trace is elevated and the heat transfer increases instead (Figure 74), the efficiency drops even more. The explanation is quite complex; a schematic figure explaining the relations is shown in Figure 76, which may support the discussion above.

In a real engine however these very small differences in efficiency is probably quite difficult to see, other effects may have higher significance e.g. combustion efficiency. Without EGR the combustion efficiency may be, let say 95%, but with EGR some of the exhaust gas is recycled and the recycled hydrocarbons gets a second chance to burn, combustion efficiency increases because less mass of unburned fractions leave the system[12]. When the combustion efficiency increases, we can expect the indicated efficiency to increase. Combustion duration will probably increase at high amount of EGR; the maximum temperature and thereby the

[12] Note that the fuel trapped inside the cylinder is used here as reference when calculating efficiencies. This amount of fuel includes residual and recirculated unburned fuel from previous cycles.

heat transfer will decrease somewhat. In summary, a less decrease in efficiency could be expected in a real engine. The higher inlet temperatures lifts the temperature level over the whole cycle and since a constant wall temperature is assumed here the heat transfer increases. If the wall temperature would have been allowed to change, it is quite clear that it would be higher with EGR than without due to the overall higher cycle temperatures. Nevertheless, the wall temperature can only increase if the overall heat transfer or if the coolant temperature increases. A thermostat usually controls the coolant temperature and it should be considered as fairly constant. Therefore, the change in heat transfer on a real engine may not be as significant as seen in the simulations here.

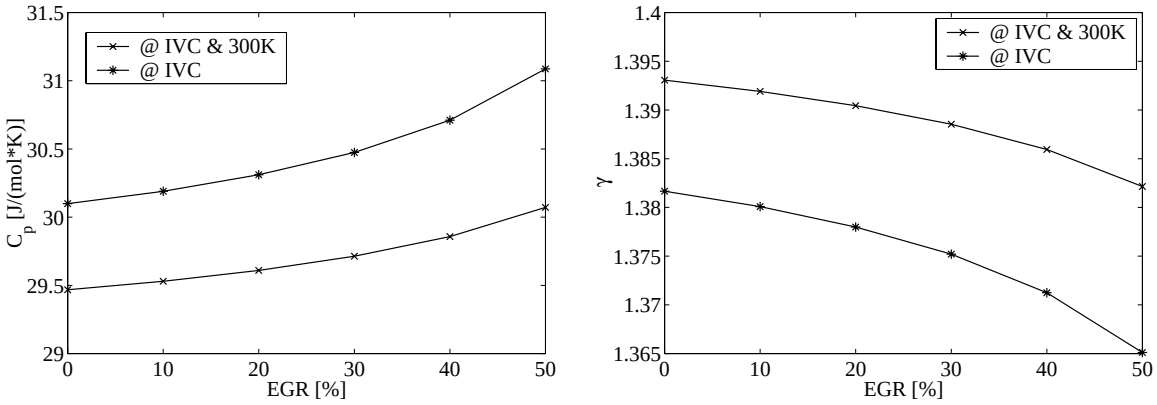

Figure 73 Specific heat at constant pressure (left) and ratio of specific heats, γ, (right) for the in-cylinder mixture at IVC. At different amount of EGR and 300K and at actual temperature at IVC.

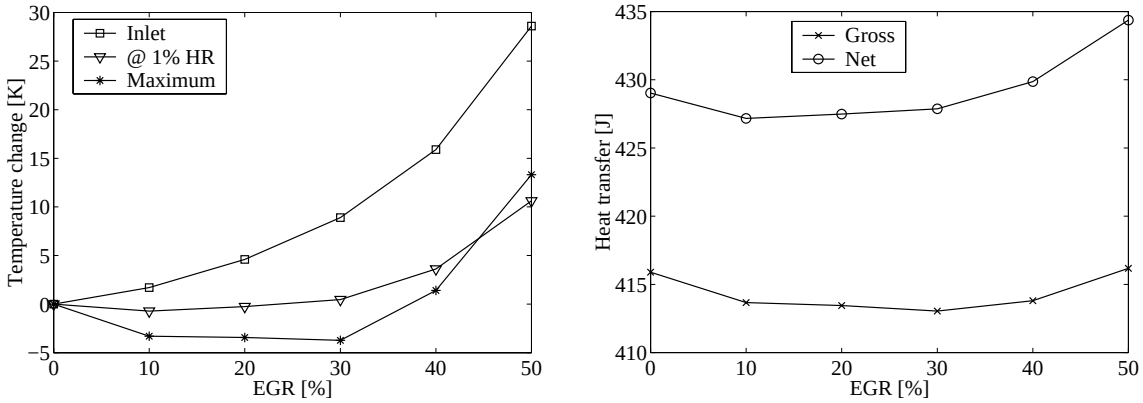

Figure 74 Change in inlet, ignition (expressed as temperature at 1% heat release, 3.6 CAD BTDC in all cases) and maximum temperatures with increasing EGR (left). Accumulated heat transfer (right).

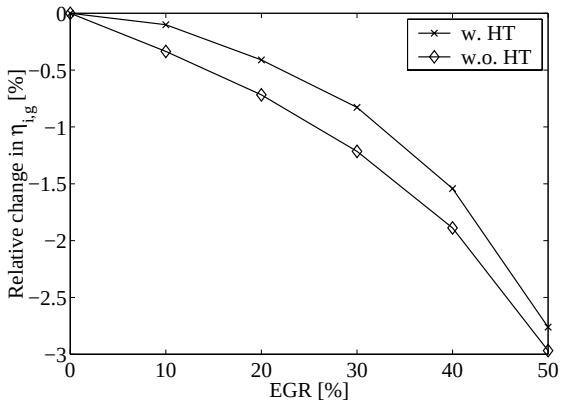

Figure 75 The relative change in efficiency due to the effect of heat transfer and EGR

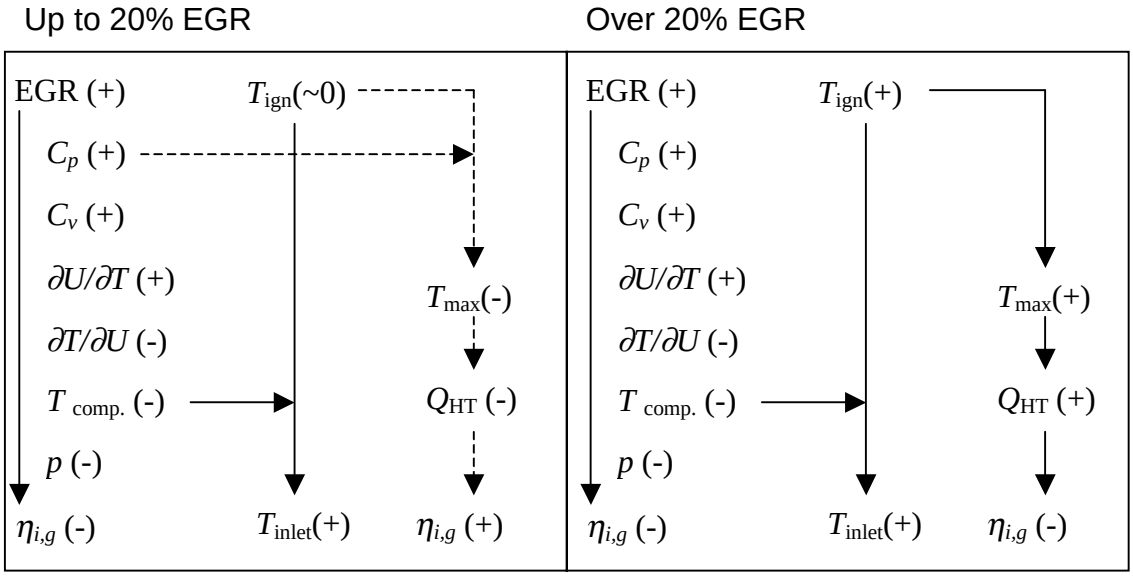

Figure 76 The effect of EGR on efficiency

The influence of the gas property is even known from ideal cycles, e.g. ideal adiabatic cycle with constant volume at TDC combustion and constant gas properties result in an ideal thermal efficiency that can be expressed like shown in Eq.113, where. As shown earlier, specific heats depend on temperature and gas composition. With EGR and/or at higher temperatures, the specific heat is increasing as seen in Figure 73. This mean that the ratio of specific heats, $\gamma = C_p/C_v = C_p/(C_p - R) = 1/(1 - R/C_p)$ decreases and therefore will the efficiency also decrease according to Eq.113.

$$\eta_{Th.} = 1 - \frac{1}{r_C^{\gamma-1}} \qquad \text{Eq.113}$$

4.4 The effect of humidification of inlet air – the HAM concept

Instead of using EGR, it is possible to dilute with other non-NOx generating gases e.g. vaporized water (or steam). Hugon used water injection into the cylinder in a non-compression flame-ignited engine to cool the double acting piston back in 1861. Later, when non-compression engines were abandoned, Prof. Bánki of the Budapest Technical University increased the compression ratio in a SI engine (to 6.5, a high value at that time) and used water injection to avoid knocking combustion. The high compression ratio gave a better efficiency but the water consumption was reported to be high, about 5 times the fuel consumption (reviewed by Cummins [97]). Later "hot-bulb" engines also employed water injection to control the temperature of the bulb and hence preventing pre-ignition. The hot-bulb engine was a very interesting engine that was frequent in fishing boats, tractors and as stationary engines in Europe from about 1900 to 1940. It was often a 2-stroke engine with direct injection of the fuel into a hot, un-cooled part of the combustion chamber. The injection timing was quite early and the engine speed was fairly low. It was vital to keep the temperature of the bulb correct and this could be a problem if the engine were running at high load for a long time. Water injection, either mixed with the air, the fuel or injected in a separate injector, was developed. Later came adjustable fuel injectors (spray angle) solving this problem without the need of any water [119].

The Humid Air Motor (HAM) concept shown in Figure 77. The patents of this method are held by Rosén and Olsson [120] and it has been developed by MUNTERS AB as a method of reducing NOx emissions in diesel engines. They have implemented this technology in large diesel engines for ferries with good results and they claim up to 70% NOx reduction without increase in fuel consumption [122]. Other positive side effect is that cylinder and valve temperatures become lower and the engine become "cleaner" i.e. there is less carbon deposit on the combustion chamber walls. The water to air mass ratio, W/A is about 0.11 at 2.5 bar/75°C and 98% relative humidity (RH).

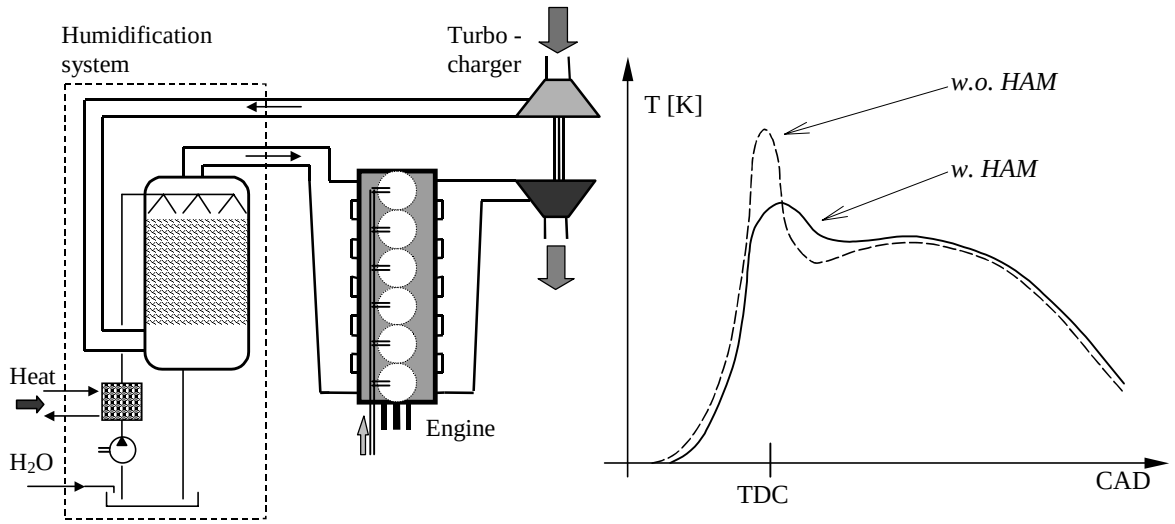

Figure 77 The HAM concept in a diesel engine (left), Revised from [121]. Schematic temperature diagram illustrating the effect on combustion (right). Water reduces heat release rate which limits the maximum temperature and hence NOx formation. Revised from [122]

Water injection in HCCI engines has been studied experimentally by Christensen [41]. The results showed that water reduces heat release rate but the combustion efficiency goes down, both CO and HC emissions increases. It should be pointed out that the heat release rate is dependent on combustion timing that was allowed to change during these experiments.

If liquid water is injected downstream the compressor, it is possible to make use of the vaporizing in terms of cooling of the inlet charge. In HCCI, this may be suitable at very high engine loads, where cooling and/or water injection could be used as a control parameter. In the HAM concept, heat from the coolant water of the engine or the exhaust gas downstream the turbine is used as a vaporization improver in the humidifier. It is possible to increase the mass flow through the turbine and hence deliver more power to the compressor. This is making this concept very interesting in HCCI engines were it may solve some of the turbocharging problem. Vaporized water, i.e. steam has a quite high specific heat; a slight decrease in efficiency of the engine should be expected but this means that the energy level upstream the turbine would also increase.

To study this further engine cycle simulation is made at turbocharged conditions and a slightly richer mixture of $\lambda = 2.5$ (without water) is selected for high load operation. The inlet and exhaust pressures are increased from the reference case 1 bar to 2.5 bar and the engine speed is increased to 1500rpm. The combustion timing is set constant as previously by adjusting the inlet temperature. The resulting inlet temperature and relative humidity for different amount of added water steam is seen in Figure 78. Without additional water, the inlet temperature is about 365K and this corresponds to an isentropic compressor efficiency of about 75% (compressor inlet temperature: 293K). Higher inlet temperature is required with more steam as expected, about 11 degrees per 0.1 in W/A-ratio. The reason why the temperature has to be higher is not due to altered ignition temperature. The ignition temperature is quite constant as seen in Figure 79, it even decreases but what happens is that the specific heat increases which reduces the temperature and pressure during compression and to compensate for this effect the inlet temperature has to be increased to maintain timing. The maximum temperature decreases as the specific heat increases.

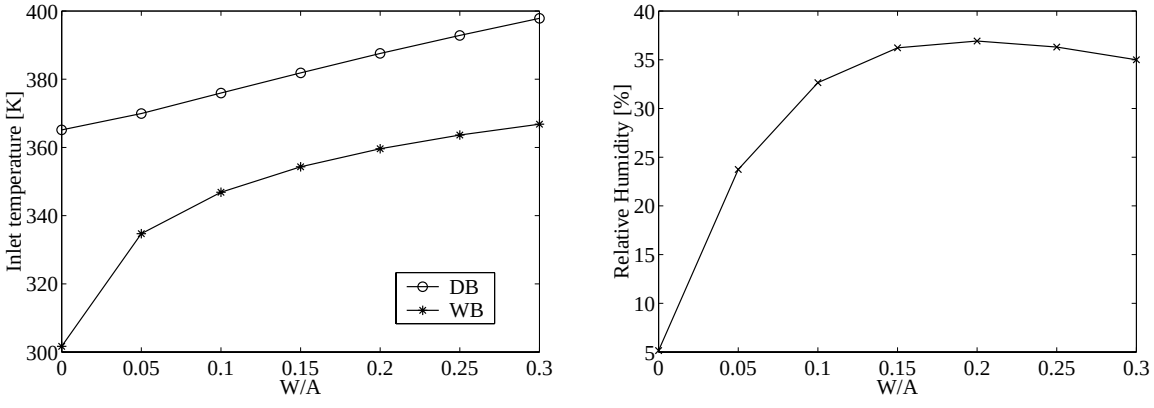

Figure 78 Required inlet (dry bulb - DB and wet bulb - WB) temperature (left) and relative humidity (right), over water to air mass ratio, W/A.

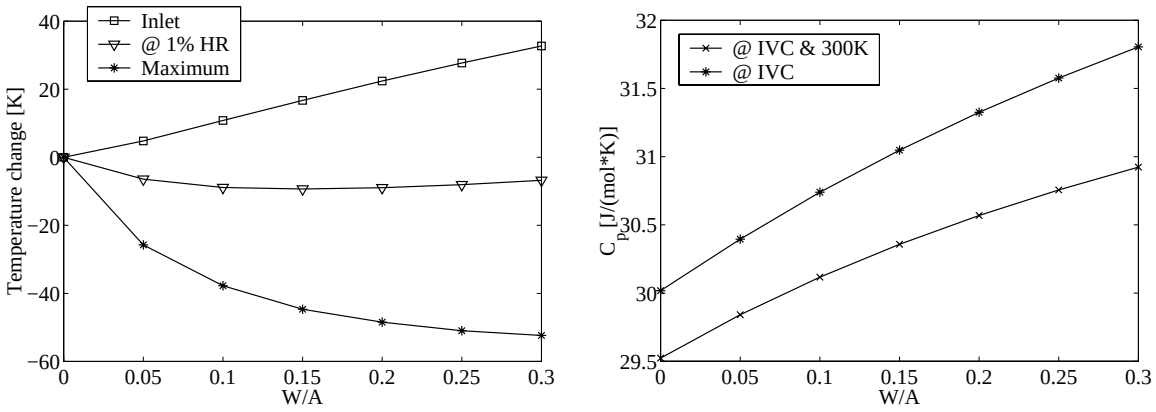

Figure 79 The change in inlet, ignition and maximum temperature (left) and specific heat at IVC (right).

As the maximum temperature decreases the heat transfer decreases, however the higher specific heat reduces the pressure, which has a greater affect on the indicated efficiency of the engine as seen in Figure 80. In the same figure, the heat balance of the engine is shown scaled to a 6-cylinder engine. The fuel energy expressed as heating power calculated from fuel flow and the lower heating value of the fuel (Q_{LHV}) is about 298kW (kept constant). The indicated work is about 140kW but decreases since the efficiency decreases. The heat transfer to the combustion chamber walls is about 70kW and decreases because the overall temperature decreases. The heat that leaves the engine with the exhaust gas is about 90kW and increases due to lower efficiency and less heat transfer. The vaporization heat at this inlet conditions (heat required to elevate the water temperature to inlet conditions is not considered) is increasing with increasing water flow and there is a brake-even with the engine heat transfer at 0.15 in water to air ratio.

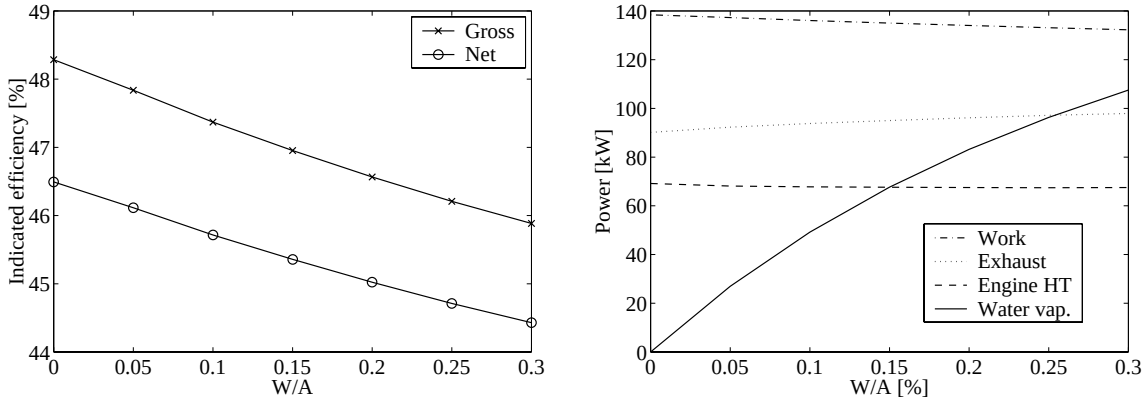

Figure 80 Indicated efficiency (left) and power levels (right). Fuel heat power (LHV) is about 298kW, "Work" – net indicated work, "Engine HT" – heat transfer over combustion chamber walls and "Exhaust" fuel heat minus work and engine heat transfer. "Water vap." – Water vaporization heat, is calculated from water flow and specific vaporization heat at 2.5 bar and the present inlet temperature.

5 More realistic prediction of heat release rate

5.1 "Slave" cycle and estimation of NO formation

The chemical kinetic calculation renders a pressure trace with a very high, close to infinite, pressure rate during combustion, which is not realistic, although HCCI has a very fast combustion at high load operation. The high combustion rate causes a very high maximum pressure and hence temperature. A very simple way to get around this problem is utilized here, however other methods are probably better and the author would like to advise the reader, if he faces the decision, to select either multi-zone models or so-called PDF models that give a better prediction of the heat release rate. At the writing moment, it may appear time-consuming in terms of computational time, but computer performance is constantly under development.

In this case, the chemical kinetics is used to find ignition timing and a "slave cycle" is then used with more reasonable estimated combustion duration. When simulating high load operation the combustion duration, from 10 to 90% burnt, is set to be 4 degrees. The Wiebe function Eq.53 is used for the heat release shape (see section 2.5.1). This means that the compression and expansion part of the cycle is calculated twice, first with kinetics and then with the Wiebe function.

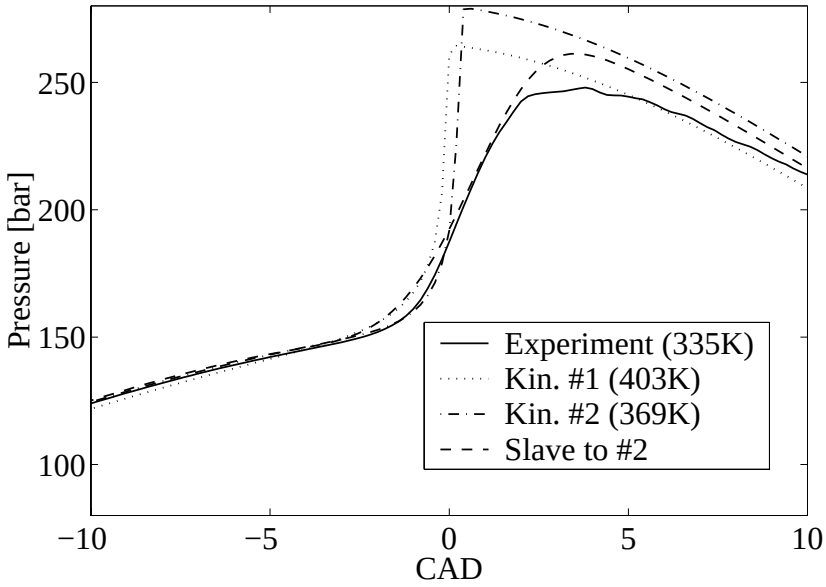

Figure 81 Slave cycle compared to kinetics and experimental pressure traces. Kin#2 is used trough out this work. Inlet temperatures are shown within brackets.

A large number of simulations with chemical kinetic based prediction of ignition timing has been done in order to find models for the full system simulation. The purpose is to reduce the

computational time for the system simulation. Depending on what resolution is used in the cycle simulation part (intake, exhaust stroke) the interaction with the chemical kinetics program takes quite some time due to interpolation.

Using the temperature and pressure trace from the slave cycle it was possible to estimate the specific NOx emissions with the extended Zeldovich mechanism as described by Heywood [96]. It gave at least the correct order of magnitude, as shown in Table 13, considering the differences in maximum pressure and hence temperatures. This mechanism could however be used as an indicator of when significant NO appear.

Table 13 Comparison between experiment and cycle simulation regarding IMEP and NOx

	Experiment [36]	Simulation
$IMEP_{net}$ [bar]	14.0	13.3
NOx [g/(kWh)$_i$] *	0.0075	0.0082

*) NO counted as NO_2 (ISO 8178-1)

5.1.1 Compression ratio optimization

In this case, cycle simulations with chemical kinetics were used to optimize the compression ratio for maximum load. The following assumptions and limitations were used:

- A maximum in-cylinder pressure of 200 bar.
- A maximum NO fraction of 10 ppm in the exhaust, calculated from the extended Zeldovich mechanism.
- Combustion timing corresponding to maximum pressure at 8 CAD ATDC
- The engine speed was set to 1500 rpm.

The λ-value basically controls the maximum temperature and hence NO formation. Inlet pressure determines the maximum pressure, and inlet temperature determines combustion timing. The selected timing is held constant, based on a compromise between efficiency and NO formation. (A very detailed study of the relation between combustion timing and stability, NOx emissions and compression ratio was made by Olsson et. al [116].) An iterative approach is used to find the proper λ, inlet temperature and pressure for each fuel and compression ratio. Two different fuels were investigated; natural gas and land fill gas. Gas composition and energy content are shown in Table 14.

The indicated efficiency became higher with higher compression ratios as shown in Figure 82, a relation well known from ideal cycles. However, the load (Figure 83) was limited with higher compression ratios due to the limited maximum pressure restricting the maximum inlet pressure. When the friction was considered, the simulated brake efficiency peaked at compression ratios between 15:1 and 17:1 (Figure 82). The friction model has no load or compression ratio dependence; the results may have been somewhat different if it did. The λ-values (Figure 83) was fairly constant indicating that the ignition temperature and the NO formation do not vary that much with different compression ratios.

The efficiency and load became higher with natural gas than with landfill gas, which can be explained by the higher ignition temperature of landfill gas that raises the required inlet temperature (Figure 84). There is also a small difference in inlet pressure that probably also can be explained by the higher inlet temperature. Higher inlet temperature limits the mass flow, and thereby the amount of fuel burned. If higher combustion temperatures are allowed due to dilution effects, (the high CO_2 content of the land-fill gas) more fuel can be burned by increasing the inlet pressure.

Table 14 Natural gas and landfill gas composition

Specie	Mole fractions	
	Natural gas	Landfill Gas
CH_4	88.11%	49.2%
C_2H_6	6.35%	10ppm
C_3H_8	2.89%	-
$N\text{-}C_4H_{10}$	0.57%	-
$I\text{-}C_4H_{10}$	0.43%	-
C_5H_{12}	0.18%	-
C_6 +	520ppm	-
N_2	1.07%	15.7%
CO_2	-	34.4%
O_2	-	0.2%

	Natural gas	Landfill Gas
$(A/F)_S$	16.58	4.93
Q_{LHV} [MJ/kg]	47.8	14.3
$Q_{stoich.\ mix}$ [MJ/kg]	2.72	2.41

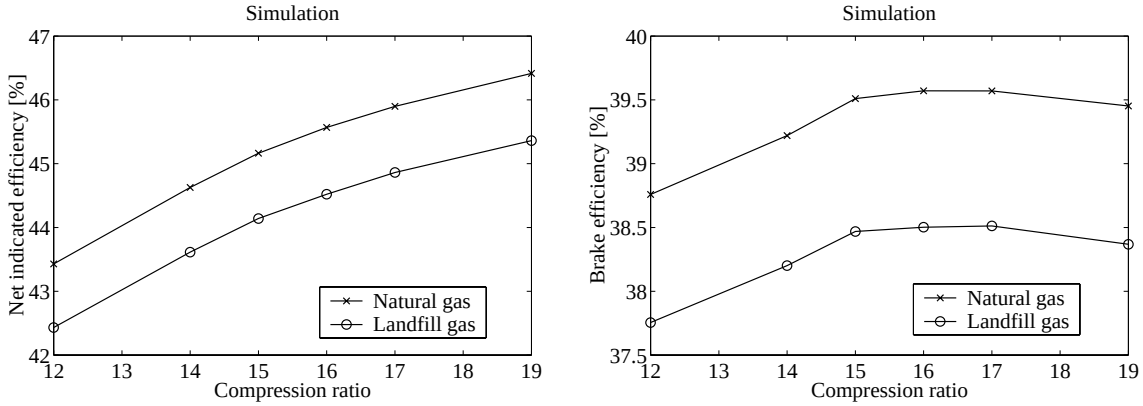

Figure 82 Left - Simulated net indicated efficiency against compression ratio. Right - Simulated brake efficiency at 1500 rpm

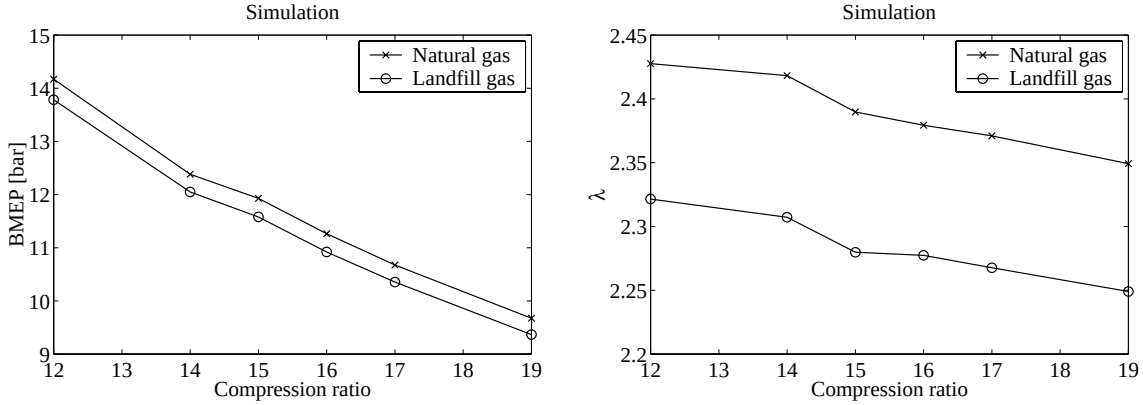

Figure 83 Left - Simulated brake mean effective pressure at 1500 rpm. Net indicated mean effective pressure is 1.71 bar higher at this speed (FMEP is 1.71 bar). Right - Simulated λ-values.

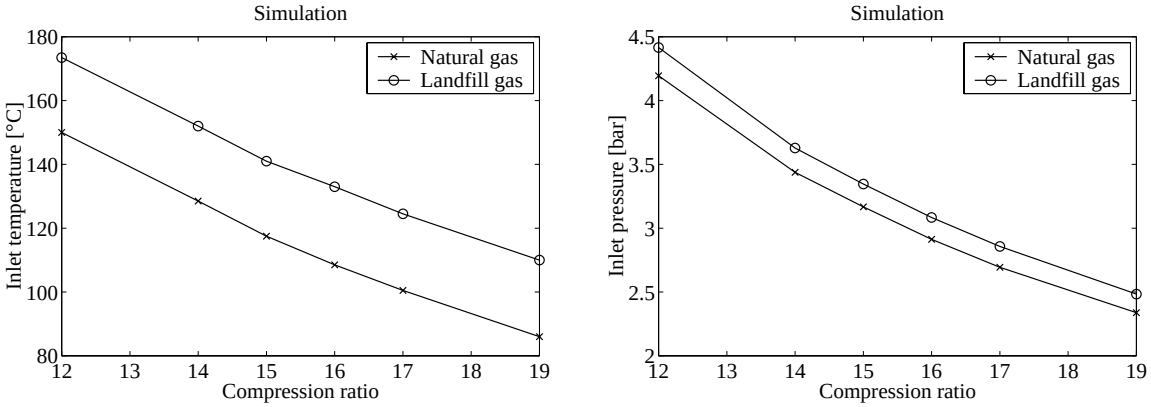

Figure 84 Required inlet temperatures (left) for proper ignition timing and required inlet pressures (right) for reaching maximum load (maximum pressure).

5.1.2 Inlet temperature control model

The previous results show that the best compression ratio is about 15:1. The efficiency then becomes almost maximum but it is still a good compromise when it comes to brake power. To achieve this efficiency the engine has to be turbocharged or supercharged to 3.5 bar (abs) which perhaps is not possible without losses. To investigate this, a full system simulation with various exhaust turbines is studied.

The current HCCI-engine setup uses the inlet temperature to control combustion timing. This is a slow control parameter. Nevertheless, it might be the only solution if no advanced engine design with e.g. variable compression ratio or dual fuel is economically feasible.

A model for desired inlet temperature is made at a compression ratio of 15:1. The required inlet temperature for combustion timing is investigated for different air-fuel ratios and inlet- and exhaust pressures. The speed is kept constant at 1500 rpm. The results are summarized in Figure 85 and Figure 86, where the dependence of fuel, inlet pressure (x-axis), exhaust pressure and λ are shown.

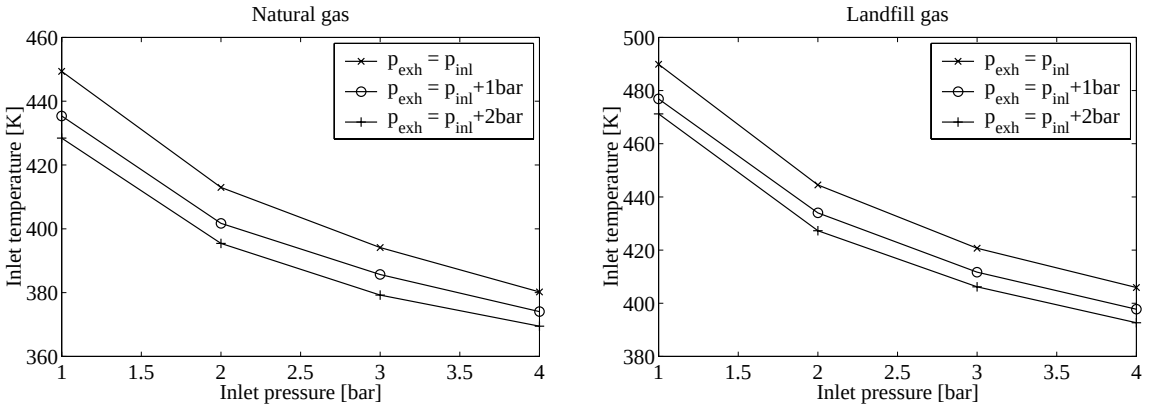

Figure 85 Required inlet temperatures depending on inlet (p_{inl}) and exhaust pressure (p_{exh}). Left – Natural gas at λ = 2.4 . Right – Land fill gas at λ = 2.3 .

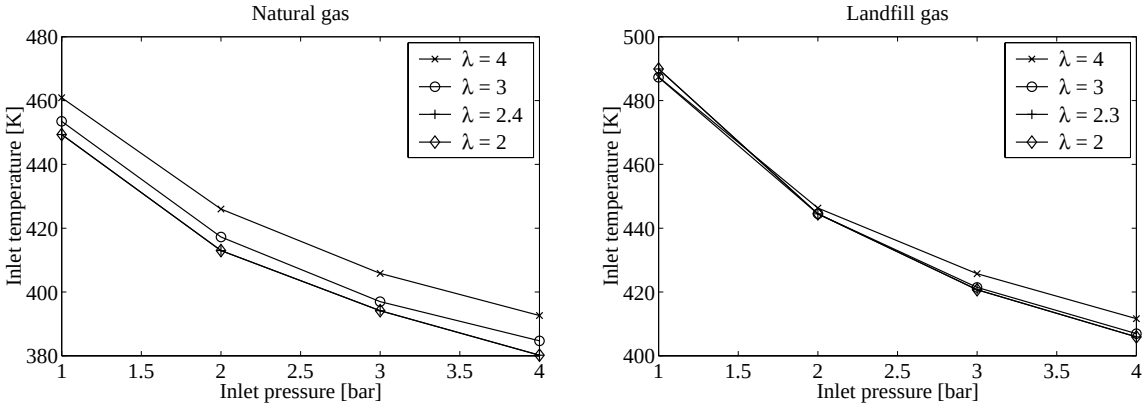

Figure 86 Required inlet temperatures depending on λ-values and engine inlet pressure.

The reason why the exhaust pressure is set higher than the inlet pressure is that we know that the turbine has to be small, compared to diesel engine configuration. This increases the exhaust pressure, but also allow more energy to be extracted.

The modeling is made through multidimensional non-linear regression of these results. This model is used in the system simulation to control proper inlet air conditioning (level of intercooling/heating). It is quite surprising that the required inlet temperature for landfill gas shows little dependence of λ-value.

5.2 System simulation

A whole engine system is simulated in order to study the effect of varying the turbine size of the turbocharger. The system is illustrated in Figure 87. Three different turbine sizes are explored, the largest one, TC-1 corresponds to the diesel engine's original turbine size (geometrical flow area: 25 cm^2) while the two smaller ones, TC-2 and TC-3 produce higher pressure ratios since they have smaller flow area (16 and 13 cm^2 respectively). Again, the simulations are made using the two different fuels mentioned earlier. The fuel is added downstream the compressor (into the inlet manifold), the efficiency of the system is not compensated for the work required to compress the fuel.

5.2.1 The effect of turbine size

Again, the turbine size is investigated using the same turbine sets from the previous investigation with isooctane/n-heptane (see section 3.3), however in this case with other fuels. A more proper estimation of required inlet conditions and the turbo model described in sections 2.6.3 - 2.6.6 is used instead of plain interpolation.

The simulations are performed with a time trace i.e. under dynamic conditions. However the reader should be aware that a number of simplifications were made to speed up the calculations. First, there is no chemical kinetics calculations made in this part, it is assumed that the timing is achieved with proper inlet air conditioning according to the model described earlier (section 5.1.2). The engine cycle is treated as a quite large damper in the system and is withdrawn from the iterative solution of the other system components i.e. for a certain time step only single-cycle calculations are made based on the inlet and exhaust states provided from the previous time step. The same goes for the simple "engine control" module used, it sets the fuel mass flow based on the air mass flow and desired λ (the fuel is injected into the inlet manifold). It also controls the inlet air "conditioner" based on air mass flow and desired

inlet temperature. The conditioner can be interpreted as a controllable charge air cooler (intercooler) or a heater of some sort. It can either cool the gas or heat the gas by removing or adding heat to the air stream. The calculation scheme for the system is shown in Figure 87. Each time step is 0.1 seconds but is allowed to be shorter if there is a problem with convergence. Then it is reduced by a factor 0.5 after each 100 iteration cycle.

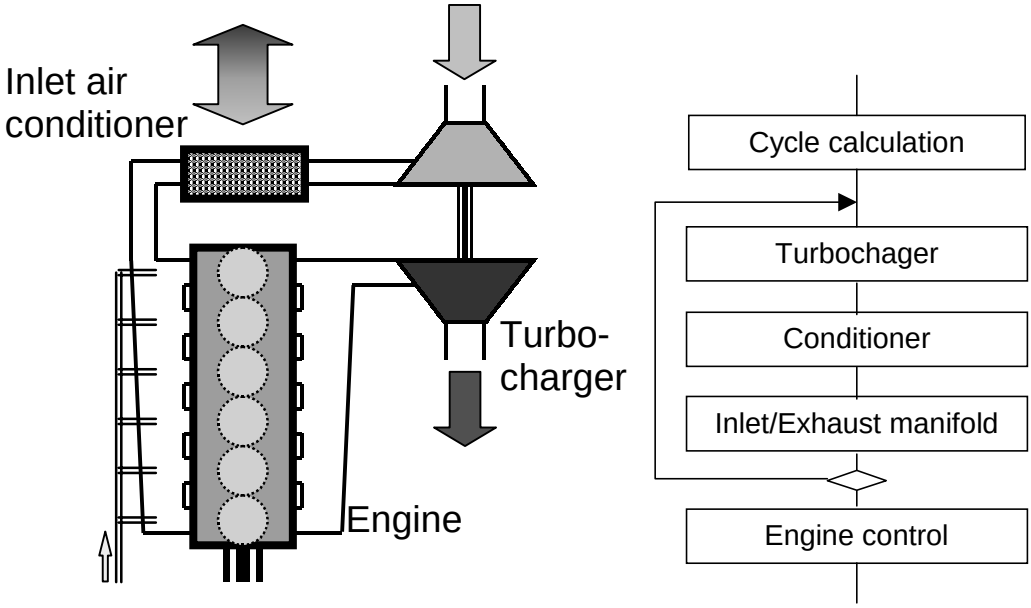

Figure 87 System layout and simplified flow chart of the system calculation, note that the engine cycle and engine control module are moved outside the iterative loop.

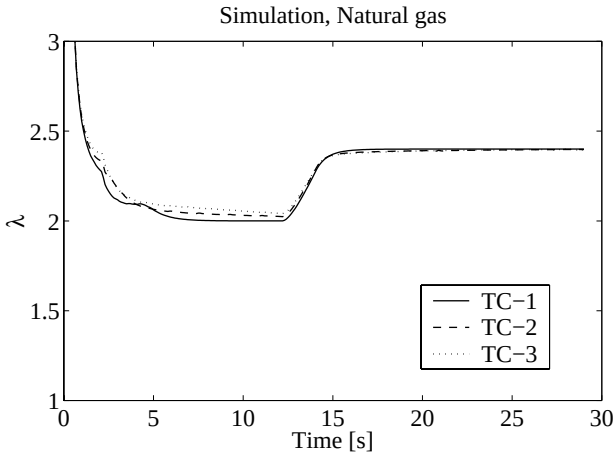

Figure 88 λ over time, 1500 rpm for natural gas. λ=2.4 at 29s. With land-fill gas the λ value is 2.3 at 29s.

During the simulation, the λ-value is varied over time. At first, the λ-value is set to a fairly low value of 2 (low for HCCI operation), simultaneously the engine is speeded up to 1500 rpm and then there is stabilization for 10 seconds where the turbine can speed up further. After that, the λ-value is lowered to the value given by the optimization earlier: 2.4 for natural gas and 2.3 for landfill gas. Everything is then allowed to reach steady state for 20 seconds. This procedure is illustrated in Figure 88. The idea is to simulate a start-up procedure under which the engine goes from idle to full load. The purpose of the middle step with a low λ is to make sure that the turbocharger speeds up, if possible. This procedure is used with three different turbine sizes and two different fuels. The resulting BMEP is shown in Figure 89 and

it is clear that the turbine does not provide enough work. The mass flow and the energy levels in the exhaust are too low.

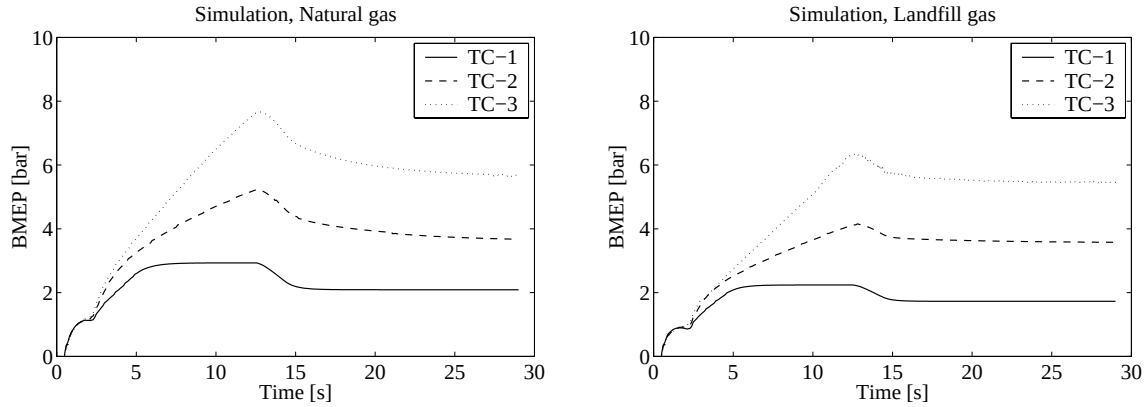

Figure 89 Simulated BMEP for three different turbochargers. Neither of them provides enough boost.

5.2.2 Quest for higher loads

As a final step, adjustments were made in order to reach higher loads. Much later ignition timing was selected; the maximum pressure was set to occur 14 CAD ATDC and the combustion duration was set to 5 CAD. The same control strategy for the inlet temperature was used, although compensated with -10 degrees per step in compression ratio, complying fairly well with the results shown in Figure 84. In addition, the λ-value was reduced to 2.2.

The resulting loads (at time = 29 s) are shown in Figure 90, and the results seem quite surprising: A higher compression ratio gave higher load. The explanation to this is the absence of proper boost pressure with a low compression ratio, which raises the required inlet temperature. This reduces mass flow through the system and consequently, the turbine cannot provide enough work. Regardless of the compression ratio the inlet pressure became 2.22 ±0.02bar. The required inlet air cooling or heating is also shown in Figure 90 and the breakeven point is somewhere between compression ratio 15 and 16.

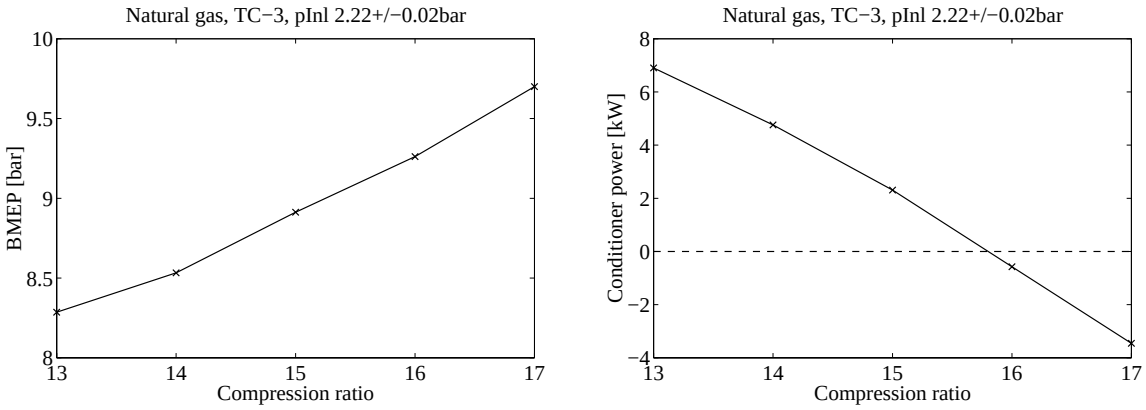

Figure 90 Left - BMEP with the smallest turbine (TC-3) and for different compression ratios. Inlet pressure (p_{Inl}) is 2.22 ±0.02 bar. Right - Required inlet air conditioning. Positive values mean heating and negative mean cooling of the air.

Without proper boost, it is the compression ratio that influences brake efficiency (Figure 91) more than friction. Since the turbocharger cannot provide enough boost, the required inlet

temperature become quite high. This effectively limits the mass flow through the system, making it even more difficult to produce boost. A higher compression ratio can actually allow higher mass flows thanks to lower inlet temperatures. In the following simulations, five different compression ratios are studied. Consequently, the efficiency became higher with higher compression ratio and the specific NO (Figure 91) went down due to the higher load. At 17:1, the efficiency became 40.3% and the NO emissions were about 22 ppm, 0.162 g/kWh, a figure far below the 20 g/kWh of the lean burn SI engine and also well below the legislation limits in Germany and Switzerland (see section 3.5) due to the much leaner mixtures. The specific load of the engine is however limited, only 9.7 bar BMEP at 17:1.

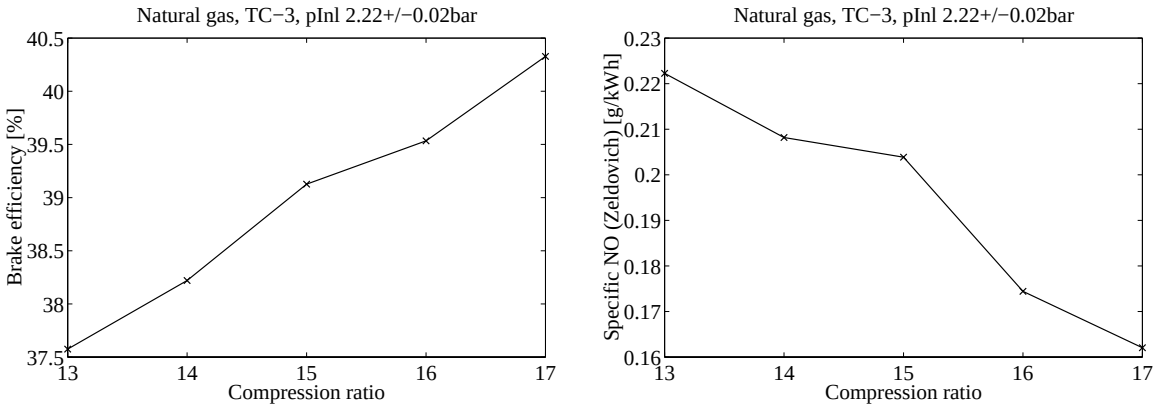

Figure 91 Left - Simulated brake efficiency. Right - Simulated specific NO emissions at λ = 2.2. At 17:1 the NO fraction is about 22 ppm.

6 System simulations with chemical kinetics

As a final step the chemical kinetics is used to predict ignition timing during system simulations, however a slave cycle is used to give a more realistic heat release prediction as shown earlier (section 5.1). The combustion efficiency is set to 95%. A combustion timing control has to be designed to get a suitable timing. The advantage of using chemical kinetics when running full system simulation is that accuracy increases, more parameters are allowed to change and more interesting inlet mixtures can be studied, on the other hand, computational time increases. The geometry of the SCANIA DSC 12 engine (Table 7) is used in all modeling although with compression ratio of 17.4:1 (except in one case were 16:1 is used) and it is fitted with the smallest turbine (TC-3: 13 cm^2 geometrical flow area). In addition, the improved turbocharger model described in section 2.6.8 is used here in order to get better accuracy in the interpolating regime in the maps.

6.1 Simple system with natural gas

A simple system with engine, turbocharger and a combined intercooler – heater ("conditioner", see section 5.2) is simulated using pure natural gas as fuel. The system setup is shown earlier in Figure 87 and the inlet temperature is used for combustion timing control as previously. The purpose is to have this simulation as a reference case for further simulations.

The simulation input, a selected λ-value over time, is shown in Figure 92, in addition the actual λ value is also shown. The compressor model gives a slight oscillation in mass flow and this is why the calculated λ-value seems "noisy", almost like experimental recordings. The chemical kinetics gives some hystheresis effect in combustion timing, which also give a noise effect on IMEP, as seen in Figure 92. The boost pressure is very limited and at λ = 2.1 only 3.3 bar BMEP is reached. The inlet temperature is 395K at this point. Previously, the same system reached 9.7 bar BMEP, 40.3% brake efficiency and 0.162 gNO/kWh at 1500 rpm and λ = 2.1, but in that case a simple model for the inlet temperature were adopted (see section 5.1.2 and 5.2.2) and richer mixtures were allowed during the first period of the simulation (λ = 2.0). It is possible that a richer mixture than λ = 2.1 may provide higher boost pressure during the startup procedure and hence bring up the turbo-speed to a level were leaner mixtures are allowed. Once the boost pressure goes up it is possible to reduce the inlet temperature, which brings up the mass flow through the engine. The increased mass flow then may provide enough energy to the turbine in order to maintain a high boost pressure. On the other hand, λ = 2.1 is a very rich mixture for HCCI combustion (without the use of EGR or any other dilute gas) and knocking combustion is very likely to occur.

A simple way of increasing the mass flow is to increase the engine speed, however at higher speed the pumping and friction losses increases and that will be a penalty on brake efficiency. In Table 15 are the results of various simulations with different air/fuel ratios shown, engine

speed and compression ratio. With higher speed, a slightly earlier timing is used. With the higher mass flow, boost pressure eventually builds up properly and engine load increases. With higher speeds, the pressure upstream the turbine also increases and the pumping losses increase rapidly, at 2000rpm, the PMEP is about twice that of 1800rpm. Friction increases as well, which reduces the overall efficiency at 2000rpm. This results comply with those in section 3.4, when increasing the engine speed a bigger turbine as the TC-2 is more suitable. The maximum pressure is higher than the selected "design limit" used earlier (200bar) and this why leaner mixtures or a lower compression ratio should be selected. A compression ratio of 16:1 is tested at 1800rpm and 220kW brake power is reached with 39.3% brake efficiency and 0.04 gNO/kWh.

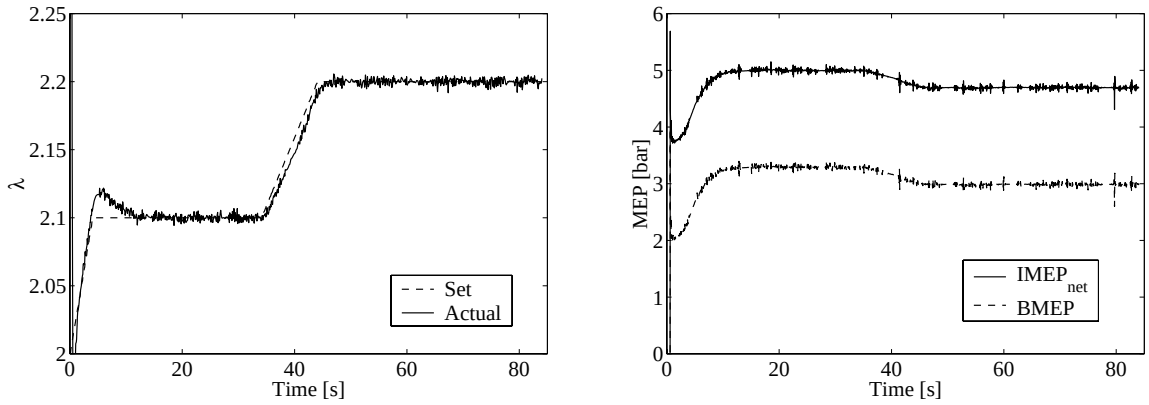

Figure 92 Left - The λ value, both set-point and actual value. Right – Load expressed as indicated – and brake mean effective pressure.

Table 15 Results with simple system using natural gas (T_1 = 298K, p_1 = p_4 = 1.013bar) At 1500 rpm 13kW of inlet air heating is required (T_{inlet}>T_2).

Speed	r_C	λ	p_{Max}		$NO_{Zeldovich}$		dm/dt_{tot}	T_{Inlet}	*Run*
[rpm]			[bar]	@CAD	[ppm]	[g/kWh]	[g/s]	[K]	
1500	17.4	2.18	71	13	7.1	0.08	127	397	Reference
1800	17.4	2.33	212	11	3.8	0.03	456	360	Speed +
1800	16.0	2.30	199	11	5.4	0.04	456	374	Speed +, r_C -
2000	17.4	2.45	223	11	1.4	0.01	541	357	Speed + +

Speed	P_b	*IMEP gross*	*IMEP net*	*PMEP*	*FMEP*	*BMEP*	$\eta_{i,n}$	η_b	p_2	p_3	T_2	T_3	T_4
[rpm]	[kW]	[bar]	[bar]	[bar]	[bar]	[bar]	[%]	[%]	[bar]	[bar]	[K]	[K]	[K]
1500	43.5	5.00	4.68	0.313	1.71	2.98	41.9	26.6	1.14	1.35	326	660	636
1800	220	15.2	14.5	0.71	1.96	12.5	46.0	39.8	3.05	3.31	445	676	543
1800	220	15.1	14.5	0.65	1.96	12.5	45.2	39.3	3.15	3.36	452	698	559
2000	237	15.6	14.3	1.34	2.13	12.2	44.6	37.9	3.29	4.01	465	679	527

6.2 Reformed natural gas fuel

A way to overcome the problem with the high inlet temperature may be to change the ignition characteristics of the fuel. A way to do that is to add other fuels that ignite more easily. However, in most cases it is convenient and more economical feasible to use only one fuel. Regarding natural gas and many other fuels it is possible to reform them into CO and H_2. This can be done through fuel rich pre-combustion in a so-called reformer. The fuel composition leaving the reformer may vary due to load, operating pressures and temperatures. In order to simplify the simulations here, it is assumed that the reformed fuel consists of 40% (volume) CO and 60% H_2 at all conditions. This "synthetic" fuel is then mixed with the natural gas in order to study the possibility to use this fuel as an ignition improver.

Here is the SCANIA engine used again with the setup shown in Figure 87. A mixture of natural gas and this fuel is used. Up to 95% reformed fuel fraction is used, if that is not enough to achieve proper combustion timing, inlet air preheating is also used. As input to the simulation the natural gas equivalent λ is used, $\lambda_{NG,set}$. This air-fuel ratio sets a desired amount of heat added to the system. The fuel flow is then calculated based on this value and compensated for the actual fuel heating value; the resulting λ become higher if reformed fuel is used. The heating value for the reformed fuel is only 20.81 MJ/kg (natural gas: 47.8 MJ/kg) but the stoichiometric air-fuel ratio is 5.63 (natural gas: 16.58) which means that both the fuel mass flow and λ differs, given the same amount of fuel-bounded heat. The heating value for a stoichiometric mixture also differs; it is 2.08 MJ/kg for reformed fuel and 2.72 MJ/kg for natural gas. If all natural gas is replaced with reformed fuel, the mass flow and λ with reformed, fuel ("ref.") can be calculated through (assumed the same airflow):

$$\dot{m}_{ref.} = \frac{Q_{LHV,NG}}{Q_{LHV,ref.}} \cdot \dot{m}_{NG} \approx 2.30 \cdot \dot{m}_{NG}$$

$$\lambda_{ref.} = \frac{\dot{m}_{air} / \dot{m}_{ref.}}{(A/F)_{s,ref.}} = \frac{Q_{LHV,ref.}}{Q_{LHV,NG}} \cdot \frac{(A/F)_{s,NG}}{(A/F)_{s,ref.}} \cdot \lambda_{NG} \approx 1.28 \cdot \lambda_{NG} \qquad \text{Eq.114}$$

The simulations are performed as previously with a richer mixture during startup, and then leaning out to the desired set point after 34 seconds as shown in Figure 93. The actual (resulting) λ is then a result of fuel heating value difference and the control dynamics.

The resulting load and efficiency are shown in Figure 94 and Figure 95. There is no noticeable difference in indicated efficiency between the two shown cases. The brake efficiency is higher with richer mixtures as expected. At $\lambda_{NG,set}$ = 2.2, the load is 12.1 bar BMEP with 39.5% brake efficiency, However, at this point there is 22 ppm NO resulting in 0.17 g NO/kWh. The maximum pressure is about 181 bar, if higher maximum pressures are allowed it is possible to increase the amount of fuel. At $\lambda_{NG,set}$ = 2.1 about 14.1 bar BMEP is reached and the brake efficiency at this point is about 40.4%. However, the NO formation also increases to 0.30 g/kWh. These results and more detailed data can be found in Table 16. In these tables comparison are also made with natural gas only. One interesting thing is that when inlet air preheating is not required, intercooling is used to some degree when running with reformatted fuel. Still, the turbocharging is not sufficient. Smaller turbine is required but unfortunately, there is not available data on smaller turbines.

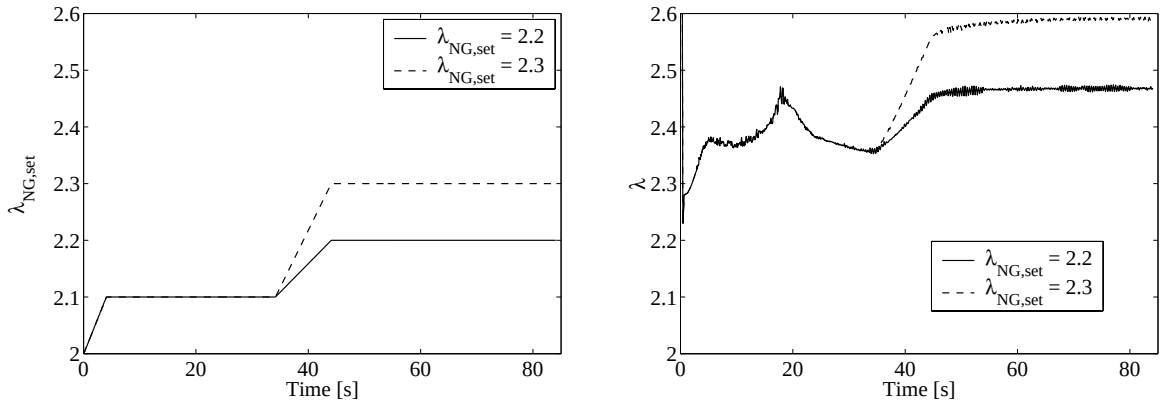

Figure 93 λ set-point (left) and actual value (right).

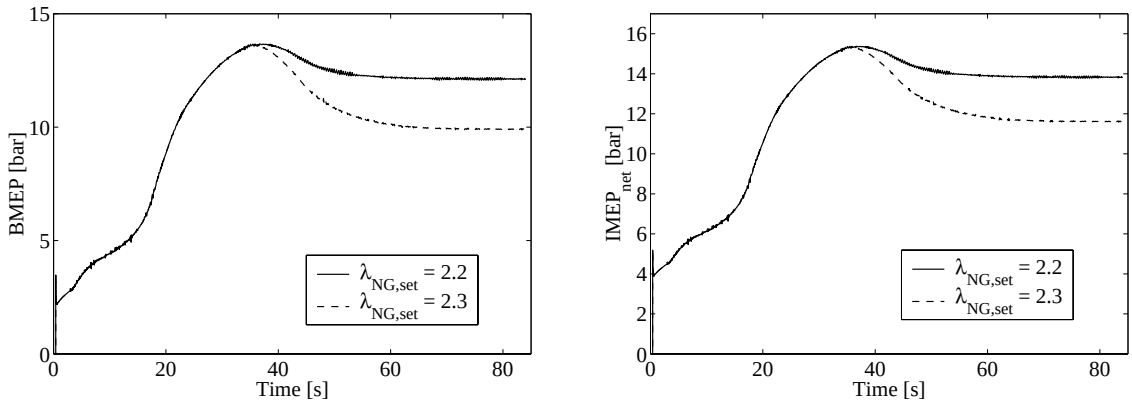

Figure 94 Resulting BMEP (left) and IMEP$_{net}$ (right).

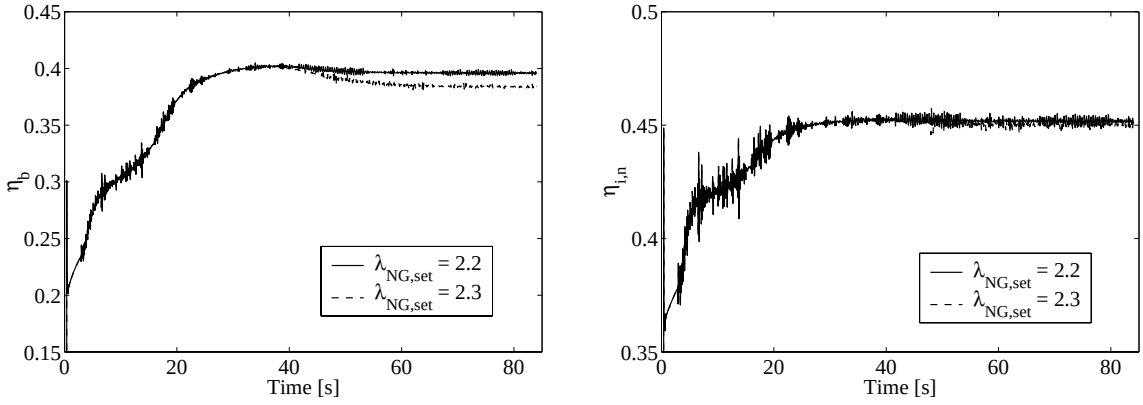

Figure 95 Resulting brake - (left) and net indicated efficiency (right).

Table 16 Results using 95% reformed fuel and 5% natural gas at 1500 rpm, except first case where only natural gas is used and showed for reference (T_1 = 298K, p_1 = p_4 = 1.013bar).

$\lambda_{NG,set}$	λ	p_{Max}	$NO_{Zeldovich}$		dm/dt_{tot}	T_{Inlet}	*Run*
		[bar]	[ppm]	[g/kWh]	[g/s]	[K]	
2.3	2.30	199	5.4	0.04	456	374	Natural gas only, 1800rpm, 16:1
2.1	*2.36*	*201*	*44*	*0.30*	*362*	*333*	*95% reformed fuel*
2.2	2.47	181	24	0.17	330	336	95% reformed fuel
2.3	2.59	154	11	0.08	291	340	95% reformed fuel

$\lambda_{NG,set}$	P_b	*Speed*	*IMEP gross*	*IMEP net*	*PMEP*	*BMEP*	$\eta_{i,n}$	η_b	p_2	p_3	T_2	T_3	T_4
	[kW]	[rpm]	[bar]	[bar]	[bar]	[bar]	[%]	[%]	[bar]	[bar]	[K]	[K]	[K]
2.3	220	1800	15.1	14.5	0.65	12.5	45.2	39.3	3.15	3.36	452	698	559
2.1	*207*	*1500*	*16.0*	*15.8*	*0.199*	*14.1*	*45.2*	*40.4*	*2.78*	*2.71*	*435*	*714*	*597*
2.2	177	1500	14.0	13.8	0.177	12.1	45.1	39.5	2.55	2.47	421	697	592
2.3	145	1500	11.8	11.6	0.164	9.90	45.1	38.4	2.27	2.21	403	680	589

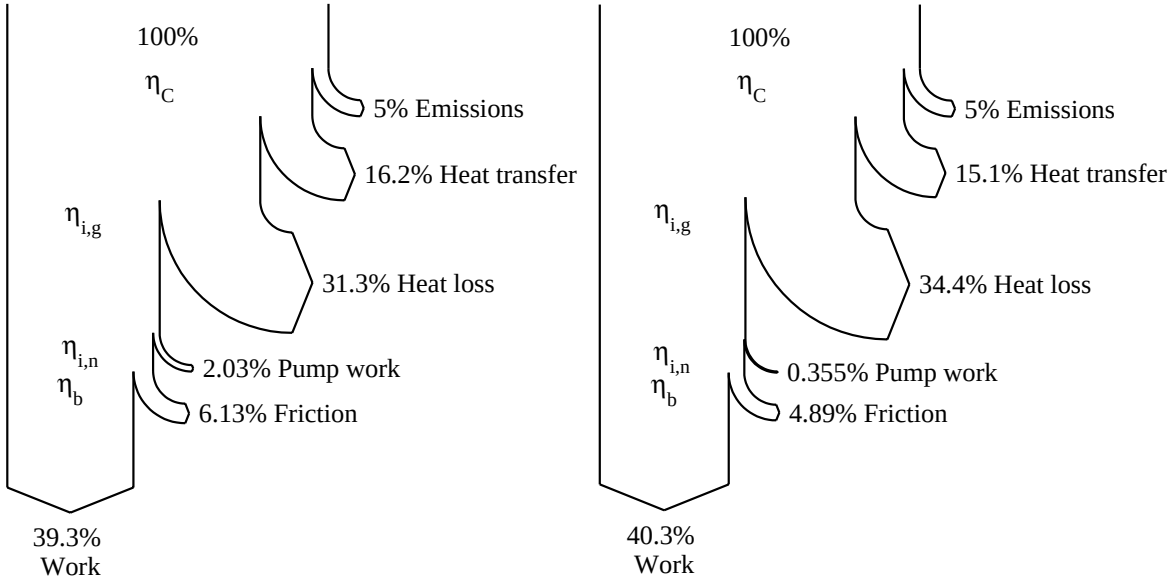

Figure 96 Sankey diagrams showing energy flow in the HCCI engine running at 1800 rpm and with natural gas (left) and at 1500rpm using reformed fuel (right).

6.3 The HAM system in combination with reformed fuel

The HAM system may be a feasible way to increase the mass flow through the turbine and simultaneously dilute the charge allowing higher engine loads without knocking combustion or NOx formation. The HAM concept is described earlier and here it is implemented in a whole turbocharged HCCI engine system simulation using the smallest turbine available (TC-3), the setup is illustrated in Figure 97. The air after the compressor is humidified to 98% relative humidity and then is the charged heated to give the necessary ignition criteria. The temperature of the heated liquid water into the humidifier is assumed to have a temperature of 70°C. There is obviously other possible system buildup but this is perhaps the simplest one. An inlet air heater for coarse control of combustion timing and reformed fuel is used for the fine adjustment. It would be better to make use of as much cooling of the humidifier as possible but that requires another ignition control parameter such as compression ratio, dual-fuel, fuel additive or any other suitable parameter.

The basic idea is to get additional mass flow from the humidification without any extra effort from the compressor. The extra water is used to dilute this mixture in a similar way as with EGR and will probably also reduce the heat release rate; knocking combustion can be avoided. The extra flow will also give extra work from the turbine and more power will be delivered to the compressor. As shown earlier (Figure 79), the specific heat of the inlet air mixture increases with more water, which results in lower indicated efficiency. Higher engine output will however reduce the friction detrimental effect on brake efficiency (FMEP assumed constant if constant engine speed).

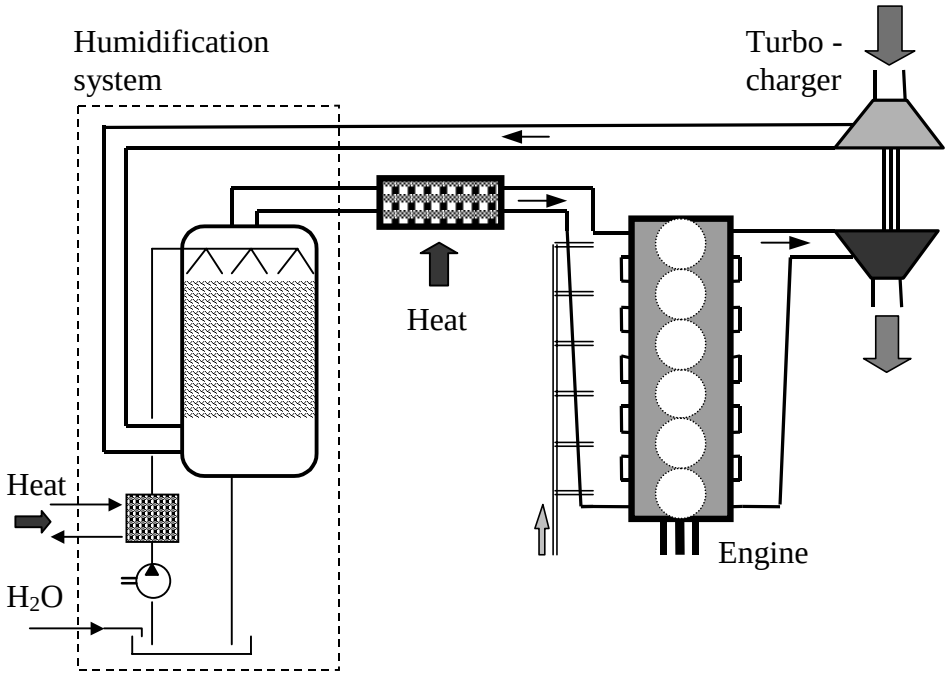

Figure 97 HAM system for HCCI operation

Reformed fuel allow much lower inlet temperatures, together with the HAM concept effective turbocharging is feasible through increased turbine mass flow. Water also suppresses NO formation by replacing oxygen in the inlet mixture which allow lower λ'as. In this simulation the effect on combustion duration cannot be seen but it would be reasonable to believe that high amount of steam will slow down combustion. Three different λ - values are tested expressed on natural gas base. This lambda value ($\lambda_{NG,set}$) is then compensated because of the

water content and the heating value of the fuel, hydrogen brings up the heating value for a stoichiometric mixture while carbon monoxide has about the same heating value for a stoichiometric mixture as natural gas. The fuel flow is then calculated and depending on the response of the system an "actual" lambda system can be calculated. The simulation is, as previously simulated as a startup procedure at 1500rpm. The λ - set point and the resulting λ is shown in Figure 98. For the two leaner cases, a slightly richer mixture is used during the first 34 seconds, then follows a 10 s ramp where the final desired value is set[13]. If the maximum in-cylinder pressure reaches 200 bar the λ set-point is increased. The primary control factor is the reformed fuel fraction but at all these cases some preheating was required; the reformed fuel fraction was set to it maximum value of 95%. 5% natural gas is left to simulate a control margin for cycle-to-cycle and cylinder-to-cylinder variation control. In order to investigate high load operation, combustion is phased quite late, as control parameter the crank angle for maximum pressure is used and the set-point is 13 CAD ATDC.

The resulting loads, both $IMEP_{net}$ and *BMEP* are shown in Figure 99. With the richer mixture, λ is reduced in order to limit maximum pressure to 200 bar so maximum load became about 14.7 bar *BMEP* at 1.71 bar *FMEP*. The efficiency also became higher with richer mixtures, about 45.2% net indicated and 40.3% brake efficiency as seen in Figure 100. The reformed fuel allowed reasonable inlet temperatures, which limited the thermal throttling. The compressor operating point became close to optimal as seen in Figure 101. In Table 17 the results of each simulation are shown. The pressure difference between engine inlet and exhaust also became positive despite the small turbine (TC-3) indicating that an even smaller turbine would be possible to use without higher pumping losses. This could allow higher boost pressures, although maximum in-cylinder pressures are already reached, so this action would require a lower compression ratio.

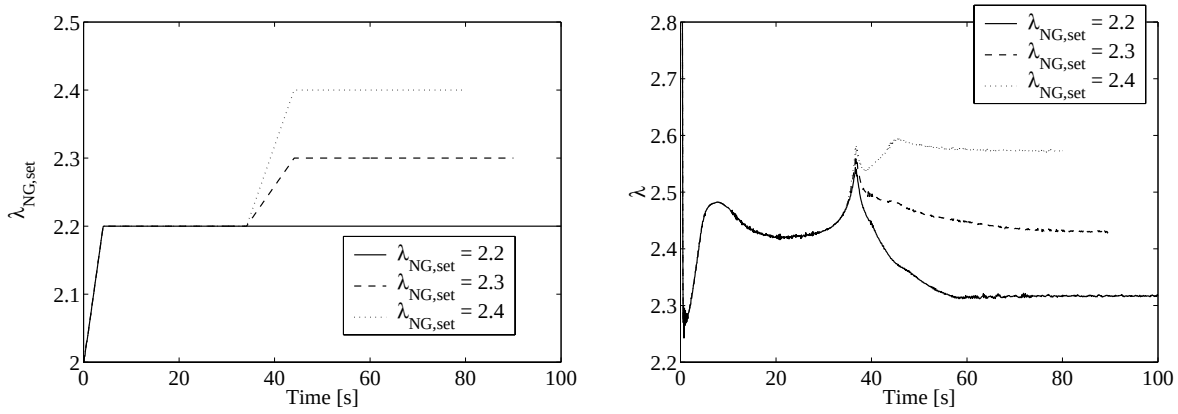

Figure 98 Left – Input to the simulation, λ for natural gas. Right - λ outcome, differs from set value ($\lambda_{NG,set}$) due to vaporized water, fuel composition and maximum pressure limitation.

[13] Required computational time (case hours:minutes): λ = 2.2 8:50, λ = 2.3 10:00, λ = 2.4 11:16, on a AMD Athlon Thunderbird 1200MHz, 256MB RAM, Windows 98 and Matlab 5.3. Functions MEX-compiled when possible. The computational time was estimated by looking at when the result files were created but the times are underestimated; it was discovered that the computer clock were delayed about 2 hours (!) after running the three simulations.

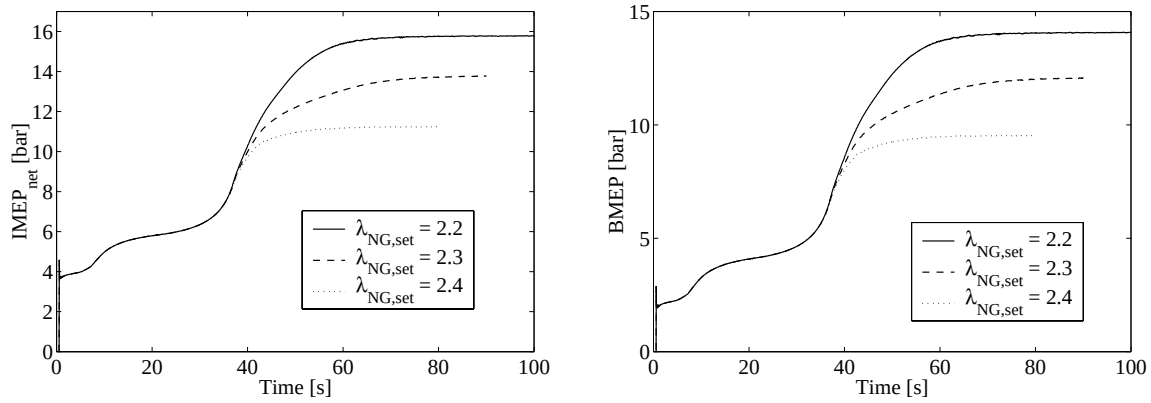

Figure 99 Left – Indicated mean effective pressure. Right – Brake mean effective pressure, FMEP is 1.71 bar

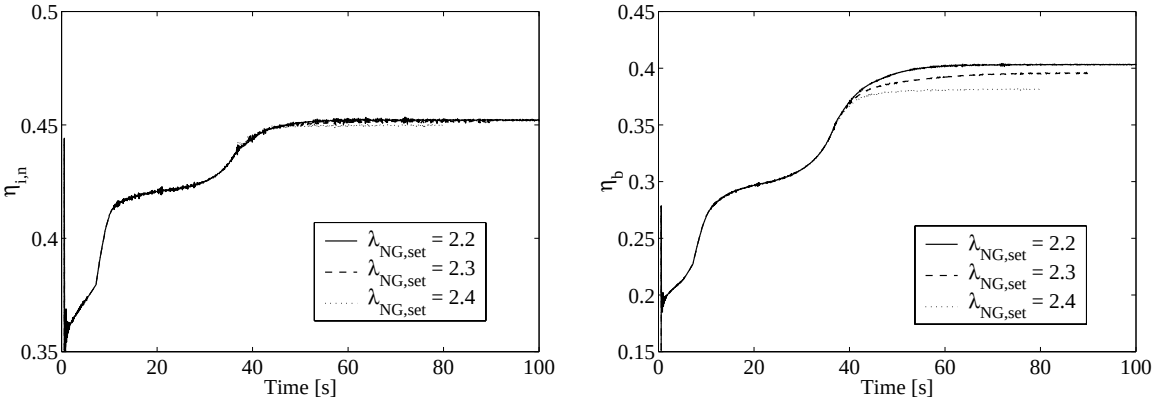

Figure 100 Left – Indicated efficiency. Right – Brake efficiency.

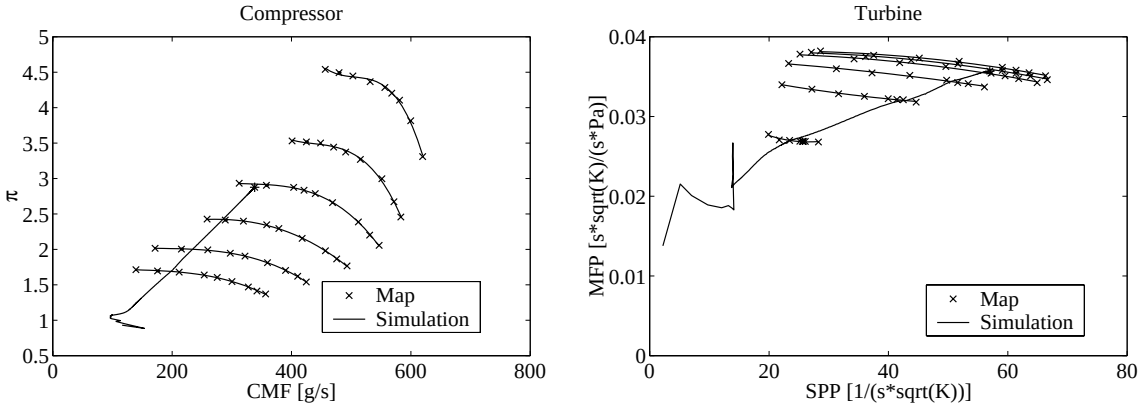

Figure 101 Compressor map (left) and turbine map (right) with the simulation ($\lambda_{NG,set}$ = 2.2) shown.

As much as 6.1 vol.-% of the inlet mixture is water, the relative humidity is assumed to be 98 % after the humidifier. The temperature drops in the humidifier due to the vaporization ($T_2 \rightarrow T_{2,HAM}$). When the air passes the heater, the relative humidity goes down and the temperature goes up depending on the heating power. The temperature in the inlet will besides the preheating also be dependant on the temperature of the fuel, and the assumption here is that it

has a temperature of 20°C before entering the inlet manifold which means that the fuel actually cools the inlet charge, this is especially clear at $\lambda_{NG,set}$ = 2.2 .

The NO formation according to Zeldovich is quite low despite the low λ. Some of this can be explained by the lower inlet temperatures than with natural gas only. Another factor may be the dilute effect of the water vapor. At $\lambda_{NG,set}$ = 2.2 the NO fraction in the exhaust gas were 12 ppm corresponding to a specific NO emission of 0.08g/kWh.

Table 17 Results with HAM using 95% reformed fuel and 5% natural gas. (T_1 = 298K, p_1 = p_4 = 1.013bar)

$\lambda_{NG,set}$	λ	p_{Max}	$NO_{Zeldovich}$		dm/dt_{tot}	dm/dt_{fuel}	$dm/dt_{H20,vap}$	x_{H2O}	T_{Inlet}	$T_{2,HAM}$
		[bar]	[ppm]	[g/kWh]	[g/s]	[g/s]	[g/s]	[%]	[K]	[K]
2.2	2.32	200	12	0.08	370	15.6	22.3	6.1	337	338
2.3	2.43	179	7	0.05	337	12.6	19.5	5.5	340	334
2.4	2.57	151	4	0.03	289	9.08	16.0	4.6	344	328

$\lambda_{NG,set}$	P_b	P_{Heater}	*IMEP gross*	*IMEP net*	*PMEP*	*BMEP*	$\eta_{i,n}$	η_b	p_2	p_3	T_2	T_3	T_4
	[kW]	[kW]	[bar]	[bar]	[bar]	[bar]	[%]	[%]	[bar]	[bar]	[K]	[K]	[K]
2.2	206	1.54	15.9	15.8	0.12	14.1	45.2	40.3	2.91	2.75	445	704	587
2.3	177	3.81	13.9	13.8	0.11	12.1	45.2	39.6	2.66	2.51	429	687	582
2.4	139	6.35	11.4	11.2	0.11	9.5	45.0	38.2	2.30	2.19	406	670	581

Figure 102 shows a Sankey plot illustrating the energy flow through the HCCI engine compared to a simulation of the diesel engine, running at peak load at 1500 rpm. The heat release parameters in the diesel engine simulation are adjusted to fit experimental data on maximum pressure, IMEP, and combustion efficiency. In the HCCI case the emissions steals a great deal of the energy and since the brake, output is less than in the diesel case the friction part is higher. The diesel engine loose quite much of the energy through the exhaust due to a slow combustion process, but gains some of this loss back due to a negative pumping work, the net indicated efficiency is higher than the gross indicated efficiency. This is possible because the higher exhaust temperatures, which makes it possible to use a much bigger turbine.

In summary, HAM in the combination with reformatted fuel seems to be a promising solution for small-scale power plant engines. With larger engines, it is a little bit questionable if HAM is required or not because of less heat transfer. In the simulation here it is not stated wherefrom the heater power for inlet air preheating is taken from. It is of cause suitable to use a heat exchanger and take heat from the exhaust gas. It should be pointed out that this system also requires a water supply of 22 g/s, about 80 liter/hour. However, during cold startup this may be a problem because of the thermal inertia of the whole system. The best operating point shown here provide 206 kW brake power, at 40.3 % brake efficiency and NO emissions of 0.08g/kWh. A big question mark is what combustion duration we would expect at this load and with this water content.

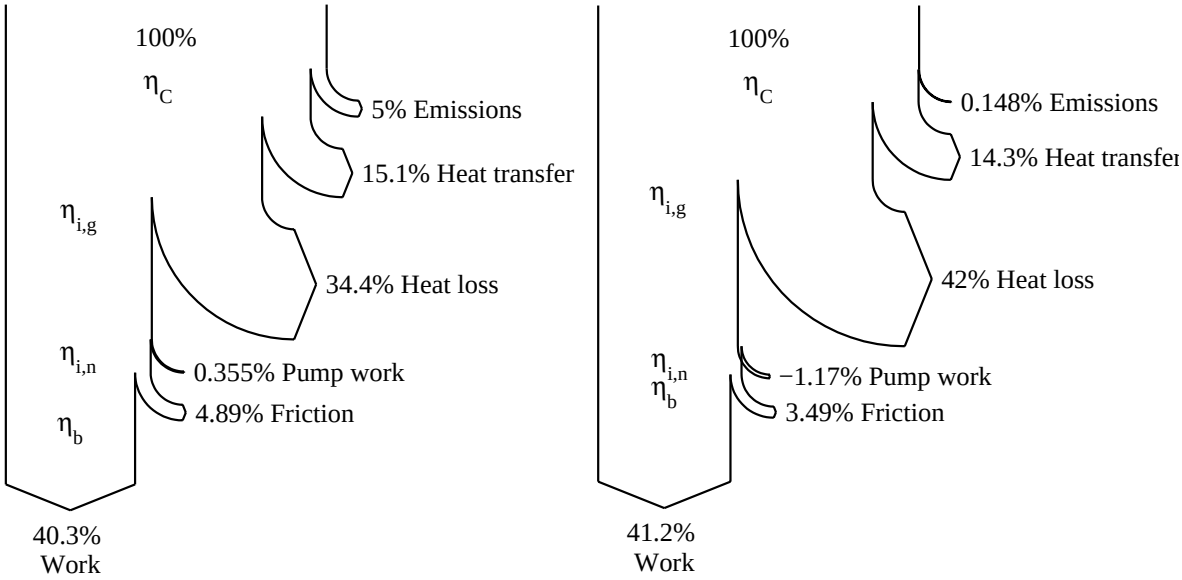

Figure 102 Sankey diagram showing the energy flow through the HCCI engine (left) using HAM and reformatted fuel ($\lambda_{NG,set}$ = 2.2) at BMEP 14.5bar, compared to simulation of a diesel engine at the same speed but at 20 bar BMEP (note the negative pump work), emissions estimated from experiments .

7 Summary

This thesis presents the predicted performance and efficiency of turbocharged natural gas driven Homogeneous Charge Compression Ignition (HCCI) engine systems. From these simulated results, we can expect that the engine load in terms of brake mean effective pressure will be lower than with conventional diesel engines, mainly due to the maximum in-cylinder pressure. The heat release rate during HCCI combustion is very high compared to diesel combustion and the peak pressures become higher. Nevertheless, for this rather small stationary engine it is possible to reach efficiency comparable to diesel engines, and with an acceptable specific power. The real benefit of HCCI is the low NOx emissions. The Zeldovich model used here give only an estimation of the NO formation, however this can still be used as an indicator of when NOx starts to form.

The most interesting cases are summarized in Table 18 and Table 19. In Table 18, comparisons are made at constant air-fuel equivalence ratio (normalized to natural gas) and in Table 19 at constant maximum pressure. The first case is the simple system with inlet air conditioner. In this case, the engine speed had to be increased in order to get proper turbocharging. The compression ratio was decreased in order to stay below a fictive design limit of 200bar peak in-cylinder pressure. Increasing the speed to 1800rpm gave both higher friction and pumping losses and the efficiency became lower.

Keeping the speed at 1500rpm and using a higher compression ratio of 17.4:1 and instead affecting the ignition characteristics of the fuel gave other results. This was done by simulate reformed natural gas, a CO (40 vol.%) and H_2 (60 vol.%) mixture. The ignition characteristics of the reformed fuel allowed lower inlet temperatures to be used and the mass flow through the turbine could be increased trough less thermal throttling of the engine. The boost pressure was lower compared to the high-speed case; the load also became lower. Using richer mixtures obviously produced more power and gave better efficiency, but the NO formation increased from 0.08g/kWh to 0.30g/kWh. The brake efficiency reached above 40% in the best operating conditions.

By also using the Humid Air Motor (HAM) concept, the mass flow through the engine and turbine could be increased at leaner mixtures. Engine load increased and hence also efficiency. Using a richer mixture, the load became higher as expected, and performance and efficiency became comparable with the case without HAM. On the other hand, the NO formation became much lower. Despite the richer mixture, the NO stayed at 0.08g/kWh. This final case would be even more interesting if the combustion duration were affected (longer) by the increased humidity. This could not be predicted with the zero dimensional models used.

Table 18 Summary of full system simulation, keeping $\lambda_{NG,set}$ at 2.3

Fuel/Case	r_C	*Speed*	λ	p_{Max}	$NO_{Zeldovich}$	P_b	P_{Heater}	*IMEP net*	*BMEP*	η_b
		[rpm]		[bar]	[g/kWh]	[kW]	[kW]	[bar]	[bar]	[%]
NG	16.0	1800	2.33	199	0.04	220	-	14.5	12.5	39.3
Reformed	17.4	1500	2.59	154	0.08	145	-	11.6	9.9	38.4
Ref. + HAM	17.4	1500	2.43	179	0.05	177	3.81	13.8	12.1	39.6

Table 19 Summary of full system simulation, keeping p_{Max} about 200bar

Fuel/Case	r_C	*Speed*	λ	p_{Max}	$NO_{Zeldovich}$	P_b	P_{Heater}	*IMEP net*	*BMEP*	η_b
		[rpm]		[bar]	[g/kWh]	[kW]	[kW]	[bar]	[bar]	[%]
NG	16.0	1800	2.33	199	0.04	220	-	14.5	12.5	39.3
Reformed	17.4	1500	2.36	201	0.30	207	-	15.8	14.1	40.4
Ref. + HAM	17.4	1500	2.32	200	0.08	206	1.54	15.8	14.1	40.3

Based on these results a suggestion would be to try these concepts on a real engine. If reformatted fuel is not possible, a temporary action could be to speed up the engine, if possible, in order to build up boost and then use the HAM concept to go down in engine speed and maintain boost pressure.

Some facts points towards better results in reality e.g. the limitation of the model about the overestimation of the inlet temperature indicate that the mass flow through the engine will become higher. Using HAM may affect combustion duration allowing slightly richer mixtures to be used without reaching maximum pressure, significant NOx formation or knocking combustion. This would lead to higher output and higher efficiency.

If bigger cylinders (larger displaced volume per cylinder) were used scale effects would probably appear. Less heat transfer would lead to higher efficiency, lower inlet temperatures and higher exhaust temperatures leading to less thermal throttling and less pumping losses if the compressor and turbine is matched properly.

8 References

1. “Pure Energy, Gas Cogeneration Plants”, pamphlet from Wärtsilä NSD Corporation, November 1997 edition
2. O. Erlandsson, ”Alvar engine An engine with variable compression ratio Experiments and test”, ISRN LUTMDN/TMVK-5304--SE
3. O. Erlandsson, Gunnar Lundholm, Fredrik Söderberg, Bengt Johansson,Victor W. Wong ”Demonstarting the Performance and Emission Characteristics of a Variable Compression Ratio, Alvar-Cycle Engine”, SAE 982682
4. S. Onishi, S. Hong Jo, K. Shoda, P Do Jo, S. Kato: ”Active Thermo-Atmosphere Combustion (ATAC) – A New Combustion Process for Internal Combustion Engines”, SAE790501
5. M. Noguchi, Y. Tanaka, T. Tanaka, Y. Takeuchi, "A Study on Gasoline Engine Combustion by Observation of Intermediate Reactive Products during Combustion", SAE 790840, 1979
6. N. Iida, "Combustion Analysis of Methanol-Fueled Active Thermo-Athmosphere Combustion (ATAC) Engine Using a Spectroscopic Observation", SAE 940684, 1994
7. P.Duret, S. Venturi, "Automotive Calibration of the IAPAC Fluid Dynamically Controlled Two-Stroke Combustion Process", SAE 960363, 1996
8. Y. Ishibashi, M. Asai, "Improving the Exhaust Emissions of Two-Stroke Engines by Applying the Activated Radical Combustion", SAE 960742, 1996
9. J. Yamaguchi, "Honda readies Activated Radical Combustion two-stroke engine for production motorcycle", Automotive Engineering, January, 1997
10. N. Iida, T. Ichikura, K. Kase, Y. Enomoto, "Self-ignition and combustion stability in a methanol fueled low heat rejection ceramic ATAC engine- analysis of cyclic variation at high wall temperatures and lean burn operation.", JSAE 9733684, 1997
11. R. Gentili, S. Frigo, L. Tognotti, P. Habert, J. Lavy, "Experimental Study on ATAC in a Two-Stroke Gasoline Engine", SAE 970363, 1997
12. N. Iida, "Alternative Fuels and Homogeneous Charge Compression Ignition Combustion Technology", SAE 972071, 1997
13. Y. Ishibashi, M. Asai, K. Nishida, "An Experimental Study of Stratified Scavenging Activated Radical Combustion Engine", SAE 972077, 1997
14. H. Oguma, T. Ichikura, N. Iida, "A Study on Adaptability of Alternative Fuels for Lean Burn Two-Stroke ATAC Engine", SAE 972097, 1997
15. E. Esterlingot, "Thermodynamical and Optical Analysis of Controlled Auto-Ignition Combustion in Two-Stroke Engines", SAE 972098, 1997
16. Y. Ishibashi, M. Asai, "A Low Pressure Pneumatic Direct Injection Two-Stroke Engine by Activated Radical Combustion Concept", SAE 980757, 1998

17. A. Hultqvist, “Characterization of the Homogeneous Charge Compression Ignition Combustion Process”, Doctoral Thesis, ISRN LUTMDN/TMVK-1030-SE
18. Homepage of Progress Aero Works, www.paw.ac, 2002-03-20
19. P.M. Najt, D. E. Foster, "Compression-Ignited Homogeneous Charge Combustion", SAE 830264, 1983
20. R.H. Thring, "Homogeneous Charge Compression Ignition (HCCI) Engines", SAE 892068, 1989
21. V. M. Stockinger, H. Schäpertöns, P. Kuhlmann, "Versuche an einem gemischansaugenden Verbrennungsmotor mit Selbstzündung", MTZ 53, 1992
22. H. Shoji, Y. Tosaka, K. Yoshida, A. Saima, "Radical Behavior in Preflame Reactions Under Knocking Operation in a Spark Ignition Engine", SAE 942061, 1994
23. T. Aoyama, Y. Hattori, J. Mizuta, Y. Sato, "An Experimental Study on Premixed-Charge Compression Ignition Gasoline Engine", SAE 960081, 1996
24. J. R. Smith, S. M. Aceves, C. Westbrook, W. Pitz, "Modeling of Homogeneous Charge Compression Ignition (HCCI) of Methane", ASME International Engine 1997 Fall Conference, Madison, Wisconsin, 1997
25. H. Yanagihara, Y. Sato, J. Mizuta, "A study of DI diesel combustion unders uniform higher dispersed mixture formation", JSAE 9725853, JSAE 9733675 1997
26. H. Suzuki, N. Koike, H. Ishii, M. Odaka, "Exhaust Purification of Diesel Engines by Homogeneous Charge with Compression Ignition Part 1", SAE 970313, 1997
27. H. Ishii, N. Koike, H. Suzuki, M. Odaka, "Exhaust Purification of Diesel Engines by Homogeneous Charge with Compression Ignition Part 2", SAE 970315, 1997
28. K. Nakagome, N. Shimazaki, K. Niimura, S. Kobayashi, "Combustion and Emission Characteristics of Premixed Lean Diesel Combustion Engine", SAE 970898, 1997
29. A.W. Grey III, T. W. Ryan III , "Homogeneous Charge Compression Ignition of Diesel Fuel", SAE 971676, 1997
30. M. Christensen, B. Johansson, P. Einewall, "Homogeneous Charge Compression Ignition (HCCI) Using Isooctane, Ethanol and Natural Gas - A Comparison with Spark Ignition Operation", SAE 972874, 1997
31. P.Amnéus, D. Nilsson, F. Mauss, M. Christensen, B. Johansson, "Homogeneous Charge Compression Ignition Engine: Experiments and Detailed Kinetic Calculations", COMODIA, 1998
32. T. Hashizume, T. Miyamoto, H. Akagawa, K. Tsujimura, "Combustion and Emission Characteristics of Multiple Stage Diesel Combustion", SAE 980505, 1998
33. H. Suzuki, N. Koike, M. Odaka, "Combustion Control Method of Homogeneous Charge Diesel Engine", SAE 980509, 1998
34. T. Seko, E. Kuroda, Y. Hamano, "Methanol Lean Burn in an Auto-Ignition DI Engine", SAE 980531, 1998
35. A. Harada, N. Shimazaki, S. Sasaki, T. Miyamoto, H. Akagawa, K. Tsujimura, "The Effects of Mixture Formation on Premixed Lean Diesel Combustion", SAE 980533, 1998
36. M. Christensen, B. Johansson, P. Amneus, F. Mauss, "Supercharged Homogeneous Charge Compression Ignition", SAE 980787, 1998
37. Y. Mase, J. Kawashima, T. Sato, M. Eguchi, "Nissan's New Multivalve DI Diesel Engine Series", SAE 981039, 1998

38. M. Christensen, B. Johansson, "Influence Of Mixture Quality on Homogeneous Charge Compression Ignition", SAE 982454, 1998
39. J. Willand, R-G. Nieberding, G. Vent, C. Enderle, "The Knock Syndrome - Its Cure and Its Potential", SAE 982483, 1998
40. N. Shimazaki, H. Akagawa, K. Tsujimura, "An Experimental Study of Premixed Lean Diesel Combustion", SAE 1999-01-0181, 1999
41. M. Christensen, B. Johansson, "Homogeneous Charge Compression Ignition with Water Injection", SAE 1999-01-0182, 1999
42. H. Akagawa, T. Miyamoto, A. Harada, S. Sasaki, N. Shimazaki, T. Hashizume, K. Tsujimura, "Approaches to Solve Problems of the Premixed Lean Diesel Combustion", SAE 1999-01-0183, 1999
43. M. Odaka, H. Suzuki, N. Koike, H. Ishii, "Search for Optimizing Control Method of Homogeneous Charge Diesel Combustion", SAE 1999-01-0184, 1999
44. Y. Iwabuchi, K. Kawai, T. Shoji, Y. Takeda, "Trial of New Concept Diesel COmbustion System - Premixed Compression -Ignited Combustion", SAE 1999-01-0185, 1999
45. T. Miyamoto, A. K. Hayashi, A. Harada, S. Susaki, K. Tsujimura, "A Computational Investigation of Premixed Lean Diesel Combustion - characteristics of fuel-air mixture formation, combustion and emissions", SAE 1999-01-0229, 1999
46. M. Richter, A. Franke, M. Aldén, A. Hultqvis, B. Johansson, "Optical Diagnostics Applied to a Natuarlly Aspirated Homogeneous Charge Compression Ignition Engine", SAE 1999-01-3649, 1999
47. M. Christensen, A. Hultqvist, B. Johansson, "Demonstrating the multi fuel capability of a homogeneous charge compression ignition engine with variable compression ratio", SAE 1999-01-3679, 1999
48. A. Hultquist, M. Christensen, B. Johansson, A. Franke, M. Richter, M. Aldén, "A Study of the Homogeneous Charge Compression Ignition Combustion Process by Chemiluminescence Imaging", SAE 1999-01-3680, 1999
49. S. Kimura, O. Aoki, H. Ogawa, S. Muranaka, Y. Enomoto, "New Combustion Concept for Ultra-Clean and High-Efficiency Small DI Diesel Engines", SAE 1999-01-3681, 1999
50. R. H. Stanglmaier, C. E. Roberts, "Homogeneous Charge Compression Ignition (HCCI): Benefits, Compromises and future Engine Applications", SAE 1999-01-3682, 1999
51. T. Løvås, D. Nilsson, P. Amnéus, F. Mauss, "Reduction of Complex Fuel Chemistry for Simulation of Combustion in an HCCI Engine", VDI Berichte Nr. 1492, p. 511, 1999
52. P. Maigaard, F. Mauss, M. Kraft, "Homogeneous Chrge Compression Ignition Engine: A Simulation Study on the Effects of Inhomogenities", ASME 2000 Spring Engine Technology Conference of the Internal Combustion Engine Division: April 9-12, 2000
53. J. Martinez-Frias, S. M. Aceves, D. Flowers, J. R. Smith, R. Dibble, "Exhaust Energy Recovery for Control of a Homogeneous Charge Compression Ignition Engine", ASME International Mechanical Engineering Congress and Exposition: Orlando, Florida, November 5-10, 2000
54. A. Hultqvist, M. Christensen, M. Richter, A. Franke, B. Johansson, "Near-Wall Combustion in a Homogeneous Charge Compression Ignition (HCCI) Engine", AVL 4. Internationales Symposium Für Verbrennungsdiagnostik, Kurhaus, Baden-Baden, 18-19 May, 2000

55. S. M. Aceves, D. L. Flowers, C. K. Westbrook, J. R. Smith, W. Pitz, R. Dibble, M. Christensen, B. Johansson, "A multi-zone model for prediction of HCCI combustion and Emissions", SAE 2000-01-0327, 2000
56. D. Flowers, S. Aceves, R. Smith, J. Torres, J. Girard, R. Dibble, "HCCI in a CFR Engine: Experiments and Detailed Kinetic Modelling", SAE 2000-01-0328, 2000
57. Z.Chen, M. Konno, M. Oguma, T. Yanai, "Experimental Study of CI Natural Gas/DME Homogeneous Charge Engine", SAE 2000-01-0329, 2000
58. A. Higashino, H. Sasaki, K. Kishiishita, S. Sekiyama, H. Kawamura, H. Iwamoto, "Compression Ignition Combustion in a Prechambered and Heat Insulated Engine Using a Homogeneous Natural Gas Mixture", SAE 2000-01-0330, 2000
59. T. Tsurushima, T. Miyamoto. H. Akagawa, Y. Aoyagi, J-H Lee, S. Goto, T. Wakisaka, T. Ishiyama, H. Kawanabe, "Effects of Initial In-Cylinder Flow Field om Mixture Formation i a Premixed Compression Ignition Engine", SAE 2000-01-0331, 2000
60. S. B.Fiveland, D. N. Assanis, "A Four-Stroke Homogeneous Charge Compression Ignition Engine Simulation for Combustion and Performance Studies", SAE 2000-01-0332, 2000
61. J-H Lee, S. Goto, T. Tsurushima, T. Miyamoto, T. Wakisaka, "Effects of Injection Conditions on Mixture Formation Process in a Premixed Compression Ignition Engine", SAE 2000-01-1831, 2000
62. N. Iida, T. Igarashi, "Auto-Ignition of n-Butane and DME/Air Mixtures in a Homogeneous Charge Compression Ignition Engine", SAE 2000-01-1832, 2000
63. A.Hultquist, M. Christensen, B. Johansson, "The Application of Ceramic and Catalytic Coatings to Reduce the Unburned Hydrocarbon Emissions from a Homogeneous Charge Compression ignition Engine", SAE 2000-01-1833, 2000
64. Y. Yamasaki, N. Iida, "Numerical Simulation of Auto-Ignition and combustion of n-Butane and Air Mixtures in a 4 Stroke HCCI Engine by Using Elementary Reactions", SAE 2000-01-1834, 2000
65. M. Christensen, B. Johansson, P. Amneus, F. Mauss, "Supercharged Homogeneous Charge Compression Ignition (HCCI) with Exhaust Gas Recirculation and Pilot Fuel", SAE 2000-01-1835, 2000
66. J. Lavy, J-C. Dabadie, C. Angelberger, P. Duret, J. Willand, A. Juretzka, J. Schäflein, T. Ma, Y. Lendresse, A. Satre, C. Schulz, H. Krämer, H. Zhao, L. Damiano, "Innovative Ultra-low Nox Auto-Ignition Combustion Process for gasoline Engines: the 4-SPACE Project", SAE 2000-01-1837, 2000
67. O. Erlandsson, B. Johansson, F. A. Silversand, "Hydrocarbon (HC) Reduction of Exhaust Gases from a Homogeneous Charge Compression Ignition (HCCI) Engine Using Different Catalytic Mesh-Coatings", SAE 2000-01-1847, 2000
68. J. - O. Olsson, O. Erlandsson, B. Johansson, "Experiments and Simulation of a Six-Cylinder Homogeneous Charge Compression Ignition (HCCI) Engine", SAE 2000-01-2867, 2000
69. M. Richter, J. Engström, A. Franke, M. Aldén, A. Hultqvist, B. Johansson, "The influence of charge inhomogenity on the HCCI combustion process", SAE 2000-01-2868, 2000
70. J. Martinez-Frias, S. Aceves, D. Flowers, J. R. Smith, R. Dibble, "HCCI Engine Control by Thermal Management", SAE 2000-01-2869, 2000
71. G. Kontarakis, N. Collins, T. Ma, "Demonstration of HCCI Using a Single Cylinder Four-stroke Engine", SAE 2000-01-2870, 2000

72. S. Kimura, O. Aoki, Y. Kitahara, E. Aiyoshizawa, "Ultra-Clean Combustion Technology Combining a Low-Temperature and Premixed Combustion Concept for Meeting Future Emissions Standards", SAE 2001-01-0200, 2001
73. T. Noda, D. E. Foster, "A Numerical Study to Control Combustion Duration of Hydrogen-fueled HCCI by Using Multi-zone Chemical Kinetics Simulation", SAE 2001-01-0250, 2001
74. D. Law, D. Kemp, J. Allen, G. Kirkpatrick, T. Copland, "Controlled Combustion in an IC-Engine with a Fully Variable Valve Train", SAE 2001-01-0251, 2001
75. T. Amano, S. Morimoto, Y. Kawabata, "Modeling of the Effect of Air/Fuel Ratio and Temperature Distribution on HCCI Engines", SAE 2001-01-1024, 2001
76. J. Zheng, W. Yang, D. L. Miller, N. P. Cernansky, "Prediction of Pre-ignition Reactivity and Ignition Delay for HCCI Using a Reduced Chemical Kinetic model", SAE 2001-01-1025, 2001
77. S.- K. Kong, C. D. Marriott, R. D. Reitz, M. Christensen , "Modelling and Experiments oa HCCI Engine Combustion Using Detailed Chemical Kinetics with Multidimensional CFD", SAE 2001-01-1026, 2001
78. S. M. Aceves, D. L. Flowers, J. Martinez-Frias, J. R. Smith, C. K. Westbrook, W. J. Pitz, R. Dibble, J. F. Wright, W. C. Akinyemi, R. P. Hessel, "A Sequential Fluid-Mechanic Chemical-Kinetic Model of Propane HCCI Combustion", SAE 2001-01-1027, 2001
79. S. B. Fiveland, D. N. Assanis, "Development of a Two-Zone HCCI Combustion Model Accounting for Boundary Layer Effects", SAE 2001-01-1028, 2001
80. W. L. Easley, A. Agarwal, G. A. Lavoie, "Modeling of HCCI combustion and Emissions Using Detailed Chemistry", SAE 2001-01-1029, 2001
81. A. Oakley, H. Zhao, N. Ladommatos, T. Ma, "Experimental Studies on Controlled Auto-ignition (CAI) Combustion of Gasoline in a 4-Stroke Engine", SAE 2001-01-1030, 2001
82. J. - O. Olsson, P. Tunestål, B. Johansson, "Closed-Loop Contol of an HCCI Engine", SAE 2001-01-1031, 2001
83. A. Hultqvist, U. Engdar, B. Johansson, J. Klingmann, "Reacting Boundary Layers in a Homogeneous Charge Compression Ignition (HCCI) Engine", SAE 2001-01-1032, 2001
84. K. Tanaka, H. Endo, A. Imamichi, Y. Oda, Y. Takeda, T. Shimada, "Study of Homogeneous Charge Compression Ignition Using a Rapid Compression Machine", SAE 2001-01-1033, 2001
85. S. S. Morimoto, Y. Kawabata, T. Sakurai, T. Amano, "Operating Characteristics of a Natural Gas-Fired Homogeneous Charge Compression Ignition Engine (Performance Improvment Using EGR)", SAE 2001-01-1034, 2001
86. N. Milovanovic, R. Chen, "A Review of Experimental and Simulation Studies on Controlled Auto-Ignition Combustion", SAE 2001-01-1890, 2001
87. T. Tsurushima, A. Harada, Y. Iwashiro, Y. Enomoto, Y. Asaaumi, Y. Aoyagi, "Thermodynamic Characteristics of Premixed Compression Ignition Combustions", SAE 2001-01-1891, 2001
88. Y. Nashijima, Y. Asaumi, Y. Aoyagi, "Premixed Lean Diesel Combustion (PREDIC) using Impingement Spray System", SAE 2001-01-1892, 2001

89. M .Christensen, B. Johansson, A. Hultqvist, "The Effect of Topland Geometry on Emissions of Unburned Hydrocarbons from a Homogeneous Charge Compression (HCCI) Engine", SAE 2001-01-1893, 2001
90. M. Y. Au, J. W. Girard, R. Dibble, D. Flowers, S. M. Aceves, J. Martinez-Frias, R. Smith, C. Seibel, U. Maas, "1.9-Liter Four-Cylinder HCCI Engine Operation with Exhaust Gas Recirculation", SAE 2001-01-1894, 2001
91. D. Flowers, S. M. Aceves, J. Martinez-Frias, J. R. Smith, M. Au, J. W. Girard, R. Dibble, "Operation of a Four-Cylinder 1.9L Propane Fueled Homogeneous Charge Compression Ignition Engine: Basic Operating Characteristics and Cylinder-to-Cylinder Effects", SAE 2001-01-1895, 2001
92. J. - O. Olsson, P. Tunestål, G. Haraldsson, B. Johansson, "A Turbocharged Dual Fuel HCCI Engine", SAE 2001-01-1896, 2001
93. R. H. Stranglmaier, T. W. Ryan III, J. S. Souder, "HCCI Operation of a Dual-Fuel Natural Gas Engine for Improved Fuel Efficency and Ultra-Low NOx Emissions at Low to Moderate Engine Loads", SAE 2001-01-1897, 2001
94. M. Christensen, ”HCCI Combustion – Engine Operation and Emission Characteristics”, Doctoral Thesis, 2002, Lund Institute of Technology, Lund, Sweden, ISBN 91-628-5424-0
95. O. Erlandsson, B. Johansson, F. Silversand, ”Hydrocarbon (HC) Reduction of Exhaust Gases from a Homogeneous Charge Compression Ignition (HCCI) Engine Using Different Catalytic Mesh-Coatings”, SAE 2000-01-1847
96. J. B. Heywood; ”Internal Combustion Engine Fundamentals”, ISBN 0-07-100499-8
97. C. L. Cummins Jr.; "Internal fire", ISBN 0-89883-765-0
98. B. J. McBride, S. Gordon, M. A. Reno; ”Coefficients for Calculating Thermodynamic and Transport Properties of Individual Species”, NASA Technical Memorandum 4513
99. Yunus A. Çengel, Michael A. Boles; ”Thermodynamics: An Engineering Approach”, ISBN 0-07-113249-X
100. O. Erlandsson, “Development of an Engine System Simulation Software Package – ESIM”, Licentiate thesis, Lund Institute of Technology, ISRN/LUTMDN/TMVK - 7043
101. C. R. Ferguson; ”Internal Combustion Engines - Applied Thermosciences”, ISBN 0-471-83705-9
102. Fredrik Söderberg; ”A Study of Fluid Flow and Combustion with Variable Valve Timing”, ISRN LUTMDN/TMHT-98/7029--SE
103. I. I. Vibe; ”Brennverlauf und Kreisprozeß von Verbrennungsmotoren”, VEB Verlag Technik Berlin
104. G. Woschni; ”A Universally Applicable Equation for the Instantaneous Heat Transfer Coefficient in the Internal Combustion Engine”, SAE 670931
105. J. A. Caton, J. B. Heywood; ”An Experimental and Analytical Study of Heat Transfer in an Engine Exhaust Port”, Int. J. Heat Mass Transfer Vol 24, No. 4, pp. 581-595, 1981
106. R. Egnell; ”A Simple Approach to Studying the Relation between Fuel Rate Heat Release and NO Formation in Diesel Engines”, SAE 1999-01-3548
107. W. W and M. Ross; “Modeling of Direct Injection Diesel Engine Fuel Consumption”, SAE 971142
108. M. Müller, E. Hendricks, S. C. Sorenson; ”Mean Value Modelling of Turbocharged Spark Ignition Engines”, SAE 980784

109. N. Watson, M. S. Janota, “Turbocharging the Internal Combustion Engine”, 1982, ISBN 0-333-24290-4
110. The NIST Reference on Constant, Units and Uncertainty; http://physics.nist.gov
111. C. Nellen, K. Boulouchos, “Natural Gas Engines for Cogeneration: Highest Efficiency and Near-Zero-Emissions through Turbocharging, EGR and 3-way Catalytic Converter”, SAE 2000-01-2825
112. P. Amneus, "Homogeneous Ignition, Chemical Kinetic Studies for IC-Engine Applications", Doctoral Thesis, ISRN LUTFD2/TFCP-81-SE, Lund Institute of Technology, Lund, Sweden
113. J. Warnatz, U. Maas, R. W. Dibble, “Combustion, - Physical and Chemical Fundamentals, Modelling and Simulation, Experiments, Pollutant Formation”, 1995, ISBN 3-540-60730-7
114. S. B. Fiveland, R. Agama, M. Christensen, B. Johansson, J. Hiltner, F. Mauss, D. N. Assanis, “Experimental and Simulated Results Detailing the Sensitivity of Natural Gas HCCI Engines to Fuel Composition”, SAE 2001-01-3609
115. DONG Energi-Service, Gas quality readings June 2002; http://www.dong.dk,
116. J. - O. Olsson, P. Tunestål, B. Johansson, S. Fiveland, R. Agama, M. Willi, D. Assanis, “Compression Ratio Influence on Maximum Load of a Natural Gas Fueled HCCI Engine”, SAE 2002-01-0111
117. L. Koopmans, I. Denbratt, “A Four Stroke Camless Engine, Operated in Homogeneous Charge Compression Ignition Mode with Commercial Gasoline”, SAE 2001-01-3610
118. L. Koopmans, O. Backlund, I. Denbratt, “Cycle to Cycle Variations: Their Influence on Cycle Resolved Gas Temperature and Unburned Hydrocarbons from a Camless Gasoline Compression Ignition Engine”, SAE 2002-01-0110.
119. O. Erlandsson, “Early Swedish Hot-Bulb Engines – Efficiency and Performance Compared to Contemporary Gasoline and Diesel Engines”, SAE 2002-01-0115
120. P. Rosén, L.-O. Olsson, “Method for supplying vapor to the intake of an internal combustion engine, and device therefore”, Patent WO 95/23286, 31 August 1995
121. T. Lindquist, P. Rosén, L. - O. Olsson, “Humid Cycles, A Novel Way To Increase Performance Of Marine Propulsion Systems”, CIMAC World Congress on Combustion Engine Technology, May 2001, Germany
122. Munters AB, Pre-cooling of diesel engines - H.A.M.; http://www.munters.com/

Symbols and Abbreviations

MEP – Mean Effective Pressures

BMEP	Brake MEP
FMEP	Friction MEP (mechanical friction)
FuelMEP	Fuel MEP
$IMEP_{net}$	Net Indicated MEP
$IMEP_{gross}$	Gross Indicated MEP (without the gas exchange strokes)
QhrMEP	Heat Release MEP
QhtMEP	Heat Transfer MEP
QlossMEP	Heat Loss MEP
QemisMEP	Emission MEP (based on heat chemically bounded in emissions)
PMEP	Pump MEP

[Pa] or [bar], 1bar = 10^5Pa ≈ 1atm

η – *Efficiencies*

η_b	Brake efficiency
η_c	Combustion efficiency
η_C , η_T	Isentropic efficiency for compressor and turbine
$\eta_{G.e.}$	Gas exchange efficiency
$\eta_{i,n}$	Net indicated efficiency
$\eta_{i,g}$	Gross indicated efficiency
$\eta_{M,e}$	Mechanical efficiency
$\eta_{Th.}$	Thermal efficiency
η_V	Volumetric efficiency

Other symbols

α	Convective heat transfer coefficient [W/(m^2·K)]
ϕ	Fuel-air equivalence ratio, $(m_f/m_a)/(m_f/m_a)_s$
γ	Ratio of specific heats
η	Dynamical viscosity [μP] or [Pa·s], 1μP = 10^{-7} Pa·s
λ	Thermal conductivity [W/(m·K)]
λ	Air-fuel equivalence ratio, $(m_a/m_f)/(m_a/m_f)_s$
ν	Kinematical viscosity
π_C, π_T	Pressure ratio for compressor and turbine
ρ	Density [g/m^3] or [kg/m^3]
τ	Time period [s]
ω	Rotational speed [1/s]

A	Area [m^2]
A_{min}	Minimum geometrical valve flow area [m^2]
A_E	Effective valve flow area [m^2]
A_p	Port area [m^2]
A0, A10	Crank angle for 0 and 10 % burned mass fraction [CAD]
A50, A90	Crank angle for 50 and 90 % burned mass fraction [CAD]
BDC	Bottom dead center
C_D	Discharge Coefficient
C_p	Specific heat at constant pressure [J/(mol·K)]
CMF	Corrected mass flow [g/s]
D	Cylinder bore [m]
$D_{0\text{-}10}$, $D_{10\text{-}90}$	Duration 0 – 10% and 10-90% burned mass fraction [CAD]
D_p	Port diameter [m]
E	Total energy [J]
EVO, EVC	Exhaust valve opening and closing (in crank angle degrees)
e	Total energy [J/mol]
h^0	Enthalpy [J/mol]
h_1 , h_2	Enthalpy upstream and downstream compressor [J/mol]
h_3 , h_4	Enthalpy upstream and downstream turbine [J/mol]
$h_{2,s}$, $h_{4,2}$	Isentropic enthalpy downstream compressor and turbine [J/mol]
h_c	Convective heat transfer coefficient [W/(m2·K)]
H	Enthalpy [J]
IVO, IVC	Intake valve opening and closing (in crank angle degrees)
J_{TC}	Inertia of the turbo shaft [kg·m^2]
l	Stroke [m]
L_{ref}	Characteristic length of the vessel [m]
M	Mole weight [g/mol]
m	Mass, [g] or [kg]
m_a	Air mass, [g] or [kg]
m_f	Fuel mass, [g] or [kg]
MFP	Mass flow parameter [g·sqrt(K)/(s·Pa)]
n	Moles [mol]
n	Engine speed [rpm]
n_R	Revolutions per cycle
N	Number of species
Nu	Nusselt number, $Nu = \alpha \cdot L_{ref} / \lambda$
p	Pressure [Pa]
p_1 , p_2	Pressure upstream and downstream compressor [Pa]
p_3 , p_4	Pressure upstream and downstream turbine [Pa]
p_{cr} , p_r	Critical and reduced pressure [Pa]
P_b	Brake power, [W] or [kW]
Q	Heat [J]
Q_{LHV}	Lower heating value of the fuel, [J/g] or [J/kg]
Q_{hr}	Heat released during combustion [J]
R	Universal gas constant [J/(mol·K)]
r_C	Compression ratio
Re	Reynolds number, $Re = \rho \cdot U_{ref} \cdot L_{ref} / \eta$
s^0	Specific entropy [J/(mol·K)]
$\overline{S}_p$	Mean piston speed [m/s], $\overline{S}_p = 2 \cdot l \cdot n / 60$

SPP	Speed parameter [1/(s·sqrt(K))]
t	Time [s]
T	Temperature [K]
T_1, T_2	Temperature upstream and downstream compressor [K]
T_3, T_4	Temperature upstream and downstream turbine [K]
T_b	Brake torque, [Nm]
T_{cr}, T_r	Critical and reduced temperature [K]
u	Internal energy [J/mol]
U	Internal energy [J]
U_{ref}	Characteristic flow velocity [m/s]
V	Volume [m^3]
V_d, $V_{d,tot}$	Displaced volume of the whole engine, or a single cylinder [m^3]
W	Work [m^3]
$\overline{w}$	Characteristic gas velocity [m/s]
x	Piston position
x_b	Burned mass fraction
y_i	Mole fraction
Z	Compressibility factor

See also figures for definitions not covered in the list, e.g. Figure 13 and Figure 14.

Abbrevations

ATAC	Active Thermo Atmosphere Combustion (Engine)
ATDC	After top dead center
BTDC	Before top dead center
ARC	Active Radical Combustion
CAC	Charge air cooler, Intercooler
CAD	Crank Angle Degrees
CFR	Cooperative Fuel Research (Engine, used for octane number determination)
EGR	Exhaust Gas Recycling (or Recirculation)
ESIM	“Engine SIMulation”, software made in-house for engine system simulation
FTIR	Fourier Transform Infra Red (analysis of the infrared absorption spectra)
HC	Hydrocarbons (emissions)
HCCI	Homogeneous Charge Compression Ignition (Engine)
HTR	Heater
IC	Internal Combustion (Engine)
KE	Kinetic energy
MK	Modulated Kinetics (diesel engine concept by Nissan Motor Co.)
NOx, NO_x	Nitrogen oxides ($NO + NO_2 + N_2O$)
PCC	Pre Combustion Chamber (Engine)
PE	Potential energy
RON	Research Octane Number (A measure of “auto-ignition resistance”)
SI	Spark Ignition (Engine)
TDC	Top Dead Center (usually the combustion TDC)
THC, UHC	Total-/Unburned hydrocarbons (including methane, CH_4. See NMHC)
NMHC	Non-methane total hydrocarbons (methane excluded), sometimes NMTHC
VCR	Variable Compression Ratio (Engine)
WOT	Wide Open Throttle (SI engines)

… and that was the beginning of the end of my Ph. D. studies.